Structures of Exocyst Subunit Exo70 from Yeast and Mouse

by

Brian A. Moore

A dissertation submitted in partial fulfillment
of the requirements for the degree of
Doctor of Philosophy
(Biological Chemistry)
in the University of Michigan
2007

Doctoral Committee:

Associate Professor Zhaohui Xu, Chair
Professor Daniel T. Klionsky
Professor Benjamin L. Margolis
Professor Edward L. Stuenkel
Assistant Professor Raymond C. Trievel

To my wife Melissa
and my son William

Acknowledgements

If my experience as a graduate student has tought me anything, it is to never give up and try everything before changing direction. I would like to thank the members of the Xu lab, Kae Yoshino-Koh, Junyu Xiao, Jiahai Zhou, Anthony Ludlam, and my mentor Zhaohui Xu, for teaching me this lesson and providing much valuable feedback over the course of my graduate career and for providing a stimulating and enjoyable environment to work in.

I would also like to thank my graduate thesis committee, Zhaohui Xu, Daniel Klionsky, Benjamin Margolis, Edward Stuenkel, and Raymond Trievel, for valuable feedback and discussion on a yearly basis, just when I seemed to be getting off track and needing some guidance from a source outside the laboratory.

The laboratory of Lois Weisman, especially Taylor Eves, Emily Kauffman, and Yui Jin, provided materials and much guidance for a number of yeast-two-hybrid experiments that ultimately did not work out. The experience was a very positive collaboration and has brought our two labs closer together.

The laboratory of Alan Saltiel, especially Xiaowei Chen, Mayumi Inoue, David Bridges, and Alan Saltiel himself, provided a mutually beneficial relationship in which I was able to provide mammalian Exo70 protein to Mayumi and receive valuable discussion in regard to mammalian Exo70 and TC10. It was a wonderful experience to work with this proficient group.

Howard Robinson of Brookhaven National Laboratory deserves thanks for collecting the final series of *S. cerevisiae* Exo70 data sets in a long-distance collaboration. His thorough and timely work was very welcome at a time when competition to publish was high.

The beamline staffs of the General Medicine and Cancer Institutes CAT and the Life Sciences CAT at APS were invaluable in technical matters. The equipment we had access to was well maintained and easy to use thanks to the help provided by these staffs.

Janet Smith and John Tesmer deserve special thanks along with the rest of the University of Michigan X-ray crystallography community for constant interest and helpful comments and interest in my structure projects.

I would also like to thank several inspirational people. My grandfather Woody Moore taught me many valuable lessons in project management, perseverance, and attitude. My scoutmaster Jack Breen provided several life lessons and fostered an early interest in science and technology. My doctor Allen Steere inspired a strong interest in biology and immunology and provided me with my first true laboratory experience. He has supported me in my scientific career throughout.

My friends Jasper Kok, David Wilson, Julia Coppola, Andrew Hauptman, Liza Rublico, Betsy Pierce, and John and Colleen Erpelding deserve many thanks for maintaining my sanity over the last five years. Their friendships have been an invaluable part of my life over the last five years.

Finally, I would like to thank my family. My brother Adam, my mother Marian, my father Jeffrey, and my Aunt Tere have each played important roles in supporting me. I am particularly grateful for my wife Melissa and my son William. They have provided

me with so much love and inspiration and they have been an instrumental part of my success at the University of Michigan.

Table of Contents

List of Figures

List of Tables

Glossary

β-me	2-mercaptoethanol
APBS	adaptive Poisson-Boltzmann solver
APS	Advanced Photon Source
ARP	Automated Refinement Procedure
ARP	actin-related protein
Arpc	actin-related protein complex
ATPase	adenosine triphosphatase
BLAST	Basic Local Alignment and Search Tool
CAT	Collaborative Access Team
CFTR	cystic fibrosis transmembrane conductance regulator
CIP	calf intestinal alkaline phosphatase
CNS	Crystallography & Nuclear Magnetic Resonance System
COG	conserved oligomeric Golgi
COP	coat protein complex
CORVET	class C core vacuole/endosome tethering
Dm (prefix)	*Drosophila melanogaster*
DMSO	Dimethyl sulfoxide
DNA	deoxyribonucleic acid
DTT	dithiothreitol

EDTA	ethylenediaminetetraacetic acid
ER	endoplasmic reticulum
ExPASy	Expert Protein Analysis System
FAPP	four-phosphate-adaptor protein
GAP	GTPase activating protein
GARP/VFT	Golgi-associated retrograde protein / Vps fifty-three
GDI	guanosine diphosphate dissociation inhibitor
GEF	guanine nucleotide exchange factor
GST	Glutathione *S*-transferase
GTPase	guanosine triphosphatase
HEPES	4-(2-hydroxyethyl)-1-piperazineethanesulfonic acid
His_8	octo-histidine
HOPS	homotypic fusion and vacuole protein sorting
IPTG	isopropyl β-D-1-thiogalactopyranoside
K_D	dissociation constant
LB	Luria-Bertani or Luria Broth or Lysogeny Broth
lgl	lethal giant larvae
MAD	multi-wavelength anomalous dispersion
MBP	maltose binding protein
MLF	maximum likelihood formalism
MLHL	maximum likelihood using Hendrickson-Lattman coefficients
Mm (prefix)	*Mus musculus*
MOPS	3-(N-morpholino)propanesulfonic acid

MPD	2-methyl-2,4-pentanediol
mRNA	messenger ribonucleic acid
NDSB	non-detergent sulfo-betaine
NLS	National Synchrotron Light Source
NMR	Nuclear Magnetic Resonance
NSF	N-ethylmaleimide sensitive fusion protein
NTA	nitrilotriacetic acid
OD	Optical Density
PCR	Polymerase Chain Reaction
PDB	protein data bank
PEG	polyethylene glycol
PH	plextrin homology
PIPES	1,4-Piperazinediethanesulfonic acid
PtdIns(3,4,5)P_3	Phosphatidylinositol (3,4,5)-trisphosphate
PM	plasma membrane
PMSF	phenylmethylsulphonyl fluoride
PVDF	polyvinylidene difluoride
RCSB	Research Collaboratory for Structural Bioinformatics
Rn (prefix)	*Rattus norvegicus*
SAD	single-wavelength anomalous dispersion
Sc (prefix)	*Saccharomyces cerevisiae*
SDS-PAGE	sodium dodecyl sulfate polyacrylamide gel rlectrophoresis
SeMet	*L*-selenomethionine

SNAP	soluble NSF attachment protein
SNARE	soluble NSF attachment protein receptor
SOB	Super Optimal Broth
Spermidine	N-(3-aminopropyl)-1,4-diaminobutane
SPR	surface plasmon resonance
TB	Transformation Broth
TCEP	*tris*(2-carboxyethyl)phosphine
TCM	Tris-Calcium-Magnesium
TEV	Tobacco Etch Virus
TRAPP	transport protein particle
Tris	2-amino-2-hydroxymethyl-1,3-propanediol
Urea	diaminomethanal
VPS	vacuole protein sorting
wARP	weighted Automated Refinement Procedure

Abstract

Exocytosis is a eukaryotic process in which vesicles deliver membrane and other cargoes to and across the plasma membrane. The exocyst is a tethering complex necessary for the polarization and fusion of exocytic vesicles with the plasma membrane. It is conserved in eukaryotes, although it exhibits increasingly complex characteristics from yeasts to mammals. Exo70 is one of eight protein subunits of the exocyst. Its interactions with a Rho family GTPase and the Arp2/3 actin branching complex are important for exocytosis.

The aim of this work is to gain greater insight into the structure and function of the exocyst and the role of Exo70 within it. The high-resolution structures of the C-terminal 90% of Exo70 from the yeast *Saccharomyces cerevisiae* and the mouse *Mus musculus* are presented here as determined by X-ray crystallography. These structures provide a unique opportunity to study a near-complete component of the exocyst and to compare and contrast this molecule between two distantly related model organisms. A conserved architecture composed of a series of unique helix-turn-helix motifs organized into a rod shape is revealed in these molecules despite low primary sequence conservation. A poor understanding of the role of this domain structure makes functional conclusions drawn from these structures difficult. These molecules also contain a novel fold that has recently been observed in other proteins participating in exocytosis. Several significant structural deviations between these molecules raise new questions about the

function of Exo70 and the interactions in which it is involved. These structures may provide information important to future studies of the exocyst and the GTPases that interact with Exo70 in both budding yeast and mammals.

Chapter 1

General Introduction

Introduction

The presence of membrane-bound compartments is one of the defining characteristics of eukaryotic cells (Stanier and van Niel, 1962). These compartments require a system for the exchange of materials between them, and vesicles, small mobile compartments, fulfill this role by transporting cargo from one compartment to another in a highly regulated process that occurs in four steps (Bonifacino and Glick, 2004). First, the vesicle must be formed from the membrane of the donor compartment and collect cargo in a process known as budding. Second, the vesicle must be transported to its destination. Third, the vesicle must make an initial interaction with the membrane of the target compartment by a process known as tethering. Finally, the vesicle must fuse with the target membrane, releasing its contents into that compartment. Molecular events that mediate and regulate these four steps will be briefly reviewed in the following sections. The third step, tethering, which is the focus of this dissertation, will be discussed last (Figure 1.1).

Vesicle budding

A class of proteins called coat proteins mediates vesicle budding (Bonifacino and Lippincott-Schwartz, 2003; Kirchhausen, 2000; McMahon and Mills, 2004). A number of

Figure 1.1: Vesicle budding, transport, tethering, and fusion

A schematic diagram depicting the four stages of vesicle-mediated transport.

1) In the first stage, budding, coat proteins (T), adapter proteins (•), and other factors play roles in the creation of a vesicle from the membrane of a donor compartment and the association of cargo within it.
2) In the second stage, transport, motor proteins such as dynein, kinesin, and myosin (●|●) carry vesicles (○) from the donor compartment along cytoskeletal components such as actin filaments or microtubules (==) to the target compartment.
3) In the third stage, tethering, multisubunit tethering complexes (Δ) associate vesicles (○) with the target compartment membrane in preparation for the fusion event, which requires the association of v-SNAREs (/) with t-SNAREs (≡).
4) In the fourth stage, fusion, the vesicle is incorporated into the target compartment membrane, releasing internal cargo across it. The association of v-SNAREs and t-SNAREs results in the formation of *trans*-SNARE complexes (///).

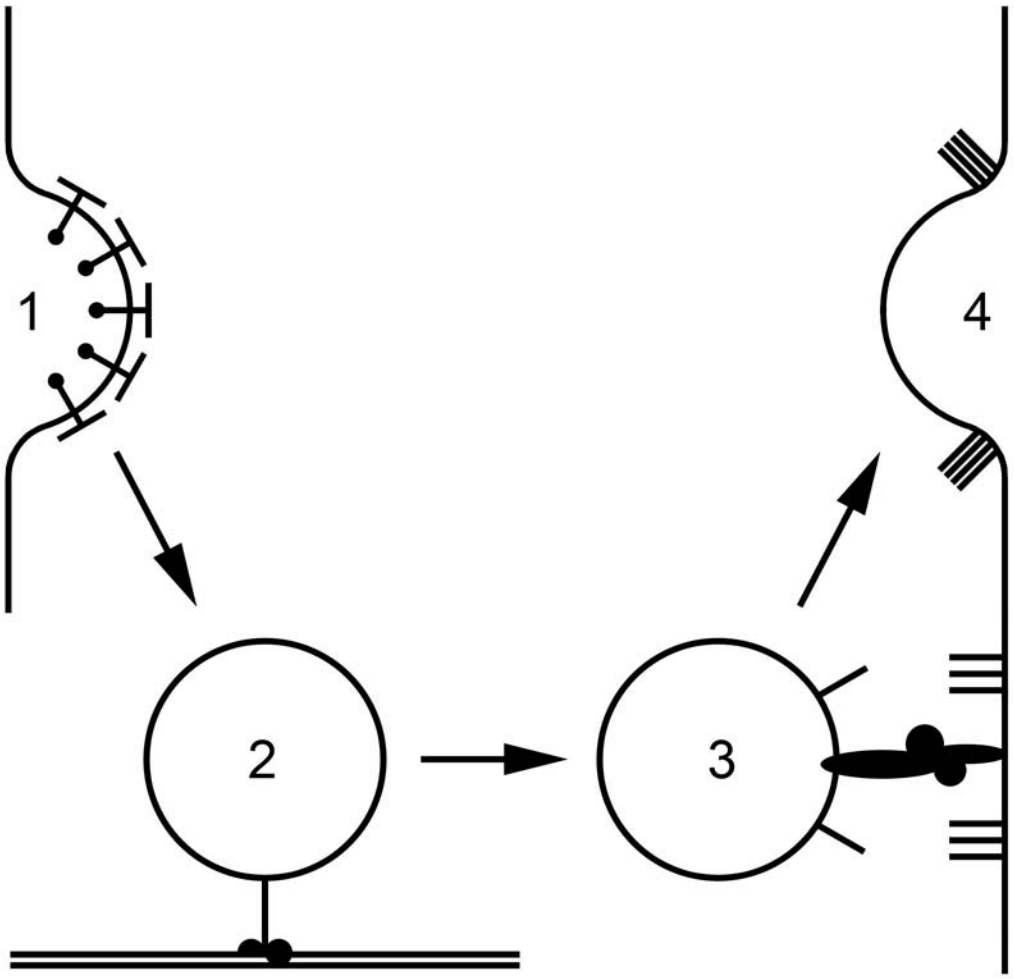
1
2
3
4

coats have been identified. The first was Clathrin, which is primarily associated with the *trans*-Golgi network and the PM (Owen *et al.*, 2004; Pearse, 1975).Other well-studied coats include COP I and II, which are involved with vesicles moving between the ER and the Golgi and within the Golgi cisternae (Barlowe *et al.*, 1994; Letourneur *et al.*, 1994; Waters *et al.*, 1991). Less well understood coats include exomer (Wang *et al.*, 2006), FAPP (Godi *et al.*, 2004), and retromer (Seaman *et al.*, 1998) coats. Coats are dynamic structures that are recruited by Arf1/Sar1 family GTPases to sites of vesicle formation (Springer *et al.*, 1999). Assembly of the coat subunits deforms the membrane into a spherical shape with a diameter consistent with the structure of the coat (Bi *et al.*, 2002; Crowther and Pearse, 1981; Weidler *et al.*, 2000). Adapter proteins such as AP1 and AP2 help the coat recruit cargo into the vesicle (Lewin and Mellman, 1998) before the vesicle is "pinched off" from the donor membrane by dynamin (Damke *et al.*, 1994).

Vesicle transport

Once a vesicle is created and separated from the donor membrane it must be transported to a site of fusion on the target membrane. Rab GTPases have been implicated in the recruitment of molecular motors, including several different dyneins, kinesins, and myosins. These motors can then transport the vesicles along microtubule or actin filaments towards target membranes (Hammer and Wu, 2002). The details of the process that targets these vesicles to the correct location are not well understood.

Membrane fusion

The final step in the transportation of cargo by vesicles is the fusion of these vesicles with the target membrane, in which the vesicle membrane is incorporated into the target membrane and the contents of the vesicle are released. The formation of a SNARE complex, which involves several proteins containing a total of four different but conserved SNARE motifs (Qa, Qb, Qc, and R) (Bock *et al.*, 2001; Fasshauer *et al.*, 1998) organized into a four-helix bundle structure (Sutton *et al.*, 1998), is sufficient for membrane fusion (Weber *et al.*, 1998). These SNARE motifs are found on several different types of proteins, including vesicle membrane-associated v-SNAREs, target membrane-associated t-SNAREs, and SNAPs. The most widely accepted model for how these complexes assemble is the zipper model, in which SNAREs catalyze membrane fusion through the release of energy derived from the creation of a favorable four-helix bundle structure (Hanson *et al.*, 1997; Lin and Scheller, 1997). NSF is a AAA+ ATPase (Hoyle *et al.*, 1996) that hydrolyzes ATP to disassemble the SNARE complex in a process requiring SNAPs, allowing for the recycling of SNARE motif proteins (Jahn and Scheller, 2006).

There are many different v-SNAREs and t-SNARES and several SNAPs (Hong, 2005). Only complimentary sets of SNAREs will interact, resulting in specific membrane fusion (McNew *et al.*, 2000; Nichols *et al.*, 1997; Parlati *et al.*, 2000). While this variety initially led to the hypothesis that SNAREs could be responsible for the specificity of vesicle fusion (Söllner *et al.*, 1993), it was eventually discarded as further evidence was acquired. The process of recycling SNAREs meant that they could be found on pathways both to and from the target for which they hold specificity (Cai *et al.*, 2007a). The interactions between various SNAREs have been shown to be promiscuous

(Fasshauer *et al.*, 1999; Tsui and Banfield, 2000; von Mollard *et al.*, 1997; Yang *et al.*, 1999), usually capable of weakly binding a number of SNARE partners. In addition, some SNAREs can be found throughout a particular system, such as in ER-Golgi transport (Cao and Barlowe, 2000; Hay *et al.*, 1998) or endosome trafficking (Antonin *et al.*, 2000). Also, SNAREs are found evenly throughout the PM despite the fact that vesicles fuse only at discrete membrane locations in *Saccharomyces cerevisiae* (Brennwald *et al.*, 1994). Furthermore, disruption of SNARE complexes did not prevent association of vesicles with the target membrane (Broadie *et al.*, 1995; Hunt *et al.*, 1994). The realization that SNAREs could not be responsible for the specificity of vesicle fusion events led to the search for components involved in this initial tethering of vesicles to the target membrane.

Vesicle tethering

Initially, a number of components in different systems were identified that played a role in the formation of physical links between a vesicle and its target membrane (Guo *et al.*, 2000; Lowe, 2000; Waters and Hughson, 2000). To date, a total of eight multisubunit tethering complexes have been identified. These are the CORVET complex (Peplowska *et al.*, 2007), the COG complex (Whyte and Munro, 2001), the Dsl1p complex (Andag *et al.*, 2001; Reilly *et al.*, 2001), the exocyst (TerBush *et al.*, 1996), the GARP/VFT complex (Conibear *et al.*, 2003), the HOPS/Class C VPS complex (Peterson and Emr, 2001), and the TRAPP I and II complexes (Cai *et al.*, 2005). Weak primary sequence and secondary structure similarity were detected among components of the COG complex, exocyst, and GARP complex (Whyte and Munro, 2001), although the

quaternary structure of the COG complex (Ungar *et al.*, 2002) more closely resembles that of the TRAPPI complex (Kim *et al.*, 2006) than the exocyst (Hsu *et al.*, 1998). The COG (Zolov and Lupashin, 2005) and TRAPPI (Cai *et al.*, 2007b) complexes are also believed to mediate only a single tethering event, while the exocyst is known to tether multiple different types of vesicles to sites of polarized growth (Munson and Novick, 2006).

The process of vesicle tethering is not well understood and is the focus of much current research. All of these tethering complexes interact with GTPases, and many of these interactions are required for proper function. All tethering complexes interact with Rab GTPases and some also interact with other classes of GTPases. In *S. cerevisiae*, the CORVET complex interacts with both the GTP- and GDP-bound forms of Vps21 through two different subunits (Peplowska *et al.*, 2007), an interaction that is probably conserved in mammals (Rink *et al.*, 2005); the *S. cerevisiae* COG complex is an effector for Ypt1 (Suvorova *et al.*, 2002); the exocyst is an effector of Sec4 in *S. cerevisiae* (Guo *et al.*, 1999b) and Rab11 in mammals (Zhang *et al.*, 2004); the *S. cerevisiae* GARP complex is an effector for Ypt6 (Siniossoglou and Pelham, 2001); the *S. cerevisiae* HOPS complex is both an effector and a guanine nucleotide exchange factor for Ypt7 (Haas *et al.*, 1995; Mayer and Wickner, 1997; Price *et al.*, 2000; Seals *et al.*, 2000; Wichmann *et al.*, 1992; Wurmser *et al.*, 2000), and the TRAPP complexes are the only tethering complexes that are not known to be Rab effectors. TRAPPI acts as an exchange factor for Ypt1 in *S. cerevisiae* (Sacher *et al.*, 2001), and it is unclear whether TRAPPII is an exchange factor for Ypt1 or Ypt31/Ypt32 (Sacher *et al.*, 2001; Wang *et al.*, 2000; Wang and Ferro-Novick, 2002). Other GTPases known to interact with some of these tethering complexes

include Cdc42 (Zhang *et al.*, 2001), Rho1 (Guo *et al.*, 2001), and Rho3 (Robinson *et al.*, 1999) which interact with the *S. cerevisiae* exocyst and Arf6 (Prigent *et al.*, 2003), RalA/B (Jin *et al.*, 2005; Moskalenko *et al.*, 2002; Moskalenko *et al.*, 2003; Sugihara *et al.*, 2002), and TC10 (Inoue *et al.*, 2003) which interact with the mammalian exocyst.

It has long been thought that coats were removed from vesicles soon after budding as the function of creating the vesicle and recruiting cargo was completed (Bonifacino and Glick, 2004). Recent work, however, has shown that tethering complexes can interact with vesicle coat proteins. COG interacts with COPI in both *S. cerevisiae* and mammals (Suvorova *et al.*, 2002; Zolov and Lupashin, 2005), Dsl1 interacts with two different subcomplexes of COPI (Andag *et al.*, 2001; Andag and Schmitt, 2003; Reilly *et al.*, 2001), TRAPPI and TRAPPII interact with COPI in both *S. cerevisiae* and mammals, and TRAPPI interacts with COPII (Cai *et al.*, 2005; Cai *et al.*, 2007b; Sacher *et al.*, 2001; Yu *et al.*, 2006). This suggests that tethering complexes interact with vesicles before they reach the target membrane, that coat proteins remain on the vesicle until reaching the target membrane, or that both of these could occur. This interaction could possibly explain how the unidirectional motion of vesicles to target membranes is maintained and possibly links vesicle tethering and uncoating, which is required to expose SNAREs on the surface of the vesicle (Cai *et al.*, 2007a). An interaction between the exocyst and coats has not yet been detected.

Tethering complexes also interact with SNAREs directly. It is not clear exactly what role this plays in membrane fusion, but it has been postulated that tethering complexes may simply bring vesicles close to the target membrane to facilitate SNARE-mediated membrane fusion (Malsam *et al.*, 2005) or that tethering complexes may

somehow actively stimulate the formation of *trans*-SNARE complexes (Shorter *et al.*, 2002). Tethering complexes also interact with SNAREs. The *S. cerevisiae* Vps51 subunit of the GARP complex binds the SNARE Tig1 (Conibear *et al.*, 2003; Siniossoglou and Pelham, 2001), and this interaction has been implicated in tethering function (Conibear and Stevens, 2000; Conibear *et al.*, 2003), although it is not essential (Fridmann-Sirkis *et al.*, 2006). The exocyst and HOPS complex may also stimulate SNARE-mediated membrane fusion through an interaction with proteins of the Sec1/Munc18 family (Jahn and Sudhof, 1999; Waters and Hughson, 2000). Sec1 (Carr *et al.*, 1999) and Munc18 (Dulubova *et al.*, 2007; Shen *et al.*, 2007) bind *trans*-SNARE complexes and promote membrane fusion. *S. cerevisiae* Sec1 has been associated with the coupling of exocyst-mediated vesicle tethering and SNARE-mediated membrane fusion (Wiederkehr *et al.*, 2004). The Vps33 subunit of the *S. cerevisiae* HOPS complex is a homolog of Sec1 and interacts with the t-SNARE Vam3, although the significance of this interaction is disputed (Laage and Ungermann, 2001; Seals *et al.*, 2000; Wang *et al.*, 2001). The *S. cerevisiae* HOPS complex also interacts with Vam7, an interaction that may participate in SNARE complex formation (Stroupe *et al.*, 2006). The *S. cerevisiae* exocyst subunit Sec6 also interacts directly with the t-SNARE Sec9 and inhibits its interaction with its partner t-SNARE, Sso1, suggesting a role in regulation of this SNARE complex (Sivaram *et al.*, 2005).

In conclusion, tethering complexes are factors whose rather complicated functions are probably regulated by Rab GTPases and several other classes of GTPases. These functions may include vesicle coat recognition and/or disassembly, tethering of vesicles to target membranes, and SNARE complex regulation, promotion or formation.

Functions of the exocyst

The exocyst is one of the best-studied tethering complexes. It is associated with specific types of exocytosis, defined as the fusion of vesicles with the PM (de Duve, 1963). At a minimum, all eukaryotic cells perform exocytosis during growth as a means for adding membrane components to the PM. Most cells also secrete various cellular products by exocytic processes. In *S. cerevisiae* the exocyst is necessary for secretion of at least invertase and acid phosphatase (Novick *et al.*, 1980), the delivery of membrane components to the bud tip during daughter cell growth, and can also be found at the mother-daughter neck during cytokinesis (Adamo *et al.*, 2001; Finger *et al.*, 1998; Guo *et al.*, 2001; Robinson *et al.*, 1999; Zajac *et al.*, 2005; Zhang *et al.*, 2005b). The functions of the exocyst in mammals are more complex than in *S. cerevisiae*. In mammals the exocyst is required for transport to the lateral, but not apical, membranes in epithelial cells (Grindstaff *et al.*, 1998); neurite branching (Lalli and Hall, 2005) and synaptogenesis, but not synaptic vesicle release, in neurons (Mehta *et al.*, 2005; Murthy *et al.*, 2003); and membrane and membrane protein delivery to the PM in recycling processes (Jafar-Nejad *et al.*, 2005; Prigent *et al.*, 2003; Sommer *et al.*, 2005). As an extension of these processes, the exocyst has also been found to be associated with membrane expansion during cytokinesis (Finger *et al.*, 1998; Gromley *et al.*, 2005; Wang *et al.*, 2002) and cell surface receptor recycling relevant to cell fate determination (Jafar-Nejad *et al.*, 2005). Recently an interaction between the ER translocation complex and the exocyst was identified (Lipschutz *et al.*, 2003; Toikkanen *et al.*, 2003), which is consistent with earlier observations that at least Sec10 localizes to the ER and is involved in an increase in synthesis and delivery of certain proteins (Lipschutz *et al.*, 2000; Lipschutz *et al.*, 2003).

In conclusion, the exocyst regulates membrane and protein addition to the PM by controlling the fusion of exocytic vesicles with the PM. The list of additional functions carried out by the exocyst continues to grow, and more have been identified in higher eukaryotes than in lower eukaryotes.

Composition and structure of the exocyst

The identification of the exocyst stems from work that initially identified 23 *S. cerevisiae* proteins involved in secretion of invertase and acid phosphatase that were sequentially named Sec1-Sec23 (Novick *et al.*, 1980). Initial study of the Sec15 protein revealed that it was present in a 19.5*S* membrane associated particle (Bowser and Novick, 1991). Sec8 was also identified to associate with Sec15 in this particle (Bowser *et al.*, 1992). Further work found that the particle contains eight proteins and identified Sec6 as one of them (TerBush and Novick, 1995). The complex was subsequently purified and named the exocyst, and the identities of four additional subunits, Sec3, Sec5, Sec10, and the novel Exo70 were identified. The eighth component was identified as a fragment of Sec3, and all subunits were determined to be present as single copies (TerBush *et al.*, 1996). Meanwhile, it was realized that many components of neuronal secretion systems shared homology with the *S. cerevisiae* secretion system, so homologs of exocyst subunits were sought and a 17*S* complex containing Sec6 and Sec8 was identified in mammals (Ting *et al.*, 1995). This complex also contained eight proteins (Hsu *et al.*, 1996), and in addition to Sec6 and Sec8, homologs of Sec5, Sec10, Sec15, and Exo70 were also identified (Kee *et al.*, 1997). Later, the 106kDa subunit was identified as a homolog of Sec3 (Brymora *et al.*, 2001; Matern *et al.*, 2001) and the 84kDa subunit was

found to be a novel subunit and was named Exo84 (Kee *et al.*, 1997). The *S. cerevisiae* homolog of Exo84 was subsequently confirmed as a component of the exocyst (Guo *et al.*, 1999a). Comparison of the *S. cerevisiae* and mammalian exocysts reveals low primary sequence conservation on the order of 10-20% identity and 30-50% similarity. Thus, the exocyst in *S. cerevisiae* and mammals is composed of eight protein subunits, Sec3, Sec5, Sec6, Sec8, Sec10, Sec15, Exo70, and Exo84.

The internal interactions between subunits of the exocyst have been probed using coimmunoprecipitation *in vitro* and *in vivo*, pull-down, and yeast two-hybrid techniques. Only three internal interactions in *S. cerevisiae* (Sec3-Sec5, Sec6-Sec8, and Sec10-Sec15) and two in mammals (Sec6-Sec8 and Sec8-Sec10) have been detected using two of these techniques, and none have been detected by all three techniques (Munson and Novick, 2006), which could suggest that different interactions are only detectable by certain methods or that some reaction conditions may promote or hinder the formation of certain interactions. Alternatively, some interactions may require the presence of additional subunits. The known interactions and how they were detected within the *S. cerevisiae* and mammalian complexes can be found in Table 1.1 and a diagram depicting both subunit and GTPase interactions can be found in Figure 1.2.

The exocyst has been imaged by quick-freeze/deep-etch electron microscopy, revealing two forms (Hsu *et al.*, 1998). When unfixed on a mica surface, the exocyst appears to be composed of four to six arms with approximate dimensions 4-6×10-30nm radiating from a central point. When fixed to the substrate with glutaraldehyde it appears as a thick stalk of dimensions 13×30nm with two smaller branches radiating from one end. It has been proposed that the unfixed state may result from disassembly on the mica

Table 1.1: Exocyst subunit-subunit interactions and detection methods

	Sc interaction	*Sc* detection	Mammal interaction	Mammal detection
Sec3	Sec5[a]	IP[i], Y2H[j]	Sec5[f]	Y2H
			Sec8[f]	Y2H
Sec5	Sec3[a]	IP, Y2H	Sec3[f]	Y2H
	Sec6[a]	IP	Sec6[f]	Y2H
	Sec10[a]	Y2H		
	Exo70[a]	Y2H		
	Exo84[b]	IP	Exo84[g]	Y2H
Sec6	Sec5[a]	IP	Sec5[f]	Y2H
	Sec6[c]	PD[k]		
	Sec8[a,d]	IP, PD	Sec8[f,h]	Y2H, PD
	Sec10[d]	PD	Sec10[h]	PD
	Exo70[e]	PD	Exo70[f]	Y2H
Sec8			Sec3[f]	Y2H
	Sec6[a,d]	IP, PD	Sec6[f,h]	Y2H, PD
			Sec10[f,h]	Y2H, PD
	Exo70[e]	PD	Exo70[h]	PD
Sec10	Sec5[a]	Y2H		
	Sec6[d]	PD	Sec6[h]	PD
			Sec8[f,h]	Y2H, PD
	Sec15[a]	IP, Y2H	Sec15[f]	Y2H
	Exo70[e]	PD	Exo70[h]	PD
	Exo84[b]	Y2H		
Sec15	Sec10[a]	IP, Y2H	Sec10[f]	Y2H
			Exo70[f]	Y2H
			Exo84[f]	Y2H
Exo70	Sec5[a]	IP		
	Sec6[e]	PD	Sec6[f]	Y2H
	Sec8[e]	PD	Sec8[h]	PD
	Sec10[e]	PD	Sec10[h]	PD
			Sec15[f]	Y2H
			Exo84[f]	Y2H
Exo84	Sec5[b]	Y2H	Sec5[g]	Y2H
	Sec10[b]	Y2H		
			Sec15[f]	Y2H
			Exo70[f]	Y2H

[a] (Guo, *et al*. 1999b)
[b] (Guo, *et al*. 1999a)
[c] (Sivaram, *et al*. 2005)
[d] (Sivaram, *et al*. 2006)
[e] (Dong, *et al*. 2005)
[f] (Matern, *et al*. 2001)
[g] (Moskalenko, *et al*. 2003)
[h] (Vega and Hsu, 2001)
[i] Detected by coimmunoprecipitation (*in vivo* or *in vitro*)
[j] Detected by yeast two-hybrid
[k] Detected by pull-down of recombinant proteins

Figure 1.2: Exocyst subunit and GTPase interactions

A diagram depicting the known subunit-subunit and subunit-GTPase interactions within the *S. cerevisiae* exocyst (A) and the mammalian exocyst (B). The exocyst subunit Exo70 is labeled and shown as a fat dark gray pill. Other exocyst subunits are labeled and shown as fat light gray pills. GTPases are labeled and shown as thin gray pills. The vesicle membrane and plasma membrane are labeled and are each represented by a pair of horizontal lines. Interactions are shown as lines; the interaction between Sec5 and Exo84 is broken by a diagonal line. GTPases thought to be important for membrane association of the exocyst are each connected to the appropriate membrane by a pair of zig-zag lines.

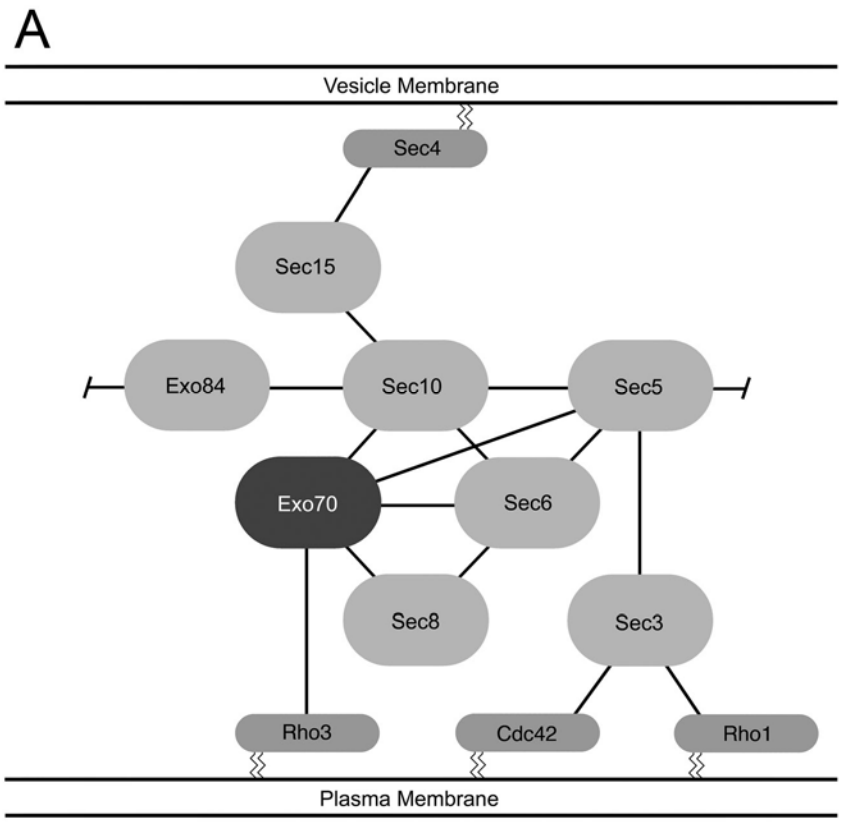
A
Vesicle Membrane
Sec4
Sec15
Exo84
Sec10
Sec5
Exo70
Sec6
Sec8
Sec3
Rho3
Cdc42
Rho1
Plasma Membrane

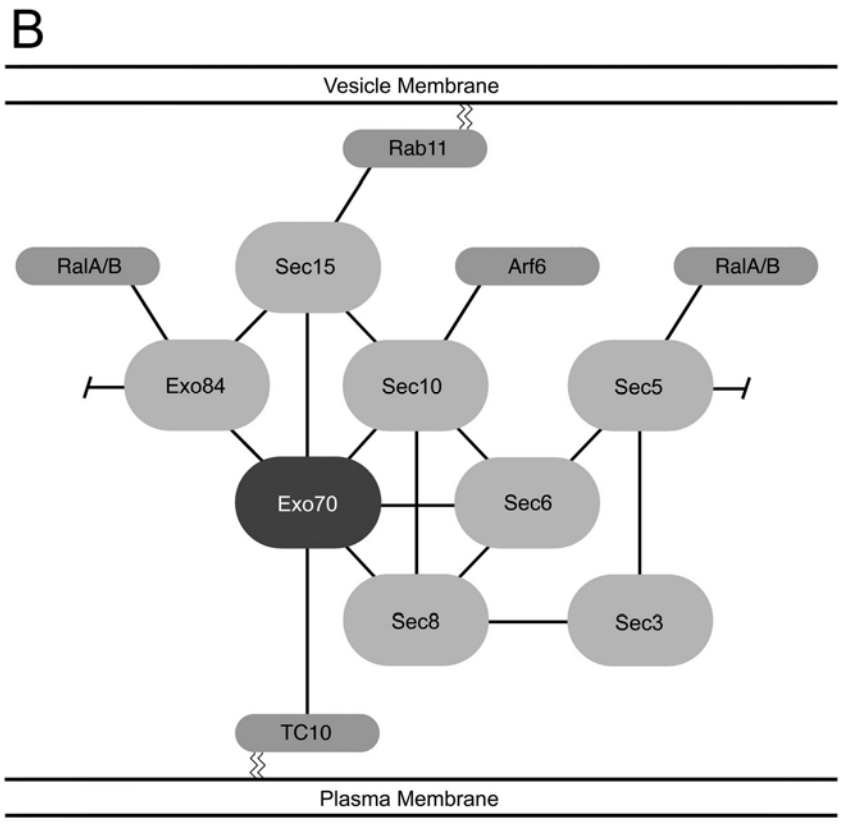
B
Vesicle Membrane
Rab11
RalA/B
Sec15
Arf6
RalA/B
Exo84
Sec10
Sec5
Exo70
Sec6
Sec8
Sec3
TC10
Plasma Membrane

substrate and could represent a partially assembled state of the exocyst, while the fixed state may more closely represent the functional state (Munson and Novick, 2006).

A speculative extended, Y-shaped architecture for the exocyst has been proposed based on several observations. First, the fixed form of the complex as observed by electron microscopy takes this shape. Second, the subunit interaction data supports the close association of most subunits with one another. Third, the structures of *Sc*Exo70, *Sc*Exo84, *Dm*Sec15, and *Sc*Sec6 each contain a series of extended α-helical bundles, leading to the prediction that other subunits may contain similar structures and have similar rod-shaped architectures (Munson and Novick, 2006). Furthermore, each domain of Exo70 interacts with exocyst subunits and some subunits interact with multiple domains of Exo70, suggesting that these subunits may pack against each other in a side-to-side fashion to form the main trunk of the complex (Dong *et al.*, 2005).

Sec3, Cdc42, and Rho1

In *S. cerevisiae*, Sec3 arrives at the PM in a vesicle- and actin-independent manner while all other components arrive in a manner similar to the vesicle-associated Sec4 (Boyd *et al.*, 2004). Sec3 is also thought to serve as a spatial marker for the localization of the exocyst (Finger *et al.*, 1998), although this finding has been disputed (Zhang *et al.*, 2005b). Sec3 is the only exocyst subunit that is not required for growth (Wiederkehr *et al.*, 2003). It also interacts with Cdc42 (Zhang *et al.*, 2001) and Rho1 (Guo *et al.*, 2001), two GTPases believed to be important in localization of the exocyst to sites of exocytosis.

Cdc42 is a member of the Rho family of small GTP-binding proteins (Johnson and Pringle, 1990) that regulate polarization, morphogenesis, membrane traffic, cell growth, and development (Cabib *et al.*, 1998; Chant, 1999; Erickson and Cerione, 2001; Johnson, 1999). In *S. cerevisiae* Cdc42 plays an important role in the initial bud site assembly and is required for polarized growth (Johnson and Pringle, 1990). It also participates in actin assembly as it is involved in type I phagocytosis (Caron and Hall, 1998) and the formation of filopodia (Nobes and Hall, 1995) through interaction with WASP, an activator of the actin branching complex Arp2/3 (Aspenström *et al.*, 1996; Symons *et al.*, 1996). Cdc42 has also been deemed necessary for the polarized localization of ASH1 mRNA to the bud (Aronov and Gerst, 2004). Cdc42 is localized to sites of budding as an mRNA (Aronov *et al*., 2007) and its localization is maintiained by landmark proteins (Chant, 1999; Schenkman *et al*., 2002). Its interaction with Sec3 controls the localization of Sec3, which is necessary for polarized secretion (Zhang *et al.*, 2001).

Rho1 is a another member of the Rho family of small GTP-binding proteins (Madaule *et al.*, 1987). It is the *S. cerevisiae* homolog of mammalian RhoA (Qadota *et al.*, 1994) and is considered to be the master regulator of cell wall integrity as it is involved in cell wall biogenesis, actin organization, and polarized secretion (Levin, 2005). It interacts with at least four different GAPs, each of which is associated with a different function of Rho1 (Levin, 2005). Its interaction with Sec3 is required for the proper localization of Sec3 and it may compete or cooperate with Cdc42 in this role (Guo *et al.*, 2001; Zhang *et al.*, 2001). Rdi1, a GDI of both Rho1 and Cdc42 (Koch *et al.*, 1997; Masuda *et al.*, 1994), is associated with the delocalization of these GTPases from the PM

(Richman *et al.*, 2004), and mammalian RhoGDIs are known to stimulate the release of Rho family GTPases from membranes (Hori *et al.*, 1991; Nomanbhoy and Cerione, 1996; Wu *et al.*, 1997). This is consistent with a model that calls for the GTPase-controlled release of the exocyst before vesicle fusion with the target membrane in mammals.

Mammalian Sec3 does not seem to serve as a spatial marker for exocyst localization as it does in *S. cerevisiae*. It does interact with GLYT1, a glycine transporter that regulates NMDA receptor function, probably to promote its insertion into membranes (Cubelos *et al.*, 2005). Sec3 is the largest subunit of the exocyst and appears to have two forms, or it may be particularly susceptible to proteolysis (TerBush *et al.*, 1996). It may be a peripheral component of the exocyst as it has the fewest known interactions among all subunits (Table 1.1).

Sec5 and RalA

In *S. cerevisiae* Sec5 was initially thought to be the central component of the exocyst due to the large number of intracomplex interactions that it was found to participate in (Guo *et al.*, 1999b), but several other subunits have since been found to have at least as many interactions in both *S. cerevisiae* and mammals, weakening this hypothesis (Table 1.1).

Mammalian Sec5 has fewer known intracomplex interactions (Munson and Novick, 2006) than *S. cerevisiae* Sec5. It competes with Exo84 for interaction with the RalA GTPase, an interaction that is important to the function of the exocyst (Fukai *et al.*, 2003; Jin *et al.*, 2005). An X-ray crystal structure of the N-terminal 99 residues of Sec5 in complex with RalA reveals that this portion of Sec5 folds into an immunoglobulin-like

β-sandwich (Fukai *et al.*, 2003). Furthermore, Sec5 interaction with RalB has been implicated in cellular migration (Rossé *et al.*, 2006).

RalA and RalB are members of the Ral family of small GTP-binding proteins (Chardin and Tavitian, 1986; Chardin and Tavitian, 1989), which regulate membrane transport, apoptosis, migration, proliferation, oncogenesis (van Dam and Robinson, 2006), neurite branching (Lalli and Hall, 2005), and cytokinesis (Chen *et al.*, 2006). Ral family GTPases also regulate secretion, filopodial function, and cell polarity through an interaction with the exocyst (Brymora *et al.*, 2001). Interaction with these Ral GTPases is required for exocytosis (Wang *et al.*, 2004a), as the assembly or stability of the exocyst depends on it (Moskalenko *et al.*, 2002).

Sec6 and Sec9

In *S. cerevisiae* Sec6 is the only component found to form a homodimer *in vitro* (Sivaram *et al.*, 2005). It also interacts with Sec9, a t-SNARE with homology to SNAP25 (Brennwald *et al.*, 1994), providing a direct link between the vesicle tethering and vesicle fusion machinery (Sivaram *et al.*, 2005). To date, neither of these functions has been identified for Sec6 in mammals. Although Sec6 was one of the first proteins identified as a subunit of the exocyst, its specific role is not yet clear. The structure of a C-terminal portion of *S. cerevisiae* Sec6 has been determined by X-ray crystallography, revealing a fold similar to other components of the exocyst (Sivaram *et al.*, 2006).

Sec8, PSD-95, and SAP97

In *S. cerevisiae* the function of Sec8 is not well understood. Mammalian Sec8 contains a PDZ binding motif (Sans *et al.*, 2003) that is involved in an interaction with PSD-95 in neurons (Riefler *et al.*, 2003) and SAP97 in adipocytes (Inoue *et al.*, 2006), both of which are associated with the delivery of proteins to specific locations. Rheumatoid arthritis has been linked to intronic single nucleotide polymorphisms in the SEC8L1 allele in a Japanese population (Hamada *et al.*, 2005), although intronic variability probably does not necessarily link Sec8 itself to disease. This is the only known link between subunits of the exocyst and a disease, although there are many links among various GTPases and cancer, including those that interact with the exocyst (Oxford and Theodorescu, 2003).

Sec10 and Arf6

In *S. cerevisiae* Sec10 is thought to be part of a soluble subcomplex of the exocyst that also includes Sec15 and requires Sec5 for association with the rest of the exocyst (Guo *et al.*, 1999b). Although this specific subcomplex has not been observed in mammals, Sec10 does interact with the Arf6 GTPase to facilitate cell motility (Prigent *et al.*, 2003).

Arf6 is a member of the ADP-ribosylation factor family of small GTP-binding proteins (Graves *et al.*, 1992), which regulate membrane trafficking through an association with vesicle coats (Donaldson *et al.*, 2005; Moss and Vaughan, 1998; Randazzo *et al.*, 2000). It localizes to the PM and endosomal membranes and it plays roles in endosome recycling, membrane remodelling, actin remodelling, and cytokinesis (D'Souza-Schorey and Chavrier, 2006). Its interaction with Sec10 in the mammalian

exocyst plays a role in the recycling of endosomal membrane to the PM at sites of dynamic reorganization (Prigent *et al.*, 2003).

Sec15, Bem1, Sec2, Sec4, and Rab11

In *S. cerevisiae* Sec15 is thought to be part of a soluble subcomplex of the exocyst that also includes Sec10 and requires Sec5 for association with the rest of the exocyst (Guo *et al.*, 1999b). It interacts with Bem1 (Drees *et al.*, 2001; Zajac *et al.*, 2005), which is thought to act as a scaffold for Cdc42 function (Moskow *et al.*, 2000). Bem1 interacts with Cdc42 and its GEF, Cdc24 (Butty *et al.*, 1998; Gulli *et al.*, 2000; Yoshinaga *et al.*, 2003), and Cdc42 also interacts with Sec3 (Zhang *et al.*, 2001). This provides a link that could possibly play a role in the assembly of the exocyst. In addition, Sec15 is an effector of the Sec4 GTPase, directly linking vesicles to the exocyst (Guo *et al.*, 1999b). Furthermore, a GEF for Sec4, Sec2, is recruited to vesicles by the Rab family GTPase Ypt32 (Ortiz *et al.*, 2002) which also interacts with Sec15 (Medkova *et al.*, 2006) and activates Sec4 (Walch-Solimena *et al.*, 1997).

Sec4 is a member of the Rab family of small GTP-binding proteins (Salminen and Novick, 1987; Zahraoui *et al.*, 1989), which regulate intracellular transportation (Seabra *et al.*, 2002; Zerial and McBride, 2001). Sec4 is localized to exocytic vesicle membranes (Goud *et al.*, 1988; Walch-Solimena *et al.*, 1997) and plays a role in membrane transport, vesicle transport (Kabcenell *et al.*, 1990; Walworth *et al.*, 1989), and ASH1 mRNA localization to the bud (Aronov and Gerst, 2004). Sro7 interacts with Sec4 (Grosshans *et al.*, 2006), and Exo84 (Zhang *et al.*, 2005b). The interaction between Sec4 and Sro7 has been implicated in cell polarity (Kagami *et al.*, 1998). Sro7 also interacts with the t-

SNARE Sec9 (Lehman *et al.*, 1999), providing a possible link between exocytic vesicles and the PM. The interaction of Sec4 with Sec15 plays an important role in vesicle targeting (Guo *et al.*, 1999b).

In mammals Sec15 is also known to interact with the Rab11 GTPase, which links vesicles directly to the exocyst (Zhang *et al.*, 2004). The structure of a C-terminal portion of *Drosophila melanogaster* Sec15 has been determined by X-ray crystallography, revealing the Rab11 binding site as well as a fold similar to other components of the exocyst with available structures (Munson and Novick, 2006), except for some deviation in α-helical positioning at the N terminus (Wu *et al.*, 2005).

Rab11 is a member of the Rab family of small GTP-binding proteins (Chavrier *et al.*, 1990) that is found on the surface of recycling compartments (Green *et al.*, 1997). It interacts with FIP2, FIP3 and FIP4 (Hales *et al.*, 2002; Hickson *et al.*, 2003), and FIP2 interacts with myosin Vb, linking this GTPase to motor proteins and transport (Hales *et al.*, 2002). Rab11 also plays a role in cell migration (Mammoto *et al.*, 1999), and the Rab family is strongly associated with invasive migration of cancers by promoting integrin transport (Caswell and Norman, 2006; Jones *et al.*, 2006). The interaction between Rab11 and Sec15 links recycling compartments to the PM through the exocyst (Zhang *et al.*, 2004). Sec4, which interacts with Sec15 in *S. cerevisiae*, is also a Rab family GTPase (Guo *et al.*, 1999b; Salminen and Novick, 1987; Zahraoui *et al.*, 1989), suggesting at least a familial relationship between the functions of these two interactions.

Exo70, Arpc1, Rho3, and TC10

In *S. cerevisiae*, Exo70 can arrive at the PM in two different manners: via an actin-independent manner similar to Sec3, and in a manner similar to the vesicle-associated Sec4 and the rest of the exocyst subunits (Boyd *et al.*, 2004). Exo70 interacts with Arpc1 through a conserved basic patch at its C-terminus (Zuo *et al.*, 2006) and promotes actin filament formation into filopodia-like structures (Wang *et al.*, 2004b; Xu *et al.*, 2005). Arpc1 is a required component of the Arp2/3 actin branching complex (Harries *et al.*, 2005; Machesky *et al.*, 1994) and has a WD40 β-propeller-like fold with a strong basic patch exposed on its surface (Nolen *et al.*, 2004; Robinson *et al.*, 2001). The interaction between Exo70 and Arpc1 links vesicle tethering to the process of local actin remodeling that is necessary for the delivery of vesicles to the PM (Eitzen, 2003). Exo70 also plays a specific role in the fusion of Bgl2-containing vesicles (He *et al.*, 2007). There are two known classes of exocytic vesicles that transport two separate sets of cargo: one that carries PM proteins and cell wall modification enzymes such as Bgl2p and the other that carries proteins such as the periplasmic enzyme invertase (Harsay and Bretscher, 1995). This function of Exo70 likely explains why the protein was not detected among the 23 original sec proteins, as the discovery of these was dependent on an assay detecting the release of invertase (Novick *et al.*, 1980). In addition, Exo70 interacts with the Rho3 GTPase, which plays several important roles in cell growth (Levin, 2005). The structure of a truncated form of Exo70 missing approximately 10% of its N-terminal sequence has been determined by X-ray crystallography in two different crystal forms (Dong *et al.*, 2005; Hamburger *et al.*, 2006), and the structure of a second construct missing both the N-terminal 10% and the C-terminal domain was also determined (Hamburger *et al.*, 2006). These structures reveal a fold with an N-terminal domain that

is similar to other components of the exocyst with available structures (Munson and Novick, 2006).

Rho3 is a member of the Rho family of small GTP-binding proteins (Matsui and Toh-e, 1992). It is required for several processes, including growth (Matsui and Toh-e, 1992), bud formation (Imai *et al.*, 1996), actin organization (Imai *et al.*, 1996; Matsui and Toh-e, 1992), efficient secretion of cell-wall hydrolases (Adamo *et al.*, 1999), localization of ASH1 mRNA to the bud (Aronov and Gerst, 2004), and, at least in *Schizosaccharomyces pombe*, cell separation (Wang *et al.*, 2003). Furthermore, Rho3 plays a role in regulation of actin polarity, transportation of exocytic vesicles from the mother cell to the bud through interaction with the unconventional class V myosin Myo2, and fusion of these vesicles with the target membrane through interaction with Exo70 (Adamo *et al.*, 1999; Robinson *et al.*, 1999). This interaction requires Exo70 residues 338-515 (Dong *et al.*, 2005) and has a K_D of 70μM as measured by SPR, which is weaker than expected and may be artificially weak due to the soluble recombinant Rho3 used for this measurement (Hamburger *et al.*, 2006).

In mammals Exo70 maintains its conserved interaction with Arpc1 (Zuo *et al.*, 2006) and the TC10 GTPase interacts with Exo70 in order to localize the exocyst to sites of exocytosis (Inoue *et al.*, 2003; Inoue *et al.*, 2006). Three different forms of Exo70 have been identified in mammals. Two have only been found in brain while the third, studied here, has been found in several tissues, but not brain (Carninci *et al.*, 2005; Guo *et al.*, 1997; Strausberg *et al.*, 2002). Exo70 found in brain appears to contain either one or two insertions in its primary sequence. Thus, an understanding of the shorter non-brain form could also serve as a basis for the understanding of the longer brain forms. Furthermore,

in plants, *Arabidopsis thaliana* appears to contain up to 23 copies of a gene homologous to Exo70 and only 1-3 copies of genes homologous to other exocyst components, suggesting that Exo70-like proteins may play an additional role, and possibly form a family, in plants (Elias *et al.*, 2003). These findings could suggest that Exo70 is modular, capable of accepting modifications to alter its function in plants and animals.

TC10 is a member of the Rho family of small GTP-binding proteins (Drivas *et al.*, 1990). It is primarily localized to the PM and can induce actin-based protrusions at the PM through an interaction with profilin, an actin-binding filament-forming protein, suggesting a role in regulation of the actin cytoskeleton and cell growth (Murphy *et al.*, 1999). TC10 also regulates the transport of the glucose transporter GLUT4 (Chiang *et al.*, 2001) and the CFTR (Cheng *et al.*, 2005) to the PM. The transport of GLUT4 to the PM requires the reorganization of actin and the recruitment of the exocyst, both of which are functions of TC10 (Kanzaki, 2006). TC10 recruits Exo70 through residues 1-384, which results in the localization of the rest of the exocyst subunits to lipid rafts on the PM where it is required for the surface exposure of GLUT4 (Inoue *et al.*, 2003; Inoue *et al.*, 2006). This work suggests that Exo70 plays an important role in exocyst localization, but in *S. cerevisiae* the localization of the exocyst is not a function of its interaction with Rho3 (Roumanie *et al.*, 2005).

Exo84, Sro7, and RalA

In *S. cerevisiae*, Exo84 was the last component to be identified, possibly because it is capable of dissociating from the exocyst under certain experimental conditions (Guo *et al.*, 1999a). It is required, along with Exo70, for the polarization and assembly of the

exocyst (Zhang *et al.*, 2005b). Exo84 interacts with Sro7 (Zhang *et al.*, 2005a), a member of the lgl family that in animal cells has been implicated in cell polarity (Kagami *et al.*, 1998). Sro7 also interacts with Sec4 (Grosshans *et al.*, 2006) and the t-SNARE Sec9 (Lehman *et al.*, 1999), providing a possible link between exocytic vesicles and the PM. A structure of the C-terminal domain of *S. cerevisiae* Exo84 has also been solved by X-ray crystallography (Dong *et al.*, 2005), revealing a fold that is similar to other components of the exocyst with available structures (Munson and Novick, 2006).

In mammals Exo84 competes with Sec5 for interaction with RalA, an interaction important to the function of the exocyst (Jin *et al.*, 2005). This interaction has been observed by X-ray crystallography, revealing a PH domain fold in Exo84 at the site of interaction (Jin *et al.*, 2005). PtdIns(3,4,5)P_3 may also compete with RalA for Exo84 interaction (Moskalenko *et al.*, 2003).

X-ray crystallography

X-ray crystallography is a powerful method capable of examining the three-dimensional structure of protein molecules at atomic or near-atomic resolution (Dauter, 2006). It is particularly suitable for the study of larger molecules such as viral capsids (Natarajan *et al.*, 2005), which are currently beyond the ability of NMR techniques (Xu *et al.*, 2006). Protein structures can reveal features and motifs important to the function of a protein. A combination of structural data with primary sequence alignments and conservation data can be used to predict important features of a molecule that may not be obvious from sequence alignment alone. In addition, the identification of a known motif can sometimes be used to infer new functions of a protein. A particularly useful

comparison can be made between two related structures, such as those of homologous molecules from two different organisms or two molecules of similar function from one organism.

One of the limitations of X-ray crystallography is the requirement of a large amount of highly purified protein capable of organizing into the ordered lattice of a crystal. A large amount of highly purified protein can usually be efficiently acquired by the over-expression of protein in *Escherichia coli* or other heterologous expression systems and purification using a series of chromatographic techniques. Protein capable of organizing into the ordered lattice of a crystal can be obtained by careful design of mutations and truncations to the gene encoding the protein of interest. In theory, the removal of domains, loops, and residues that interfere with crystal packing can improve both the ability of a protein to crystallize and the resolution of X-ray diffraction obtained from that crystal (Helliwell, 2005). This process is somewhat subjective, as there are no clear rules defining how to modify a protein for crystallization, although limited proteolysis is a technique that can often provide useful information (Fontana *et al.*, 2004). In addition, the process of crystallization itself is not completely understood (Kashchiev *et al.*, 2005; Vekilov, 2005), making the prediction of conditions under which a particular protein will crystallize difficult. For this task many screens have been developed that include a wide variety of chemical conditions in order to maximize the chance of identifying one or more that produce useful protein crystals (Page and Stevens, 2004). This initial screening process for crystallization conditions also contributes to the requirement of a large amount of purified protein.

Several techniques are available for the crystallization of protein, although the sitting drop method based the principle of vapor diffusion is the most common (Forsythe *et al.*, 2002). In this technique a small μL-scale drop containing protein and dilute precipitant is separated from a larger reservoir of concentrated precipitant in a closed environment. In theory, vapor diffusion occurs, transferring water from the drop to the reservoir driven by the unequal precipitant concentrations between them. This results in the slow increase in protein concentration within the drop, and at the saturation point protein begins to leave the solution. In the right chemical environment and with a proper protein construct, the protein will organize into crystals as it leaves solution. Crystallization takes place in two steps: nucleation and growth. Nucleation is the formation of small nuclei with crystalline organization. Growth is the process of increasing the size of the nucleus to a maximum, usually on the order of several hundred μm. Some chemical environments may only promote one of these two steps. In a case where nucleation is not strongly promoted, existing crystals can be ground up and distributed as nuclei into the drop to bypass this obstacle in a technique known as seeding.

Conclusions

The exocyst is composed of eight protein subunits that have received varying levels of study. The contributions of each subunit to the exocyst as a whole are being determined through the study of mutants and interactions with components outside the exocyst. These studies have revealed a number of differences between the interactions and functions of each subunit across species, particularly between the distantly related *S.*

cerevisiae and mammals. Exo70 is an important subunit of the exocyst. It mediates several interactions that are important to cellular function, including the polarization of exocytosis, the assembly of the exocyst, and the regulation of the actin cytoskeleton. The goal of the work presented here was to provide insight into the interactions of Exo70 and therefore the function of the exocyst.

The identification, purification, crystallization, and X-ray characterization of the *S. cerevisiae* and *M. musculus* Exo70 molecules are described in Chapters 2 and 3, respectively. Chapter 4 gives a detailed description and comparison of both structures. Chapter 5 further elaborates on the observations made in Chapter 4 and presents several avenues for further study of Exo70 as a result of this work.

REFERENCES

Adamo, J. E., Rossi, G., and Brennwald, P. (1999). The Rho Gtpase Rho3 Has a Direct Role in Exocytosis That Is Distinct from Its Role in Actin Polarity. *Molecular biology of the cell* **10**, 4121-4133.

Adamo, J. E., Moskow, J. J., Gladfelter, A. S., Viterbo, D., Lew, D. J., and Brennwald, P. J. (2001). Yeast Cdc42 Functions at a Late Step in Exocytosis, Specifically During Polarized Growth of the Emerging Bud. *The Journal of cell biology* **155**, 581-592.

Andag, U., Neumann, T., and Schmitt, H. D. (2001). The Coatomer-Interacting Protein Dsl1p Is Required for Golgi-to-Endoplasmic Reticulum Retrieval in Yeast. *The Journal of biological chemistry* **276**, 39150-39160.

Andag, U. and Schmitt, H. D. (2003). Dsl1p, an Essential Component of the Golgi-Endoplasmic Reticulum Retrieval System in Yeast, Uses the Same Sequence Motif to Interact with Different Subunits of the Copi Vesicle Coat. *The Journal of biological chemistry* **278**, 51722-51734.

Antonin, W., Holroyd, C., Tikkanen, R., Honing, S., and Jahn, R. (2000). The R-Snare Endobrevin/Vamp-8 Mediates Homotypic Fusion of Early Endosomes and Late Endosomes. *Molecular biology of the cell* **11**, 3289-3298.

Aronov, S. and Gerst, J. E. (2004). Involvement of the Late Secretory Pathway in Actin Regulation and Mrna Transport in Yeast. *The Journal of biological chemistry* **279**, 36962-36971.

Aronov, S., Gelin-Licht, R., Zipor, G., Haim, L., Safran, E., and Gerst, J. E. (2007). mRNAs Encoding Polarity and Exocytosis Factors Are Cotransported with the Cortical Endoplasmic Reticulum to the Incipient Bud in *Saccharomyces cerevisiae*. *Molecular and cellular biology* **27**, 3441-3455.

Aspenström, P., Lindberg, U., and Hall, A. (1996). Two Gtpases, Cdc42 and Rac, Bind Directly to a Protein Implicated in the Immunodeficiency Disorder Wiskott-Aldrich Syndrome. *Curr Biol* **6**, 70-75.

Barlowe, C., Orci, L., Yeung, T., Hosobuchi, M., Hamamoto, S., Salama, N., Rexach, M. F., Ravazzola, M., Amherdt, M., and Schekman, R. (1994). Copii: A Membrane Coat Formed by Sec Proteins That Drive Vesicle Budding from the Endoplasmic Reticulum. *Cell* **77**, 895-907.

Bi, X., Corpina, R. A., and Goldberg, J. (2002). Structure of the Sec23/24-Sar1 Pre-Budding Complex of the Copii Vesicle Coat. *Nature* **419**, 271-277.

Bock, J. B., Matern, H. T., Peden, A. A., and Scheller, R. H. (2001). A Genomic Perspective on Membrane Compartment Organization. *Nature* **409**, 839-841.

Bonifacino, J. S. and Lippincott-Schwartz, J. (2003). Coat Proteins: Shaping Membrane Transport. *Nature reviews* **4**, 409-414.

Bonifacino, J. S. and Glick, B. S. (2004). The Mechanisms of Vesicle Budding and Fusion. *Cell* **116**, 153-166.

Bowser, R. and Novick, P. (1991). Sec15 Protein, an Essential Component of the Exocytotic Apparatus, Is Associated with the Plasma Membrane and with a Soluble 19.5s Particle. *The Journal of cell biology* **112**, 1117-1131.

Bowser, R., Muller, H., Govindan, B., and Novick, P. (1992). Sec8p and Sec15p Are Components of a Plasma Membrane-Associated 19.5s Particle That May Function Downstream of Sec4p to Control Exocytosis. *The Journal of cell biology* **118**, 1041-1056.

Boyd, C., Hughes, T., Pypaert, M., and Novick, P. (2004). Vesicles Carry Most Exocyst Subunits to Exocytic Sites Marked by the Remaining Two Subunits, Sec3p and Exo70p. *The Journal of cell biology* **167**, 889-901.

Brennwald, P., Kearns, B., Champion, K., Keranen, S., Bankaitis, V., and Novick, P. (1994). Sec9 Is a Snap-25-Like Component of a Yeast Snare Complex That May Be the Effector of Sec4 Function in Exocytosis. *Cell* **79**, 245-258.

Broadie, K., Prokop, A., Bellen, H. J., O'Kane, C. J., Schulze, K. L., and Sweeney, S. T. (1995). Syntaxin and Synaptobrevin Function Downstream of Vesicle Docking in Drosophila. *Neuron* **15**, 663-673.

Brymora, A., Valova, V. A., Larsen, M. R., Roufogalis, B. D., and Robinson, P. J. (2001). The Brain Exocyst Complex Interacts with Rala in a Gtp-Dependent Manner: Identification of a Novel Mammalian Sec3 Gene and a Second Sec15 Gene. *The Journal of biological chemistry* **276**, 29792-29797.

Butty, A. C., Pryciak, P. M., Huang, L. S., Herskowitz, I., and Peter, M. (1998). The Role of Far1p in Linking the Heterotrimeric G Protein to Polarity Establishment Proteins During Yeast Mating. *Science (New York, NY* **282**, 1511-1516.

Cabib, E., Drgonova, J., and Drgon, T. (1998). Role of Small G Proteins in Yeast Cell Polarization and Wall Biosynthesis. *Annual review of biochemistry* **67**, 307-333.

Cai, H., Zhang, Y., Pypaert, M., Walker, L., and Ferro-Novick, S. (2005). Mutants in Trs120 Disrupt Traffic from the Early Endosome to the Late Golgi. *The Journal of cell biology* **171**, 823-833.

Cai, H., Reinisch, K., and Ferro-Novick, S. (2007a). Coats, Tethers, Rabs, and Snares Work Together to Mediate the Intracellular Destination of a Transport Vesicle. *Developmental cell* **12**, 671-682.

Cai, H., Yu, S., Menon, S., Cai, Y., Lazarova, D., Fu, C., Reinisch, K., Hay, J. C., and Ferro-Novick, S. (2007b). Trappi Tethers Copii Vesicles by Binding the Coat Subunit Sec23. *Nature* **445**, 941-944.

Cao, X. and Barlowe, C. (2000). Asymmetric Requirements for a Rab Gtpase and Snare Proteins in Fusion of Copii Vesicles with Acceptor Membranes. *The Journal of cell biology* **149**, 55-66.

Carninci, P. and Kasukawa, T. and Katayama, S. and Gough, J. and Frith, M. C. and Maeda, N. and Oyama, R. and Ravasi, T. and Lenhard, B. and Wells, C. and Kodzius, R. and Shimokawa, K. and Bajic, V. B. and Brenner, S. E. and Batalov, S. and Forrest, A. R. and Zavolan, M. and Davis, M. J. and Wilming, L. G. and Aidinis, V. and Allen, J. E. and Ambesi-Impiombato, A. and Apweiler, R. and Aturaliya, R. N. and Bailey, T. L. and Bansal, M. and Baxter, L. and Beisel, K. W. and Bersano, T. and Bono, H. and Chalk, A. M. and Chiu, K. P. and Choudhary, V. and Christoffels, A. and Clutterbuck, D. R. and Crowe, M. L. and Dalla, E. and Dalrymple, B. P. and de Bono, B. and Della Gatta, G. and di Bernardo, D. and Down, T. and Engstrom, P. and Fagiolini, M. and Faulkner, G. and Fletcher, C. F. and Fukushima, T. and Furuno, M. and Futaki, S. and Gariboldi, M. and Georgii-Hemming, P. and Gingeras, T. R. and Gojobori, T. and Green, R. E. and Gustincich, S. and Harbers, M. and Hayashi, Y. and Hensch, T. K. and Hirokawa, N. and Hill, D. and Huminiecki, L. and Iacono, M. and Ikeo, K. and Iwama, A. and Ishikawa, T. and Jakt, M. and Kanapin, A. and Katoh, M. and Kawasawa, Y. and Kelso, J. and Kitamura, H. and Kitano, H. and Kollias, G. and Krishnan, S. P. and Kruger, A. and Kummerfeld, S. K. and Kurochkin, I. V. and Lareau, L. F. and Lazarevic, D. and Lipovich, L. and Liu, J. and Liuni, S. and McWilliam, S. and Madan Babu, M. and Madera, M. and Marchionni, L. and Matsuda, H. and Matsuzawa, S. and Miki, H. and Mignone, F. and Miyake, S. and Morris, K. and Mottagui-Tabar, S. and Mulder, N. and Nakano, N. and Nakauchi, H. and Ng, P. and Nilsson, R. and Nishiguchi, S. and Nishikawa, S., *et al.* (2005). The Transcriptional Landscape of the Mammalian Genome. *Science (New York, NY* **309**, 1559-1563.

Caron, E. and Hall, A. (1998). Identification of Two Distinct Mechanisms of Phagocytosis Controlled by Different Rho Gtpases. *Science (New York, NY* **282**, 1717-1721.

Carr, C. M., Grote, E., Munson, M., Hughson, F. M., and Novick, P. J. (1999). Sec1p Binds to Snare Complexes and Concentrates at Sites of Secretion. *The Journal of cell biology* **146**, 333-344.

Caswell, P. T. and Norman, J. C. (2006). Integrin Trafficking and the Control of Cell Migration. *Traffic (Copenhagen, Denmark)* **7**, 14-21.

Chant, J. (1999). Cell Polarity in Yeast. *Annual review of cell and developmental biology* **15**, 365-391.

Chardin, P. and Tavitian, A. (1986). The Ral Gene: A New Ras Related Gene Isolated by the Use of a Synthetic Probe. *The EMBO journal* **5**, 2203-2208.

Chardin, P. and Tavitian, A. (1989). Coding Sequences of Human Rala and Ralb Cdnas. *Nucleic acids research* **17**, 4380.

Chavrier, P., Vingron, M., Sander, C., Simons, K., and Zerial, M. (1990). Molecular Cloning of Ypt1/Sec4-Related Cdnas from an Epithelial Cell Line. *Molecular and cellular biology* **10**, 6578-6585.

Chen, X. W., Inoue, M., Hsu, S. C., and Saltiel, A. R. (2006). Rala-Exocyst-Dependent Recycling Endosome Trafficking Is Required for the Completion of Cytokinesis. *The Journal of biological chemistry* **281**, 38609-38616.

Cheng, J., Wang, H., and Guggino, W. B. (2005). Regulation of Cystic Fibrosis Transmembrane Regulator Trafficking and Protein Expression by a Rho Family Small Gtpase Tc10. *The Journal of biological chemistry* **280**, 3731-3739.

Chiang, S. H., Baumann, C. A., Kanzaki, M., Thurmond, D. C., Watson, R. T., Neudauer, C. L., Macara, I. G., Pessin, J. E., and Saltiel, A. R. (2001). Insulin-Stimulated Glut4 Translocation Requires the Cap-Dependent Activation of Tc10. *Nature* **410**, 944-948.

Conibear, E. and Stevens, T. H. (2000). Vps52p, Vps53p, and Vps54p Form a Novel Multisubunit Complex Required for Protein Sorting at the Yeast Late Golgi. *Molecular biology of the cell* **11**, 305-323.

Conibear, E., Cleck, J. N., and Stevens, T. H. (2003). Vps51p Mediates the Association of the Garp (Vps52/53/54) Complex with the Late Golgi T-Snare Tlg1p. *Molecular biology of the cell* **14**, 1610-1623.

Crowther, R. A. and Pearse, B. M. (1981). Assembly and Packing of Clathrin into Coats. *The Journal of cell biology* **91**, 790-797.

Cubelos, B., Gimenez, C., and Zafra, F. (2005). The Glycine Transporter Glyt1 Interacts with Sec3, a Component of the Exocyst Complex. *Neuropharmacology* **49**, 935-944.

D'Souza-Schorey, C. and Chavrier, P. (2006). Arf Proteins: Roles in Membrane Traffic and Beyond. *Nature reviews* **7**, 347-358.

Damke, H., Baba, T., Warnock, D. E., and Schmid, S. L. (1994). Induction of Mutant Dynamin Specifically Blocks Endocytic Coated Vesicle Formation. *The Journal of cell biology* **127**, 915-934.

Dauter, Z. (2006). Current State and Prospects of Macromolecular Crystallography. *Acta crystallographica* **62**, 1-11.

de Duve, C. (1963). *Ciba Foundation Symposium on Lysosomes*, *London*.

Donaldson, J. G., Honda, A., and Weigert, R. (2005). Multiple Activities for Arf1 at the Golgi Complex. *Biochimica et biophysica acta* **1744**, 364-373.

Dong, G., Hutagalung, A. H., Fu, C., Novick, P., and Reinisch, K. M. (2005). The Structures of Exocyst Subunit Exo70p and the Exo84p C-Terminal Domains Reveal a Common Motif. *Nat Struct Mol Biol* **12**, 1094-1100.

Drees, B. L., Sundin, B., Brazeau, E., Caviston, J. P., Chen, G. C., Guo, W., Kozminski, K. G., Lau, M. W., Moskow, J. J., Tong, A., Schenkman, L. R., McKenzie, A., 3rd, Brennwald, P., Longtine, M., Bi, E., Chan, C., Novick, P., Boone, C., Pringle, J. R., Davis, T. N., Fields, S., and Drubin, D. G. (2001). A Protein Interaction Map for Cell Polarity Development. *The Journal of cell biology* **154**, 549-571.

Drivas, G. T., Shih, A., Coutavas, E., Rush, M. G., and D'Eustachio, P. (1990). Characterization of Four Novel Ras-Like Genes Expressed in a Human Teratocarcinoma Cell Line. *Molecular and cellular biology* **10**, 1793-1798.

Dulubova, I., Khvotchev, M., Liu, S., Huryeva, I., Sudhof, T. C., and Rizo, J. (2007). Munc18-1 Binds Directly to the Neuronal Snare Complex. *Proceedings of the National Academy of Sciences of the United States of America* **104**, 2697-2702.

Eitzen, G. (2003). Actin Remodeling to Facilitate Membrane Fusion. *Biochimica et biophysica acta* **1641**, 175-181.

Elias, M., Drdova, E., Ziak, D., Bavlnka, B., Hala, M., Cvrckova, F., Soukupova, H., and Zarsky, V. (2003). The Exocyst Complex in Plants. *Cell Biol Int* **27**, 199-201.

Erickson, J. W. and Cerione, R. A. (2001). Multiple Roles for Cdc42 in Cell Regulation. *Current opinion in cell biology* **13**, 153-157.

Fasshauer, D., Sutton, R. B., Brunger, A. T., and Jahn, R. (1998). Conserved Structural Features of the Synaptic Fusion Complex: Snare Proteins Reclassified as Q- and R-Snares. *Proceedings of the National Academy of Sciences of the United States of America* **95**, 15781-15786.

Fasshauer, D., Antonin, W., Margittai, M., Pabst, S., and Jahn, R. (1999). Mixed and Non-Cognate Snare Complexes. Characterization of Assembly and Biophysical Properties. *The Journal of biological chemistry* **274**, 15440-15446.

Finger, F. P., Hughes, T. E., and Novick, P. (1998). Sec3p Is a Spatial Landmark for Polarized Secretion in Budding Yeast. *Cell* **92**, 559-571.

Fontana, A., de Laureto, P. P., Spolaore, B., Frare, E., Picotti, P., and Zambonin, M. (2004). Probing Protein Structure by Limited Proteolysis. *Acta biochimica Polonica* **51**, 299-321.

Forsythe, E. L., Maxwell, D. L., and Pusey, M. (2002). Vapor Diffusion, Nucleation Rates and the Reservoir to Crystallization Volume Ratio. *Acta crystallographica* **58**, 1601-1605.

Fridmann-Sirkis, Y., Kent, H. M., Lewis, M. J., Evans, P. R., and Pelham, H. R. (2006). Structural Analysis of the Interaction between the Snare Tlg1 and Vps51. *Traffic (Copenhagen, Denmark)* **7**, 182-190.

Fukai, S., Matern, H. T., Jagath, J. R., Scheller, R. H., and Brunger, A. T. (2003). Structural Basis of the Interaction between Rala and Sec5, a Subunit of the Sec6/8 Complex. *The EMBO journal* **22**, 3267-3278.

Godi, A., Di Campli, A., Konstantakopoulos, A., Di Tullio, G., Alessi, D. R., Kular, G. S., Daniele, T., Marra, P., Lucocq, J. M., and De Matteis, M. A. (2004). Fapps Control Golgi-to-Cell-Surface Membrane Traffic by Binding to Arf and Ptdins(4)P. *Nature cell biology* **6**, 393-404.

Goud, B., Salminen, A., Walworth, N. C., and Novick, P. J. (1988). A Gtp-Binding Protein Required for Secretion Rapidly Associates with Secretory Vesicles and the Plasma Membrane in Yeast. *Cell* **53**, 753-768.

Graves, R. A., Tontonoz, P., and Spiegelman, B. M. (1992). Analysis of a Tissue-Specific Enhancer: Arf6 Regulates Adipogenic Gene Expression. *Molecular and cellular biology* **12**, 3313.

Green, E. G., Ramm, E., Riley, N. M., Spiro, D. J., Goldenring, J. R., and Wessling-Resnick, M. (1997). Rab11 Is Associated with Transferrin-Containing Recycling Compartments in K562 Cells. *Biochemical and biophysical research communications* **239**, 612-616.

Grindstaff, K. K., Yeaman, C., Anandasabapathy, N., Hsu, S. C., Rodriguez-Boulan, E., Scheller, R. H., and Nelson, W. J. (1998). Sec6/8 Complex Is Recruited to Cell-Cell Contacts and Specifies Transport Vesicle Delivery to the Basal-Lateral Membrane in Epithelial Cells. *Cell* **93**, 731-740.

Gromley, A., Yeaman, C., Rosa, J., Redick, S., Chen, C. T., Mirabelle, S., Guha, M., Sillibourne, J., and Doxsey, S. J. (2005). Centriolin Anchoring of Exocyst and Snare Complexes at the Midbody Is Required for Secretory-Vesicle-Mediated Abscission. *Cell* **123**, 75-87.

Grosshans, B. L., Andreeva, A., Gangar, A., Niessen, S., Yates, J. R., 3rd, Brennwald, P., and Novick, P. (2006). The Yeast Lgl Family Member Sro7p Is an Effector of the Secretory Rab Gtpase Sec4p. *The Journal of cell biology* **172**, 55-66.

Gulli, M. P., Jaquenoud, M., Shimada, Y., Niederhauser, G., Wiget, P., and Peter, M. (2000). Phosphorylation of the Cdc42 Exchange Factor Cdc24 by the Pak-Like Kinase Cla4 May Regulate Polarized Growth in Yeast. *Molecular cell* **6**, 1155-1167.

Guo, W., Roth, D., Gatti, E., De Camilli, P., and Novick, P. (1997). Identification and Characterization of Homologues of the Exocyst Component Sec10p. *FEBS letters* **404**, 135-139.

Guo, W., Grant, A., and Novick, P. (1999a). Exo84p Is an Exocyst Protein Essential for Secretion. *The Journal of biological chemistry* **274**, 23558-23564.

Guo, W., Roth, D., Walch-Solimena, C., and Novick, P. (1999b). The Exocyst Is an Effector for Sec4p, Targeting Secretory Vesicles to Sites of Exocytosis. *The EMBO journal* **18**, 1071-1080.

Guo, W., Sacher, M., Barrowman, J., Ferro-Novick, S., and Novick, P. (2000). Protein Complexes in Transport Vesicle Targeting. *Trends in cell biology* **10**, 251-255.

Guo, W., Tamanoi, F., and Novick, P. (2001). Spatial Regulation of the Exocyst Complex by Rho1 Gtpase. *Nature cell biology* **3**, 353-360.

Haas, A., Scheglmann, D., Lazar, T., Gallwitz, D., and Wickner, W. (1995). The Gtpase Ypt7p of Saccharomyces Cerevisiae Is Required on Both Partner Vacuoles for the Homotypic Fusion Step of Vacuole Inheritance. *The EMBO journal* **14**, 5258-5270.

Hales, C. M., Vaerman, J. P., and Goldenring, J. R. (2002). Rab11 Family Interacting Protein 2 Associates with Myosin Vb and Regulates Plasma Membrane Recycling. *The Journal of biological chemistry* **277**, 50415-50421.

Hamada, D., Takata, Y., Osabe, D., Nomura, K., Shinohara, S., Egawa, H., Nakano, S., Shinomiya, F., Scafe, C. R., Reeve, V. M., Miyamoto, T., Moritani, M., Kunika, K., Inoue, H., Yasui, N., and Itakura, M. (2005). Association between Single-Nucleotide Polymorphisms in the Sec8l1 Gene, Which Encodes a Subunit of the Exocyst Complex, and Rheumatoid Arthritis in a Japanese Population. *Arthritis Rheum* **52**, 1371-1380.

Hamburger, Z. A., Hamburger, A. E., West, A. P., Jr., and Weis, W. I. (2006). Crystal Structure of the S.Cerevisiae Exocyst Component Exo70p. *Journal of molecular biology* **356**, 9-21.

Hammer, J. A., 3rd and Wu, X. S. (2002). Rabs Grab Motors: Defining the Connections between Rab Gtpases and Motor Proteins. *Current opinion in cell biology* **14**, 69-75.

Hanson, P. I., Roth, R., Morisaki, H., Jahn, R., and Heuser, J. E. (1997). Structure and Conformational Changes in Nsf and Its Membrane Receptor Complexes Visualized by Quick-Freeze/Deep-Etch Electron Microscopy. *Cell* **90**, 523-535.

Harries, P. A., Pan, A., and Quatrano, R. S. (2005). Actin-Related Protein2/3 Complex Component Arpc1 Is Required for Proper Cell Morphogenesis and Polarized Cell Growth in Physcomitrella Patens. *The Plant cell* **17**, 2327-2339.

Harsay, E. and Bretscher, A. (1995). Parallel Secretory Pathways to the Cell Surface in Yeast. *The Journal of cell biology* **131**, 297-310.

Hay, J. C., Klumperman, J., Oorschot, V., Steegmaier, M., Kuo, C. S., and Scheller, R. H. (1998). Localization, Dynamics, and Protein Interactions Reveal Distinct Roles for Er and Golgi Snares. *The Journal of cell biology* **141**, 1489-1502.

He, B., Xi, F., Zhang, J., Terbush, D., Zhang, X., and Guo, W. (2007). Exo70p Mediates the Secretion of Specific Exocytic Vesicles at Early Stages of the Cell Cycle for Polarized Cell Growth. *The Journal of cell biology* **176**, 771-777.

Helliwell, J. R. (2005). Protein Crystal Perfection and Its Application. *Acta crystallographica* **61**, 793-798.

Hickson, G. R., Matheson, J., Riggs, B., Maier, V. H., Fielding, A. B., Prekeris, R., Sullivan, W., Barr, F. A., and Gould, G. W. (2003). Arfophilins Are Dual Arf/Rab 11 Binding Proteins That Regulate Recycling Endosome Distribution and Are Related to Drosophila Nuclear Fallout. *Molecular biology of the cell* **14**, 2908-2920.

Hong, W. (2005). Snares and Traffic. *Biochimica et biophysica acta* **1744**, 120-144.

Hori, Y., Kikuchi, A., Isomura, M., Katayama, M., Miura, Y., Fujioka, H., Kaibuchi, K., and Takai, Y. (1991). Post-Translational Modifications of the C-Terminal Region of the Rho Protein Are Important for Its Interaction with Membranes and the Stimulatory and Inhibitory Gdp/Gtp Exchange Proteins. *Oncogene* **6**, 515-522.

Hoyle, J., Phelan, J. P., Bermingham, N., and Fisher, E. M. (1996). Localization of Human and Mouse N-Ethylmaleimide-Sensitive Factor (Nsf) Gene: A Two-Domain Member of the Aaa Family That Is Involved in Membrane Fusion. *Mamm Genome* **7**, 850-852.

Hsu, S. C., Ting, A. E., Hazuka, C. D., Davanger, S., Kenny, J. W., Kee, Y., and Scheller, R. H. (1996). The Mammalian Brain Rsec6/8 Complex. *Neuron* **17**, 1209-1219.

Hsu, S. C., Hazuka, C. D., Roth, R., Foletti, D. L., Heuser, J., and Scheller, R. H. (1998). Subunit Composition, Protein Interactions, and Structures of the Mammalian Brain Sec6/8 Complex and Septin Filaments. *Neuron* **20**, 1111-1122.

Hunt, J. M., Bommert, K., Charlton, M. P., Kistner, A., Habermann, E., Augustine, G. J., and Betz, H. (1994). A Post-Docking Role for Synaptobrevin in Synaptic Vesicle Fusion. *Neuron* **12**, 1269-1279.

Imai, J., Toh-e, A., and Matsui, Y. (1996). Genetic Analysis of the Saccharomyces Cerevisiae Rho3 Gene, Encoding a Rho-Type Small Gtpase, Provides Evidence for a Role in Bud Formation. *Genetics* **142**, 359-369.

Inoue, M., Chang, L., Hwang, J., Chiang, S. H., and Saltiel, A. R. (2003). The Exocyst Complex Is Required for Targeting of Glut4 to the Plasma Membrane by Insulin. *Nature* **422**, 629-633.

Inoue, M., Chiang, S. H., Chang, L., Chen, X. W., and Saltiel, A. R. (2006). Compartmentalization of the Exocyst Complex in Lipid Rafts Controls Glut4 Vesicle Tethering. *Molecular biology of the cell* **17**, 2303-2311.

Jafar-Nejad, H., Andrews, H. K., Acar, M., Bayat, V., Wirtz-Peitz, F., Mehta, S. Q., Knoblich, J. A., and Bellen, H. J. (2005). Sec15, a Component of the Exocyst, Promotes Notch Signaling During the Asymmetric Division of Drosophila Sensory Organ Precursors. *Developmental cell* **9**, 351-363.

Jahn, R. and Sudhof, T. C. (1999). Membrane Fusion and Exocytosis. *Annual review of biochemistry* **68**, 863-911.

Jahn, R. and Scheller, R. H. (2006). Snares--Engines for Membrane Fusion. *Nature reviews* **7**, 631-643.

Jin, R., Junutula, J. R., Matern, H. T., Ervin, K. E., Scheller, R. H., and Brunger, A. T. (2005). Exo84 and Sec5 Are Competitive Regulatory Sec6/8 Effectors to the Rala Gtpase. *The EMBO journal* **24**, 2064-2074.

Johnson, D. I. and Pringle, J. R. (1990). Molecular Characterization of Cdc42, a Saccharomyces Cerevisiae Gene Involved in the Development of Cell Polarity. *The Journal of cell biology* **111**, 143-152.

Johnson, D. I. (1999). Cdc42: An Essential Rho-Type Gtpase Controlling Eukaryotic Cell Polarity. *Microbiol Mol Biol Rev* **63**, 54-105.

Jones, M. C., Caswell, P. T., and Norman, J. C. (2006). Endocytic Recycling Pathways: Emerging Regulators of Cell Migration. *Current opinion in cell biology* **18**, 549-557.

Kabcenell, A. K., Goud, B., Northup, J. K., and Novick, P. J. (1990). Binding and Hydrolysis of Guanine Nucleotides by Sec4p, a Yeast Protein Involved in the Regulation of Vesicular Traffic. *The Journal of biological chemistry* **265**, 9366-9372.

Kagami, M., Toh-e, A., and Matsui, Y. (1998). Sro7p, a Saccharomyces Cerevisiae Counterpart of the Tumor Suppressor L(2)Gl Protein, Is Related to Myosins in Function. *Genetics* **149**, 1717-1727.

Kanzaki, M. (2006). Insulin Receptor Signals Regulating Glut4 Translocation and Actin Dynamics. *Endocrine journal* **53**, 267-293.

Kashchiev, D., Vekilov, P. G., and Kolomeisky, A. B. (2005). Kinetics of Two-Step Nucleation of Crystals. *The Journal of chemical physics* **122**, 244706.

Kee, Y., Yoo, J. S., Hazuka, C. D., Peterson, K. E., Hsu, S. C., and Scheller, R. H. (1997). Subunit Structure of the Mammalian Exocyst Complex. *Proceedings of the National Academy of Sciences of the United States of America* **94**, 14438-14443.

Kim, Y. G., Raunser, S., Munger, C., Wagner, J., Song, Y. L., Cygler, M., Walz, T., Oh, B. H., and Sacher, M. (2006). The Architecture of the Multisubunit Trapp I Complex Suggests a Model for Vesicle Tethering. *Cell* **127**, 817-830.

Kirchhausen, T. (2000). Three Ways to Make a Vesicle. *Nature reviews* **1**, 187-198.

Koch, G., Tanaka, K., Masuda, T., Yamochi, W., Nonaka, H., and Takai, Y. (1997). Association of the Rho Family Small Gtp-Binding Proteins with Rho Gdp Dissociation Inhibitor (Rho Gdi) in Saccharomyces Cerevisiae. *Oncogene* **15**, 417-422.

Laage, R. and Ungermann, C. (2001). The N-Terminal Domain of the T-Snare Vam3p Coordinates Priming and Docking in Yeast Vacuole Fusion. *Molecular biology of the cell* **12**, 3375-3385.

Lalli, G. and Hall, A. (2005). Ral Gtpases Regulate Neurite Branching through Gap-43 and the Exocyst Complex. *The Journal of cell biology* **171**, 857-869.

Lehman, K., Rossi, G., Adamo, J. E., and Brennwald, P. (1999). Yeast Homologues of Tomosyn and Lethal Giant Larvae Function in Exocytosis and Are Associated with the Plasma Membrane Snare, Sec9. *The Journal of cell biology* **146**, 125-140.

Letourneur, F., Gaynor, E. C., Hennecke, S., Demolliere, C., Duden, R., Emr, S. D., Riezman, H., and Cosson, P. (1994). Coatomer Is Essential for Retrieval of Dilysine-Tagged Proteins to the Endoplasmic Reticulum. *Cell* **79**, 1199-1207.

Levin, D. E. (2005). Cell Wall Integrity Signaling in Saccharomyces Cerevisiae. *Microbiol Mol Biol Rev* **69**, 262-291.

Lewin, D. A. and Mellman, I. (1998). Sorting out Adaptors. *Biochimica et biophysica acta* **1401**, 129-145.

Lin, R. C. and Scheller, R. H. (1997). Structural Organization of the Synaptic Exocytosis Core Complex. *Neuron* **19**, 1087-1094.

Lipschutz, J. H., Guo, W., O'Brien, L. E., Nguyen, Y. H., Novick, P., and Mostov, K. E. (2000). Exocyst Is Involved in Cystogenesis and Tubulogenesis and Acts by Modulating Synthesis and Delivery of Basolateral Plasma Membrane and Secretory Proteins. *Molecular biology of the cell* **11**, 4259-4275.

Lipschutz, J. H., Lingappa, V. R., and Mostov, K. E. (2003). The Exocyst Affects Protein Synthesis by Acting on the Translocation Machinery of the Endoplasmic Reticulum. *The Journal of biological chemistry* **278**, 20954-20960.

Lowe, M. (2000). Membrane Transport: Tethers and Trapps. *Curr Biol* **10**, R407-409.

Machesky, L. M., Atkinson, S. J., Ampe, C., Vandekerckhove, J., and Pollard, T. D. (1994). Purification of a Cortical Complex Containing Two Unconventional Actins from Acanthamoeba by Affinity Chromatography on Profilin-Agarose. *The Journal of cell biology* **127**, 107-115.

Madaule, P., Axel, R., and Myers, A. M. (1987). Characterization of Two Members of the Rho Gene Family from the Yeast Saccharomyces Cerevisiae. *Proceedings of the National Academy of Sciences of the United States of America* **84**, 779-783.

Malsam, J., Satoh, A., Pelletier, L., and Warren, G. (2005). Golgin Tethers Define Subpopulations of Copi Vesicles. *Science (New York, NY* **307**, 1095-1098.

Mammoto, A., Ohtsuka, T., Hotta, I., Sasaki, T., and Takai, Y. (1999). Rab11bp/Rabphilin-11, a Downstream Target of Rab11 Small G Protein Implicated in Vesicle Recycling. *The Journal of biological chemistry* **274**, 25517-25524.

Masuda, T., Tanaka, K., Nonaka, H., Yamochi, W., Maeda, A., and Takai, Y. (1994). Molecular Cloning and Characterization of Yeast Rho Gdp Dissociation Inhibitor. *The Journal of biological chemistry* **269**, 19713-19718.

Matern, H. T., Yeaman, C., Nelson, W. J., and Scheller, R. H. (2001). The Sec6/8 Complex in Mammalian Cells: Characterization of Mammalian Sec3, Subunit Interactions, and Expression of Subunits in Polarized Cells. *Proceedings of the National Academy of Sciences of the United States of America* **98**, 9648-9653.

Matsui, Y. and Toh-e, A. (1992). Isolation and Characterization of Two Novel Ras Superfamily Genes in Saccharomyces Cerevisiae. *Gene* **114**, 43-49.

Mayer, A. and Wickner, W. (1997). Docking of Yeast Vacuoles Is Catalyzed by the Ras-Like Gtpase Ypt7p after Symmetric Priming by Sec18p (Nsf). *The Journal of cell biology* **136**, 307-317.

McMahon, H. T. and Mills, I. G. (2004). Cop and Clathrin-Coated Vesicle Budding: Different Pathways, Common Approaches. *Current opinion in cell biology* **16**, 379-391.

McNew, J. A., Parlati, F., Fukuda, R., Johnston, R. J., Paz, K., Paumet, F., Sollner, T. H., and Rothman, J. E. (2000). Compartmental Specificity of Cellular Membrane Fusion Encoded in Snare Proteins. *Nature* **407**, 153-159.

Medkova, M., France, Y. E., Coleman, J., and Novick, P. (2006). The Rab Exchange Factor Sec2p Reversibly Associates with the Exocyst. *Molecular biology of the cell* **17**, 2757-2769.

Mehta, S. Q., Hiesinger, P. R., Beronja, S., Zhai, R. G., Schulze, K. L., Verstreken, P., Cao, Y., Zhou, Y., Tepass, U., Crair, M. C., and Bellen, H. J. (2005). Mutations in Drosophila Sec15 Reveal a Function in Neuronal Targeting for a Subset of Exocyst Components. *Neuron* **46**, 219-232.

Moskalenko, S., Henry, D. O., Rosse, C., Mirey, G., Camonis, J. H., and White, M. A. (2002). The Exocyst Is a Ral Effector Complex. *Nature cell biology* **4**, 66-72.

Moskalenko, S., Tong, C., Rosse, C., Mirey, G., Formstecher, E., Daviet, L., Camonis, J., and White, M. A. (2003). Ral Gtpases Regulate Exocyst Assembly through Dual Subunit Interactions. *The Journal of biological chemistry* **278**, 51743-51748.

Moskow, J. J., Gladfelter, A. S., Lamson, R. E., Pryciak, P. M., and Lew, D. J. (2000). Role of Cdc42p in Pheromone-Stimulated Signal Transduction in Saccharomyces Cerevisiae. *Molecular and cellular biology* **20**, 7559-7571.

Moss, J. and Vaughan, M. (1998). Molecules in the Arf Orbit. *The Journal of biological chemistry* **273**, 21431-21434.

Munson, M. and Novick, P. (2006). The Exocyst Defrocked, a Framework of Rods Revealed. *Nat Struct Mol Biol* **13**, 577-581.

Murphy, G. A., Solski, P. A., Jillian, S. A., Perez de la Ossa, P., D'Eustachio, P., Der, C. J., and Rush, M. G. (1999). Cellular Functions of Tc10, a Rho Family Gtpase: Regulation of Morphology, Signal Transduction and Cell Growth. *Oncogene* **18**, 3831-3845.

Murthy, M., Garza, D., Scheller, R. H., and Schwarz, T. L. (2003). Mutations in the Exocyst Component Sec5 Disrupt Neuronal Membrane Traffic, but Neurotransmitter Release Persists. *Neuron* **37**, 433-447.

Natarajan, P., Lander, G. C., Shepherd, C. M., Reddy, V. S., Brooks, C. L., 3rd, and Johnson, J. E. (2005). Exploring Icosahedral Virus Structures with Viper. *Nat Rev Microbiol* **3**, 809-817.

Nichols, B. J., Ungermann, C., Pelham, H. R., Wickner, W. T., and Haas, A. (1997). Homotypic Vacuolar Fusion Mediated by T- and V-Snares. *Nature* **387**, 199-202.

Nobes, C. D. and Hall, A. (1995). Rho, Rac, and Cdc42 Gtpases Regulate the Assembly of Multimolecular Focal Complexes Associated with Actin Stress Fibers, Lamellipodia, and Filopodia. *Cell* **81**, 53-62.

Nolen, B. J., Littlefield, R. S., and Pollard, T. D. (2004). Crystal Structures of Actin-Related Protein 2/3 Complex with Bound Atp or Adp. *Proceedings of the National Academy of Sciences of the United States of America* **101**, 15627-15632.

Nomanbhoy, T. K. and Cerione, R. (1996). Characterization of the Interaction between Rhogdi and Cdc42hs Using Fluorescence Spectroscopy. *The Journal of biological chemistry* **271**, 10004-10009.

Novick, P., Field, C., and Schekman, R. (1980). Identification of 23 Complementation Groups Required for Post-Translational Events in the Yeast Secretory Pathway. *Cell* **21**, 205-215.

Ortiz, D., Medkova, M., Walch-Solimena, C., and Novick, P. (2002). Ypt32 Recruits the Sec4p Guanine Nucleotide Exchange Factor, Sec2p, to Secretory Vesicles; Evidence for a Rab Cascade in Yeast. *The Journal of cell biology* **157**, 1005-1015.

Owen, D. J., Collins, B. M., and Evans, P. R. (2004). Adaptors for Clathrin Coats: Structure and Function. *Annual review of cell and developmental biology* **20**, 153-191.

Oxford, G. and Theodorescu, D. (2003). Ras Superfamily Monomeric G Proteins in Carcinoma Cell Motility. *Cancer letters* **189**, 117-128.

Page, R. and Stevens, R. C. (2004). Crystallization Data Mining in Structural Genomics: Using Positive and Negative Results to Optimize Protein Crystallization Screens. *Methods (San Diego, Calif* **34**, 373-389.

Parlati, F., McNew, J. A., Fukuda, R., Miller, R., Sollner, T. H., and Rothman, J. E. (2000). Topological Restriction of Snare-Dependent Membrane Fusion. *Nature* **407**, 194-198.

Pearse, B. M. (1975). Coated Vesicles from Pig Brain: Purification and Biochemical Characterization. *Journal of molecular biology* **97**, 93-98.

Peplowska, K., Markgraf, D. F., Ostrowicz, C. W., Bange, G., and Ungermann, C. (2007). The Corvet Tethering Complex Interacts with the Yeast Rab5 Homolog Vps21 and Is Involved in Endo-Lysosomal Biogenesis. *Developmental cell* **12**, 739-750.

Peterson, M. R. and Emr, S. D. (2001). The Class C Vps Complex Functions at Multiple Stages of the Vacuolar Transport Pathway. *Traffic (Copenhagen, Denmark)* **2**, 476-486.

Price, A., Seals, D., Wickner, W., and Ungermann, C. (2000). The Docking Stage of Yeast Vacuole Fusion Requires the Transfer of Proteins from a Cis-Snare Complex to a Rab/Ypt Protein. *The Journal of cell biology* **148**, 1231-1238.

Prigent, M., Dubois, T., Raposo, G., Derrien, V., Tenza, D., Rosse, C., Camonis, J., and Chavrier, P. (2003). Arf6 Controls Post-Endocytic Recycling through Its Downstream Exocyst Complex Effector. *The Journal of cell biology* **163**, 1111-1121.

Qadota, H., Anraku, Y., Botstein, D., and Ohya, Y. (1994). Conditional Lethality of a Yeast Strain Expressing Human Rhoa in Place of Rho1. *Proceedings of the National Academy of Sciences of the United States of America* **91**, 9317-9321.

Randazzo, P. A., Nie, Z., Miura, K., and Hsu, V. W. (2000). Molecular Aspects of the Cellular Activities of Adp-Ribosylation Factors. *Sci STKE* **2000**, RE1.

Reilly, B. A., Kraynack, B. A., VanRheenen, S. M., and Waters, M. G. (2001). Golgi-to-Endoplasmic Reticulum (Er) Retrograde Traffic in Yeast Requires Dsl1p, a Component of the Er Target Site That Interacts with a Copi Coat Subunit. *Molecular biology of the cell* **12**, 3783-3796.

Richman, T. J., Toenjes, K. A., Morales, S. E., Cole, K. C., Wasserman, B. T., Taylor, C. M., Koster, J. A., Whelihan, M. F., and Johnson, D. I. (2004). Analysis of Cell-Cycle Specific Localization of the Rdi1p Rhogdi and the Structural Determinants Required for Cdc42p Membrane Localization and Clustering at Sites of Polarized Growth. *Current genetics* **45**, 339-349.

Riefler, G. M., Balasingam, G., Lucas, K. G., Wang, S., Hsu, S. C., and Firestein, B. L. (2003). Exocyst Complex Subunit Sec8 Binds to Postsynaptic Density Protein-95 (Psd-95): A Novel Interaction Regulated by Cypin (Cytosolic Psd-95 Interactor). *The Biochemical journal* **373**, 49-55.

Rink, J., Ghigo, E., Kalaidzidis, Y., and Zerial, M. (2005). Rab Conversion as a Mechanism of Progression from Early to Late Endosomes. *Cell* **122**, 735-749.

Robinson, N. G., Guo, L., Imai, J., Toh, E. A., Matsui, Y., and Tamanoi, F. (1999). Rho3 of Saccharomyces Cerevisiae, Which Regulates the Actin Cytoskeleton and Exocytosis, Is a Gtpase Which Interacts with Myo2 and Exo70. *Molecular and cellular biology* **19**, 3580-3587.

Robinson, R. C., Turbedsky, K., Kaiser, D. A., Marchand, J. B., Higgs, H. N., Choe, S., and Pollard, T. D. (2001). Crystal Structure of Arp2/3 Complex. *Science (New York, NY* **294**, 1679-1684.

Rossé, C., Hatzoglou, A., Parrini, M. C., White, M. A., Chavrier, P., and Camonis, J. (2006). Ralb Mobilizes the Exocyst to Drive Cell Migration. *Molecular and cellular biology* **26**, 727-734.

Roumanie, O., Wu, H., Molk, J. N., Rossi, G., Bloom, K., and Brennwald, P. (2005). Rho Gtpase Regulation of Exocytosis in Yeast Is Independent of Gtp Hydrolysis and Polarization of the Exocyst Complex. *The Journal of cell biology* **170**, 583-594.

Sacher, M., Barrowman, J., Wang, W., Horecka, J., Zhang, Y., Pypaert, M., and Ferro-Novick, S. (2001). Trapp I Implicated in the Specificity of Tethering in Er-to-Golgi Transport. *Molecular cell* **7**, 433-442.

Salminen, A. and Novick, P. J. (1987). A Ras-Like Protein Is Required for a Post-Golgi Event in Yeast Secretion. *Cell* **49**, 527-538.

Sans, N., Prybylowski, K., Petralia, R. S., Chang, K., Wang, Y. X., Racca, C., Vicini, S., and Wenthold, R. J. (2003). Nmda Receptor Trafficking through an Interaction between Pdz Proteins and the Exocyst Complex. *Nature cell biology* **5**, 520-530.

Schenkman, L. R., Caruso, C., Page, N., and Pringle, J. R. (2002). The Role of Cell Cycle-Regulated Expression in the Localization of Spatial Landmark Proteins in Yeast. *The Journal of cell biology* **156**, 829-841.

Seabra, M. C., Mules, E. H., and Hume, A. N. (2002). Rab Gtpases, Intracellular Traffic and Disease. *Trends in molecular medicine* **8**, 23-30.

Seals, D. F., Eitzen, G., Margolis, N., Wickner, W. T., and Price, A. (2000). A Ypt/Rab Effector Complex Containing the Sec1 Homolog Vps33p Is Required for Homotypic Vacuole Fusion. *Proceedings of the National Academy of Sciences of the United States of America* **97**, 9402-9407.

Seaman, M. N., McCaffery, J. M., and Emr, S. D. (1998). A Membrane Coat Complex Essential for Endosome-to-Golgi Retrograde Transport in Yeast. *The Journal of cell biology* **142**, 665-681.

Shen, J., Tareste, D. C., Paumet, F., Rothman, J. E., and Melia, T. J. (2007). Selective Activation of Cognate Snarepins by Sec1/Munc18 Proteins. *Cell* **128**, 183-195.

Shorter, J., Beard, M. B., Seemann, J., Dirac-Svejstrup, A. B., and Warren, G. (2002). Sequential Tethering of Golgins and Catalysis of Snarepin Assembly by the Vesicle-Tethering Protein P115. *The Journal of cell biology* **157**, 45-62.

Siniossoglou, S. and Pelham, H. R. (2001). An Effector of Ypt6p Binds the Snare Tlg1p and Mediates Selective Fusion of Vesicles with Late Golgi Membranes. *The EMBO journal* **20**, 5991-5998.

Sivaram, M. V., Saporita, J. A., Furgason, M. L., Boettcher, A. J., and Munson, M. (2005). Dimerization of the Exocyst Protein Sec6p and Its Interaction with the T-Snare Sec9p. *Biochemistry* **44**, 6302-6311.

Sivaram, M. V., Furgason, M. L., Brewer, D. N., and Munson, M. (2006). The Structure of the Exocyst Subunit Sec6p Defines a Conserved Architecture with Diverse Roles. *Nat Struct Mol Biol* **13**, 555-556.

Söllner, T., Bennett, M. K., Whiteheart, S. W., Scheller, R. H., and Rothman, J. E. (1993). A Protein Assembly-Disassembly Pathway in Vitro That May Correspond to Sequential Steps of Synaptic Vesicle Docking, Activation, and Fusion. *Cell* **75**, 409-418.

Sommer, B., Oprins, A., Rabouille, C., and Munro, S. (2005). The Exocyst Component Sec5 Is Present on Endocytic Vesicles in the Oocyte of Drosophila Melanogaster. *The Journal of cell biology* **169**, 953-963.

Springer, S., Spang, A., and Schekman, R. (1999). A Primer on Vesicle Budding. *Cell* **97**, 145-148.

Stanier, R. Y. and van Niel, C. B. (1962). The Concept of a Bacterium. *Archiv fur Mikrobiologie* **42**, 17-35.

Strausberg, R. L., Feingold, E. A., Grouse, L. H., Derge, J. G., Klausner, R. D., Collins, F. S., Wagner, L., Shenmen, C. M., Schuler, G. D., Altschul, S. F., Zeeberg, B., Buetow, K. H., Schaefer, C. F., Bhat, N. K., Hopkins, R. F., Jordan, H., Moore, T., Max, S. I., Wang, J., Hsieh, F., Diatchenko, L., Marusina, K., Farmer, A. A., Rubin, G. M., Hong, L., Stapleton, M., Soares, M. B., Bonaldo, M. F., Casavant, T. L., Scheetz, T. E., Brownstein, M. J., Usdin, T. B., Toshiyuki, S., Carninci, P., Prange, C., Raha, S. S., Loquellano, N. A., Peters, G. J., Abramson, R. D., Mullahy, S. J., Bosak, S. A., McEwan, P. J., McKernan, K. J., Malek, J. A., Gunaratne, P. H., Richards, S., Worley, K. C., Hale, S., Garcia, A. M., Gay, L. J., Hulyk, S. W., Villalon, D. K., Muzny, D. M., Sodergren, E. J., Lu, X., Gibbs, R. A., Fahey, J., Helton, E., Ketteman, M., Madan, A., Rodrigues, S., Sanchez, A., Whiting, M., Madan, A., Young, A. C., Shevchenko, Y., Bouffard, G. G., Blakesley, R. W., Touchman, J. W., Green, E. D., Dickson, M. C., Rodriguez, A. C., Grimwood, J., Schmutz, J., Myers, R. M., Butterfield, Y. S., Krzywinski, M. I., Skalska, U., Smailus, D. E., Schnerch, A., Schein, J. E., Jones, S. J., and Marra, M. A. (2002). Generation and Initial Analysis of More Than 15,000 Full-Length Human and Mouse Cdna Sequences. *Proceedings of the National Academy of Sciences of the United States of America* **99**, 16899-16903.

Stroupe, C., Collins, K. M., Fratti, R. A., and Wickner, W. (2006). Purification of Active Hops Complex Reveals Its Affinities for Phosphoinositides and the Snare Vam7p. *The EMBO journal* **25**, 1579-1589.

Sugihara, K., Asano, S., Tanaka, K., Iwamatsu, A., Okawa, K., and Ohta, Y. (2002). The Exocyst Complex Binds the Small Gtpase Rala to Mediate Filopodia Formation. *Nature cell biology* **4**, 73-78.

Sutton, R. B., Fasshauer, D., Jahn, R., and Brunger, A. T. (1998). Crystal Structure of a Snare Complex Involved in Synaptic Exocytosis at 2.4 a Resolution. *Nature* **395**, 347-353.

Suvorova, E. S., Duden, R., and Lupashin, V. V. (2002). The Sec34/Sec35p Complex, a Ypt1p Effector Required for Retrograde Intra-Golgi Trafficking, Interacts with Golgi Snares and Copi Vesicle Coat Proteins. *The Journal of cell biology* **157**, 631-643.

Symons, M., Derry, J. M., Karlak, B., Jiang, S., Lemahieu, V., McCormick, F., Francke, U., and Abo, A. (1996). Wiskott-Aldrich Syndrome Protein, a Novel Effector for the Gtpase Cdc42hs, Is Implicated in Actin Polymerization. *Cell* **84**, 723-734.

TerBush, D. R. and Novick, P. (1995). Sec6, Sec8, and Sec15 Are Components of a Multisubunit Complex Which Localizes to Small Bud Tips in Saccharomyces Cerevisiae. *The Journal of cell biology* **130**, 299-312.

TerBush, D. R., Maurice, T., Roth, D., and Novick, P. (1996). The Exocyst Is a Multiprotein Complex Required for Exocytosis in Saccharomyces Cerevisiae. *The EMBO journal* **15**, 6483-6494.

Ting, A. E., Hazuka, C. D., Hsu, S. C., Kirk, M. D., Bean, A. J., and Scheller, R. H. (1995). Rsec6 and Rsec8, Mammalian Homologs of Yeast Proteins Essential for Secretion. *Proceedings of the National Academy of Sciences of the United States of America* **92**, 9613-9617.

Toikkanen, J. H., Miller, K. J., Soderlund, H., Jantti, J., and Keranen, S. (2003). The Beta Subunit of the Sec61p Endoplasmic Reticulum Translocon Interacts with the Exocyst Complex in Saccharomyces Cerevisiae. *The Journal of biological chemistry* **278**, 20946-20953.

Tsui, M. M. and Banfield, D. K. (2000). Yeast Golgi Snare Interactions Are Promiscuous. *Journal of cell science* **113 (Pt 1)**, 145-152.

Ungar, D., Oka, T., Brittle, E. E., Vasile, E., Lupashin, V. V., Chatterton, J. E., Heuser, J. E., Krieger, M., and Waters, M. G. (2002). Characterization of a Mammalian Golgi-Localized Protein Complex, Cog, That Is Required for Normal Golgi Morphology and Function. *The Journal of cell biology* **157**, 405-415.

van Dam, E. M. and Robinson, P. J. (2006). Ral: Mediator of Membrane Trafficking. *Int J Biochem Cell Biol* **38**, 1841-1847.

Vega, I. E. and Hsu, S. C. (2001). The Exocyst Complex Associates with Microtubules to Mediate Vesicle Targeting and Neurite Outgrowth. *J Neurosci* **21**, 3839-3848.

Vekilov, P. G. (2005). Kinetics and Mechanisms of Protein Crystallization at the Molecular Level. *Methods in molecular biology (Clifton, NJ* **300**, 15-52.

von Mollard, G. F., Nothwehr, S. F., and Stevens, T. H. (1997). The Yeast V-Snare Vti1p Mediates Two Vesicle Transport Pathways through Interactions with the T-Snares Sed5p and Pep12p. *The Journal of cell biology* **137**, 1511-1524.

Walch-Solimena, C., Collins, R. N., and Novick, P. J. (1997). Sec2p Mediates Nucleotide Exchange on Sec4p and Is Involved in Polarized Delivery of Post-Golgi Vesicles. *The Journal of cell biology* **137**, 1495-1509.

Walworth, N. C., Goud, B., Kabcenell, A. K., and Novick, P. J. (1989). Mutational Analysis of Sec4 Suggests a Cyclical Mechanism for the Regulation of Vesicular Traffic. *The EMBO journal* **8**, 1685-1693.

Wang, C. W., Hamamoto, S., Orci, L., and Schekman, R. (2006). Exomer: A Coat Complex for Transport of Select Membrane Proteins from the Trans-Golgi Network to the Plasma Membrane in Yeast. *The Journal of cell biology* **174**, 973-983.

Wang, H., Tang, X., Liu, J., Trautmann, S., Balasundaram, D., McCollum, D., and Balasubramanian, M. K. (2002). The Multiprotein Exocyst Complex Is Essential for Cell Separation in Schizosaccharomyces Pombe. *Molecular biology of the cell* **13**, 515-529.

Wang, H., Tang, X., and Balasubramanian, M. K. (2003). Rho3p Regulates Cell Separation by Modulating Exocyst Function in Schizosaccharomyces Pombe. *Genetics* **164**, 1323-1331.

Wang, L., Li, G., and Sugita, S. (2004a). Rala-Exocyst Interaction Mediates Gtp-Dependent Exocytosis. *The Journal of biological chemistry* **279**, 19875-19881.

Wang, S., Liu, Y., Adamson, C. L., Valdez, G., Guo, W., and Hsu, S. C. (2004b). The Mammalian Exocyst, a Complex Required for Exocytosis, Inhibits Tubulin Polymerization. *The Journal of biological chemistry* **279**, 35958-35966.

Wang, W., Sacher, M., and Ferro-Novick, S. (2000). Trapp Stimulates Guanine Nucleotide Exchange on Ypt1p. *The Journal of cell biology* **151**, 289-296.

Wang, W. and Ferro-Novick, S. (2002). A Ypt32p Exchange Factor Is a Putative Effector of Ypt1p. *Molecular biology of the cell* **13**, 3336-3343.

Wang, Y., Dulubova, I., Rizo, J., and Sudhof, T. C. (2001). Functional Analysis of Conserved Structural Elements in Yeast Syntaxin Vam3p. *The Journal of biological chemistry* **276**, 28598-28605.

Waters, M. G., Serafini, T., and Rothman, J. E. (1991). 'Coatomer': A Cytosolic Protein Complex Containing Subunits of Non-Clathrin-Coated Golgi Transport Vesicles. *Nature* **349**, 248-251.

Waters, M. G. and Hughson, F. M. (2000). Membrane Tethering and Fusion in the Secretory and Endocytic Pathways. *Traffic (Copenhagen, Denmark)* **1**, 588-597.

Weber, T., Zemelman, B. V., McNew, J. A., Westermann, B., Gmachl, M., Parlati, F., Sollner, T. H., and Rothman, J. E. (1998). Snarepins: Minimal Machinery for Membrane Fusion. *Cell* **92**, 759-772.

Weidler, M., Reinhard, C., Friedrich, G., Wieland, F. T., and Rosch, P. (2000). Structure of the Cytoplasmic Domain of P23 in Solution: Implications for the Formation of Copi Vesicles. *Biochemical and biophysical research communications* **271**, 401-408.

Whyte, J. R. and Munro, S. (2001). The Sec34/35 Golgi Transport Complex Is Related to the Exocyst, Defining a Family of Complexes Involved in Multiple Steps of Membrane Traffic. *Developmental cell* **1**, 527-537.

Wichmann, H., Hengst, L., and Gallwitz, D. (1992). Endocytosis in Yeast: Evidence for the Involvement of a Small Gtp-Binding Protein (Ypt7p). *Cell* **71**, 1131-1142.

Wiederkehr, A., Du, Y., Pypaert, M., Ferro-Novick, S., and Novick, P. (2003). Sec3p Is Needed for the Spatial Regulation of Secretion and for the Inheritance of the Cortical Endoplasmic Reticulum. *Molecular biology of the cell* **14**, 4770-4782.

Wiederkehr, A., De Craene, J. O., Ferro-Novick, S., and Novick, P. (2004). Functional Specialization within a Vesicle Tethering Complex: Bypass of a Subset of Exocyst Deletion Mutants by Sec1p or Sec4p. *The Journal of cell biology* **167**, 875-887.

Wu, S., Mehta, S. Q., Pichaud, F., Bellen, H. J., and Quiocho, F. A. (2005). Sec15 Interacts with Rab11 Via a Novel Domain and Affects Rab11 Localization in Vivo. *Nat Struct Mol Biol* **12**, 879-885.

Wu, W. J., Leonard, D. A., R, A. C., and Manor, D. (1997). Interaction between Cdc42hs and Rhogdi Is Mediated through the Rho Insert Region. *The Journal of biological chemistry* **272**, 26153-26158.

Wurmser, A. E., Sato, T. K., and Emr, S. D. (2000). New Component of the Vacuolar Class C-Vps Complex Couples Nucleotide Exchange on the Ypt7 Gtpase to Snare-Dependent Docking and Fusion. *The Journal of cell biology* **151**, 551-562.

Xu, K. F., Shen, X., Li, H., Pacheco-Rodriguez, G., Moss, J., and Vaughan, M. (2005). Interaction of Big2, a Brefeldin a-Inhibited Guanine Nucleotide-Exchange Protein, with

Exocyst Protein Exo70. *Proceedings of the National Academy of Sciences of the United States of America* **102**, 2784-2789.

Xu, Y., Zheng, Y., Fan, J. S., and Yang, D. (2006). A New Strategy for Structure Determination of Large Proteins in Solution without Deuteration. *Nature methods* **3**, 931-937.

Yang, B., Gonzalez, L., Jr., Prekeris, R., Steegmaier, M., Advani, R. J., and Scheller, R. H. (1999). Snare Interactions Are Not Selective. Implications for Membrane Fusion Specificity. *The Journal of biological chemistry* **274**, 5649-5653.

Yoshinaga, S., Kohjima, M., Ogura, K., Yokochi, M., Takeya, R., Ito, T., Sumimoto, H., and Inagaki, F. (2003). The Pb1 Domain and the Pc Motif-Containing Region Are Structurally Similar Protein Binding Modules. *The EMBO journal* **22**, 4888-4897.

Yu, S., Satoh, A., Pypaert, M., Mullen, K., Hay, J. C., and Ferro-Novick, S. (2006). Mbet3p Is Required for Homotypic Copii Vesicle Tethering in Mammalian Cells. *The Journal of cell biology* **174**, 359-368.

Zahraoui, A., Touchot, N., Chardin, P., and Tavitian, A. (1989). The Human Rab Genes Encode a Family of Gtp-Binding Proteins Related to Yeast Ypt1 and Sec4 Products Involved in Secretion. *The Journal of biological chemistry* **264**, 12394-12401.

Zajac, A., Sun, X., Zhang, J., and Guo, W. (2005). Cyclical Regulation of the Exocyst and Cell Polarity Determinants for Polarized Cell Growth. *Molecular biology of the cell* **16**, 1500-1512.

Zerial, M. and McBride, H. (2001). Rab Proteins as Membrane Organizers. *Nature reviews* **2**, 107-117.

Zhang, X., Bi, E., Novick, P., Du, L., Kozminski, K. G., Lipschutz, J. H., and Guo, W. (2001). Cdc42 Interacts with the Exocyst and Regulates Polarized Secretion. *The Journal of biological chemistry* **276**, 46745-46750.

Zhang, X., Wang, P., Gangar, A., Zhang, J., Brennwald, P., TerBush, D., and Guo, W. (2005a). Lethal Giant Larvae Proteins Interact with the Exocyst Complex and Are Involved in Polarized Exocytosis. *The Journal of cell biology* **170**, 273-283.

Zhang, X., Zajac, A., Zhang, J., Wang, P., Li, M., Murray, J., TerBush, D., and Guo, W. (2005b). The Critical Role of Exo84p in the Organization and Polarized Localization of the Exocyst Complex. *The Journal of biological chemistry* **280**, 20356-20364.

Zhang, X. M., Ellis, S., Sriratana, A., Mitchell, C. A., and Rowe, T. (2004). Sec15 Is an Effector for the Rab11 Gtpase in Mammalian Cells. *The Journal of biological chemistry* **279**, 43027-43034.

Zolov, S. N. and Lupashin, V. V. (2005). Cog3p Depletion Blocks Vesicle-Mediated Golgi Retrograde Trafficking in Hela Cells. *The Journal of cell biology* **168**, 747-759.

Zuo, X., Zhang, J., Zhang, Y., Hsu, S. C., Zhou, D., and Guo, W. (2006). Exo70 Interacts with the Arp2/3 Complex and Regulates Cell Migration. *Nature cell biology* **8**, 1383-1388.

Chapter 2

*Sc*Exo70 Expression, Purification, and X-ray Crystallography

ABSTRACT

The function of Exo70 in the exocyst and its interactions with Arpc1 and GTPases are not well understood. In this chapter X-ray crystallographic data for *Saccharomyces cerevisiae* Exo70 were collected and processed. In preparation for data collection, several different Exo70 constructs were created, over-expressed, purified, and crystallized. The most successful construct contains a deletion of the N-terminal 62 residues. It crystallized in 20 conditions, including two small, three-dimensional forms. One of these three-dimensional crystals yielded a high-resolution X-ray diffraction data set to 2.1Å.

INTRODUCTION

At the start of this project there was no published information on the structure of the exocyst or its subunits and little information on the interactions between these and other cellular components. The initial goal of this project was to learn more about the structure and function of the exocyst by employing X-ray crystallographic techniques. Early published literature hinted at the importance of the role played by Exo70, which has been well established over the last several years. It was hoped that structural information would add significantly to our knowledge of the function of this protein as a subunit of a tethering complex and a member of the cellular transport systems.

This study begins with exocyst subunits from the yeast *S. cerevisiae* as they were readily available and *S. cerevisiae* is considered to be a model eukaryotic organism (Skoneczna, 2006). The activities performed by the unicellular *S. cerevisiae* are simpler than multicellular organisms such as mammals, but many essential cell functions are conserved. The simplicity and well-studied nature of *S. cerevisiae* provides a eukaryotic system in which genetic manipulation, isolation of genes, and the study of individual proteins are all relatively easy to accomplish, making it a reasonable choice for initial work on a particular system. In particular, these features make it simple to knock out genes, as there are rarely pseudogenes (Cherry *et al.*, 1998; Esnault *et al.*, 2000; Mewes *et al.*, 2000; Spingola *et al.*, 1999) or multiple copies (Gu *et al.*, 2002) to consider, and the scarcity of introns (Dujon, 2006) makes genes easy to identify and clone. Also, the number of protein modifications in *S. cerevisiae* is fewer, making manipulation and study simpler once again. Certainly the most valuable information comes from the study of human and other mammalian organisms, but the value of the model yeast *S. cerevisiae* has proven itself to be a valuable tool and focus for most studies interested in eukaryotic functions and features.

MATERIALS & METHODS

Plasmids, *Escherichia coli* strains, and source DNA

The pSJ series of plasmids were employed in the constructs used in this work. pSJ3 is based on pET21a (Novagen) and includes a His_8 tag and a TEV protease cleavage site upstream of the BamHI restriction site as well as an insert containing the NdeI restriction site and the gene encoding a fragment of DnaK from $pGEX_{2t}$ (Novagen)

between the BamHI and EcoRI restriction sites. pSJ4 is based on pET30a (Novagen) and incorporates the same inserts used in pSJ3. pSJ5, pSJ6, and pSJ7 were created by insertion of a His_8 tag and TEV protease cleavage site upstream of the BamHI restriction site in pET32a, pET41a, and pET43.1a (Novagen), respectively. pSJ5 contains a Thioredoxin tag, pSJ6 contains a GST tag, and pSJ7 contains a Nus tag, each upstream of the inserted sequence. pSJ7D is a modified version of pSJ7 to include a shorter linker sequence between the Nus and His_8 tags in an attempt to improve expression and purification. pSJ3, pSJ5, pSJ7, and pSJ7D contain a Ampicilin antibiotic resistance gene; pSJ4 and pSJ6 contain a Kanamycin antibiotic resistance gene.

Wei Guo (Univeristy of Pennsylvania) provided all eight *S. cerevisiae* exocyst genes in various 2μ plasmids. For primers used in this study, see Table A.1.

Four strains of *Escherichia coli* were used in this work. DH5α was used for initial selection and amplification of plasmids. BL21(DE3) was used for expression of all native exocyst proteins. B834(DE3) was used for expression of all SeMet-substituted proteins. BL21(DE3) pLysS was used for the expression of TEV protease (see Appendix). Competent cell stocks were prepared using calcium-dependent methods (see Appendix).

Amplification and cloning

The Touchdown method of PCR (Don *et al.*, 1991) was used to amplify genes and insert restriction sites at the start and end of genes. It uses a series of cycles in which the annealing temperature is slowly decreased in four stages. The adaptation of the thermocycling protocol used for this work is as follows: 95°C for 3min, four cycles of stage 1, four cycles of stage 2, four cycles of stage 3, eighteen cycles of stage 4, and

10min at 72°C. Stage 1 includes 2min at 95°C followed by 1.5min at 66°C and 1.5min at 72°C. Stage 2 is like stage 1 except for a decreased annealing temperature of 63°C. Stage 3 is also like stage 1 except for a further decreased annealing temperature of 60°C. Stage 4 is again the same as stage 1 except for a decreased dissociation time of 1min, decreased annealing temperature of 55°C, and decreased annealing time of 1min. PCR products may be stored at -20°C if necessary before purification using a PCR purification kit (Qiagen).

Double restriction digestions were performed when both restriction enzymes performed sufficiently in the same reaction buffer following manufacturer protocol (New England Biolabs). 10 units of CIP (New England Biolabs) were added during the final 30min of digestion to vector digestion reactions. Products were purified by gel extraction on a 1.0% agarose gel using a gel extraction kit (Qiagen).

Restriction-digested plasmids and genes were ligated in a 16°C water bath overnight following manufacturer protocol (New England Biolabs). All ligation products and controls were transformed into ultra-competent DH5α *E. coli* (see Appendix) and plated on LB-agar plates containing the appropriate selective antibiotics using a standard protocol. Plasmids were isolated from expanded single-colony cultures by miniprep (Qiagen) and digested with the appropriate restriction enzymes as before, except for a period of 1hr and without the addition of CIP. Products were run on a 1.0% agarose gel to confirm the presence of both vector and gene. Construct DNA sequences were confirmed by DNA sequencing of a concentrated plasmid sent to the University of Michigan DNA Sequencing Core.

Protein expression

Plasmids containing genes of interest were transformed into BL21(DE3) *E. coli*, and colonies were tested for over-expression of the desired genes using a standard protocol and visualized by SDS-PAGE. After identification of an appropriate expression condition by test expression, large-scale expression was performed using these conditions. 5mL of a dense starter culture was added to each of six flasks containing 1L LB and the appropriate selective antibiotic and shaken at 37°C to an OD of approximately 0.375 at 595nm. The temperature was then shifted to the appropriate temperature, if necessary, before overnight expression with 400μM IPTG. Cell pellets were collected and pellets not immediately used for protein purification were stored at -80°C.

Protein purification

All steps were performed at 4°C or on ice. Cell pellets were thawed and 4-10g of cell pellet was resuspended in 50mL buffer A (20mM Tris pH8.0, 10% glycerol, 300mM NaCl, 0-20mM imidazole·HCl, 0.07% β-me, 20μg/mL PMSF, filtered at 45μm). Resuspended pellets were sonicated six times on ice for 30sec at power 8 on a Branson Sonifier 450 with 30sec breaks between pulses. Sonicated cells were centrifuged and the supernatant was collected.

A Ni^{2+}-NTA column was washed and equilibrated in buffer A. The sonicated supernatant was pumped over the column and washed 3 × with buffer A. In some cases the addition of a small amount of imidazole·HCl to buffer A improved washing. A linear gradient of buffer B (20mM Tris pH8.0, 10% glycerol, 300mM NaCl, 250mM imidazole·HCl, 0.07% β-me, 20μg/mL PMSF, filtered at 45μm) was applied from 0 to

100% and fractions with a strong UV signal were analyzed by SDS-PAGE. Fractions containing an appropriate concentration and purity of the desired protein were collected and concentrated by centrifugation in a Centriprep YM-10 concentrator (Amicon).

Concentrated protein was then dialyzed in a 10000 molecular weight cut-off dialysis bag with 1mL TEV protease (see Appendix) against 2L buffer C (20mM Tris pH8.0, 100mM NaCl, 0.07% β-me, 20μg/mL PMSF) overnight. The efficiency of the TEV protease digestion of the construct was analyzed by SDS-PAGE.

Dialyzed protein was exchanged into buffer D (20mM Tris pH8.0, 300mM NaCl, 0.07% β-me, 20μg/mL PMSF, filtered at 45μm) as before and loaded onto a second Ni^{2+}-NTA column equilibrated in buffer D. The column was washed with buffer D to elute untagged protein and washed with buffer B to remove column-bound material. Fractions containing an appropriate concentration and purity of the desired protein were identified by SDS-PAGE and were concentrated as before. In some cases a significant amount of contaminant also eluted with the desired protein. In this case, collected and concentrated protein was passed back over the same column re-equilibrated in buffer D and the process was repeated up to two more times in order to improve the purity of the desired protein.

Protein was exchanged into buffer E (20mM Tris pH8.0, 0-50mM NaCl, 1mM DTT, 1mM EDTA, filtered at 20μm) as before, then loaded onto a Source Q or Mono Q ion exchange column equilibrated in buffer E. Protein was eluted with a linear gradient of 0 to 40% buffer F (20mM Tris pH8.0, 1M NaCl, 1mM DTT, 1mM EDTA, filtered at 20μm) and fractions with a strong UV signal and fractions were analyzed by SDS-PAGE.

In some early purifications gel filtration was also performed in search of additional useful purification steps and to analyze the protein. Concentrated protein was

exchanged into buffer G (20mM Tris pH8.0, 100mM NaCl, 1mM DTT, 1mM EDTA, filtered at 20μm) before loading onto either a Superdex 75 or Superdex 200 column equilibrated in buffer G. 90mL of buffer G was passed over the column and fractions were identified by SDS-PAGE.

Purified protein was exchanged into crystallization buffer (20mM Tris pH8.0, 150mM NaCl, 1mM TCEP) and concentrated appropriately for crystallization. The concentration was estimated by comparison of the UV spectrum of the purified protein to its theoretical extinction coefficient before storage in 50-100μL aliquots at -80°C.

Limited Proteolysis and N-terminal sequencing

The proteases trypsin, chymotrypsin, or subtilisin are added to protein in either a concentration course or time course experiment. In a concentration course experiment 1mg/mL protein is mixed with a series of diluted protease in digestion buffer (20 mM Hepes, pH7.5, 200 mM NaCl, 10% glycerol, 1mM DTT) for 30min. The reaction is stopped with 2μg PMSF and digestion products are analyzed by SDS-PAGE. In a time course experiment a single concentration of protease is chosen, usually based on the results of a concentration course experiment, and reacted for varying periods of time, typically 30, 60, 90, 120, 240, and 360 min, and at varying temperatures. The reaction is stopped with PMSF and digestion products are analyzed by SDS-PAGE.

Limited proteolysis products can be analyzed by N-terminal sequencing. Unstained protein on an SDS-PAGE gel is electroblotted onto a PVDF membrane by the method of Matsudaira (Matsudaira, 1987) using a BioRad electroblotting apparatus. 80V was applied for 2hr. and the membrane is stained with Ponceau S. The band of interest is

excised from the membrane and sent to the Michigan State University Protein Sequencing Core for N-terminal sequencing.

Protein Crystallization

Protein crystallization was performed using the sitting drop method at two temperatures. Initial screening for crystal-producing conditions used the Hampton I and Hampton II screening kits (Hampton Research; Table A.2) and the X screen kit (Table A.3). 0.5-2μL of purified protein is mixed with an equal volume of precipitant from the kit in the presence of a reservoir containing 500μL precipitant, all sealed in the well of a 24-well sitting drop plate (Cryshem). These are stored in a 4°C or 20°C temperature-controlled room and observed for a period of days to months. Conditions producing crystals were optimized for crystal size, shape, and attachment to other crystals and surfaces using grid screens around the conditions of the original crystal. Drop size, protein:precipitant ratio, precipitant composition (buffer species, pH, PEG concentration, salt concentration, precipitant analogs), precipitant concentration, and protein concentration were all optimized. Once an optimal condition was identified, the Hampton Additive Screen kit (Hampton Research; Table A.4) was applied to search for any additional improvements in crystal attributes. Optimized crystals were harvested, equilibrated in a drop containing a cryo solution based on the growth conditions and selected to yield a transparent solid when frozen, and snap-frozen in liquid nitrogen.

RESULTS AND DISCUSSION

Identification of a *Sc*Exo70 construct as a candidate for structural studies

The first goal of this project was to identify one or more proteins of the exocyst complex as a candidate for structural studies. Plasmids containing each of the eight subunits of the *S. cerevisiae* exocyst were amplified by PCR and inserted into the pSJ4 vector. Initial analysis found that *Sc*Exo70 expressed well but insolubly in BL21(DE3) *Escherichia coli* at 37°C. Expression at 20°C and 16°C revealed increasing solubility with decreasing temperature. None of the other tested exocyst subunits expressed as well as *Sc*Exo70. Purification of *Sc*Exo70 from the pSJ4 construct was attempted, but it precipitated after concentration of the affinity-purified product. *Sc*Exo70 was then subcloned into pSJ5, pSJ6 and pSJ7. It expressed strongly but insolubly in pSJ5, weakly in pSJ6, and moderately in pSJ7 at 16°C.

Purification of *Sc*Exo70

*Sc*Exo70 was expressed from pSJ7 in BL21(DE3) *E. coli*. The protein eluted from a Ni^{2+}-NTA column with 75mM imidazole. Overnight dialysis at 4°C with TEV protease was sufficient to cleave >95% of protein with some precipitation apparent. The digested protein was passed over another Ni^{2+}-NTA column twice to remove >90% of the tags and TEV protease. Finally, *Sc*Exo70 eluted from a MonoQ ion exchange column with 150mM NaCl. The final yield was 7.0mg/L of culture. Purified protein was exchanged into crystallization buffer (20mM Tris pH8.0, 150mM NaCl, 1mM TCEP) at a concentration of 10.8mg/mL and stored in aliquots at -80°C. Protein stored at 4°C precipitated over a period of weeks. Further purification was not achieved by gel filtration. *Sc*Exo70 eluted from a Superdex 200 column as a single peak at a volume of 69mL, which corresponds to an apparent molecular weight of 140kDa. This result raised

the possibility that *Sc*Exo70 may form a homodimer, but this result was later interpreted as an artifact of the elongated shape of the molecule.

Crystallization and diffraction of *Sc*Exo70

The sitting drop method was employed with the Hampton Crystal Screens I and II and the X screen at 4°C and 20°C to screen *Sc*Exo70 for crystal formation. Only one condition in the X screen produced crystals, which appeared at 4°C within 24 hours and reached full size within 7 days. Optimized crystals grew in a 1:2 protein:precipitant ratio in a 3μL drop with a precipitant containing 150mM HEPES pH8.0, 18% ethylene glycol, 2% PEG 2000, and 10mM NaCl. Crystals were mostly <0.1mm rod-shaped crystals with an occasional larger "football-shaped" crystal (Figure 2.1). These diffracted to a maximum resolution of approximately 8Å on beamline 23-ID-D (General Medicine and Cancer Institutes CAT) at APS. Other crystals grown in a similar condition, but in the absence of PEG or in the presence of the additive NDSB 195, diffracted similarly.

Limited proteolysis of *Sc*Exo70

*Sc*Exo70 was digested with subtilisin, trypsin or chymotrypsin in a concentration course experiment. Analysis of digestion products by SDS-PAGE revealed that all three proteases produced an approximately 61kDa fragment as the largest product. The band produced by trypsin was the easiest to separate from other digestion products (Figure 2.2) and was excised for N-terminal sequencing, which identified Asn63 as the N-terminal residue of this fragment (*Sc*Exo70$_{\Delta 62}$). Subtilisin digestion also produced two strong fragments, one of which was also produced by trypsin. These bands were approximately

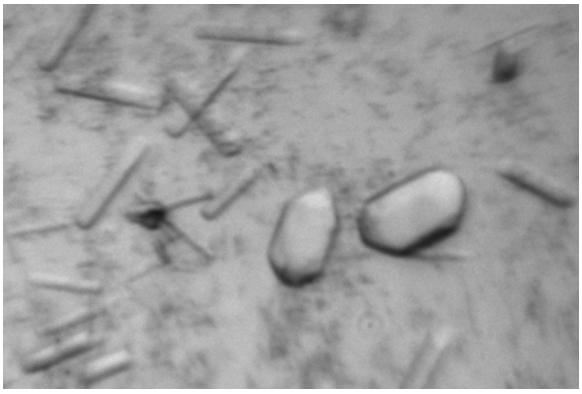

Figure 2.1: *Sc*Exo70 crystals

A photograph of *Sc*Exo70 crystals grown in a precipitant containing approximately 150mM HEPES pH8.0, 18% ethylene glycol, 2% PEG 2000, and 10mM NaCl. Several rod-shaped and two football-shaped crystals can be seen in the presence of light precipitation.

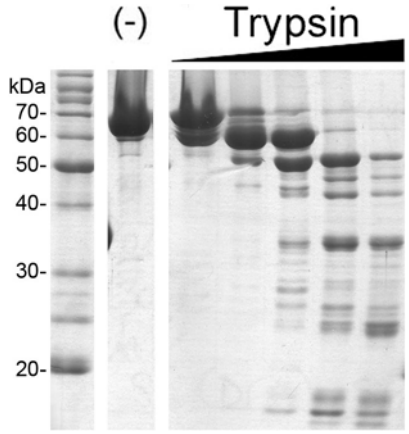

Figure 2.2: Limited proteolysis of *Sc*Exo70

A photograph of a 12% SDS-PAGE gel stained with Coomassie blue.
Left lane: Benchmark standard (Invitrogen) with 20-70kDa bands labeled.
(-): Purified *Sc*Exo70 treated with no trypsin protease.
Trypsin lanes: From left to right, *Sc*Exo70 treated with a 1:1000, 1:300, 1:100, 1:30, or 1:10 molar ratio of trypsin:*Sc*Exo70 for 30 minutes on ice.

50kDa and 35kDa. Constructs lacking the first 168 (*Sc*Exo70$_{\Delta 168}$) and 294 residues (*Sc*Exo70$_{\Delta 294}$) were designed based on these sizes, secondary structure prediction, and the location of subtilisin-susceptible sites in the primary sequence identified by the ExPASy PeptideCutter tool (Gasteiger *et al.*, 2005). Both of these constructs exhibited soluble expression in pSJ7 at 15°C. *Sc*Exo70$_{\Delta 168}$ precipitated heavily during purification. *Sc*Exo70$_{\Delta 294}$ also precipitated to a lesser degree and a small amount was successfully purified, but no conditions were found to produce crystals.

Preparation and purification of *Sc*Exo70$_{\Delta 62}$

The *Sc*Exo70$_{\Delta 62}$ gene was amplified by PCR and inserted into the pSJ7D vector. Protein expression in BL21(DE3) *E. coli* was strong and soluble at 37°C. The protein eluted from a Ni^{2+}-NTA column with 75mM imidazole (Figure 2.3). Overnight dialysis with TEV protease was sufficient to cleave >95% of protein. Digested protein was passed over a second Ni^{2+}-NTA column twice for improved purification and removal of >95% of the tag and TEV protease. Finally, *Sc*Exo70$_{\Delta 62}$ eluted from a MonoQ ion exchange column with 150mM NaCl. Final yield was estimated at 12.0mg/L of culture. Protein was exchanged into crystallization buffer at a concentration of 15.8mg/mL and stored in aliquots at -80°C.

Crystallization of *Sc*Exo70$_{\Delta 62}$

*Sc*Exo70$_{\Delta 62}$ was screened for crystal formation with the Hampton Crystal Screens I and II at 4°C and 20°C and the X screen at 4°C using the sitting drop method. The

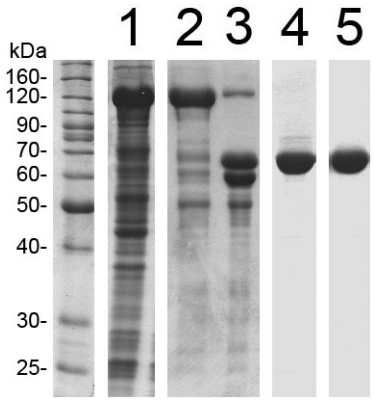

Figure 2.3: Purification of *Sc*Exo70$_{\Delta 62}$

A photograph of a 12% SDS-PAGE gel stained with Coomassie blue. 120kDa bands represent MBP-tagged *Sc*Exo70, 70kDa bands represent untagged *Sc*Exo70, and the 60kDa band represents the MBP tag.
Left lane: Benchmark standard (Invitrogen) with 25-160kDa bands labeled.
1: Soluble protein from sonicated *E. coli*, diluted 1:4 in buffer A (see text).
2: Protein after two passes over a Ni^{2+}-NTA affinity column.
3: Protein after overnight digestion with TEV protease.
4: Protein after passage over a second Ni^{2+}-NTA column.
5: Final purified *Sc*Exo70$_{\Delta 62}$ after passage over a MonoQ ion exchange column.

Hampton screens produced crystals in five conditions at 4°C and two at 20°C, and the X screen yielded thirteen at 4°C (Table 2.1). Some crystals appeared as quickly as overnight while others required up to three weeks to form. Most of these crystals grew from precipitants of various PEG/salt conditions, a few of them appeared in salt only conditions, and one appeared in an MPD/PEG condition. About half of the conditions, mostly PEG/salt conditions, produced clusters of flat, plate-like crystals of various sizes and shapes (Figure 2.4a,b). Four PEG/salt conditions produced fast-growing clusters of rod-shaped crystals of various sizes and lengths (Figure 2.4c,d). Limited success was had in attempts to improve size and prevent clustering of these crystals. The optimized condition for producing crystals of this type was 100mM Tris pH8.5, 16% PEG 8000, 200mM $CaCl_2$, 20°C. The Hampton Additive Screen (Hampton Research) yielded one additive, spermine·4HCl, which produced long, thick clustered rods that could potentially be broken away from the rest of the cluster (Figure 2.4e). These large crystals could not be repeated and were found to be soft when harvested. A third type of crystal observed in two salt-only conditions was a plentiful small, unclustered needle (Figure 2.4f). No improvement in size or shape was achieved. A fourth type of crystal grew in two conditions and yielded small three-dimensional crystals. The MPD/PEG condition produced small, nearly square 3D tablet-shaped crystals, but these could not be reproduced. The PEG/salt condition produced slow-growing, small 3D trapezoidal tablet-shaped crystals with thick, clean edges (Figure 2.4g). These crystals appeared in about ten days and continued to grow for an additional seven to fourteen days. They grew optimally at 4°C in a 2µL drop with a 1:1 ratio of protein to precipitant and a precipitant composition of 100mM glycine pH9.5, 20.5% PEG 300, 200mM LiCl. Two conditions in

Table 2.1: *Sc*Exo70$_{\Delta 62}$ crystals produced by initial screening

Crystal Type	Appearance Time (days)	Screen Condition
Clustered plates	8 – 18	0.1M sodium cacodylate pH5.5, 8% PEG 8000, 0.2M LiCl, 4°C
Clustered plates	8 – 18	0.1M sodium cacodylate pH5.5, 16% PEG 8000, 4°C
Clustered plates	1 – 3	0.1M sodium cacodylate pH5.5, 16% PEG 8000, 0.2M $(NH_4)_2SO_4$, 4°C
Clustered plates	1 – 2	0.1M HEPES pH7.5, 16% PEG 8000, 0.2M $(NH_4)_2SO_4$, 4°C
Clustered plates	1	0.1M Glycine pH9.5, 16% PEG 8000, 0.2M $(NH_4)_2SO_4$, 4°C
Clustered plates	8 – 18	0.1M MES pH6.5, 12% PEG 20000, 4°C
Clustered plates	7 – 17	0.1M HEPES pH7.5, 8% PEG 2000, 4°C
Clustered plates	2 – 6	0.1M HEPES pH7.5, 8% PEG 8000, 0.2M LiCl, 4°C
Clustered plates	2 – 6	0.1M Glycine pH9.5, 8% PEG 8000, 0.2M LiCl, 4°C
Clustered plates	1 – 3	0.1M Bicine pH9.0, 30% PEG MME 550, 0.1M NaCl, 4°C
Clustered rods	2	0.1M Glycine pH9.5, 16% PEG 8000, 0.2M $MgCl_2$, 4°C
Clustered rods	1 – 3	0.1M sodium cacodylate pH6.5, 20% PEG 8000, 0.2M magnesium acetate, 20°C
Clustered rods	1 – 3	0.1M sodium cacodylate pH6.5, 18% PEG 8000, 0.2M calcium acetate, 20°C
Clustered rods	1 – 3	0.1M sodium cacodylate pH6.5, 18% PEG 8000, 0.2M calcium acetate, 4°C
Single needles	8 – 18	0.1M sodium citrate pH5.6, 1M Li_2SO_4, 0.5M $(NH_4)_2SO_4$, 4°C
Single needles	8 – 18	0.1M Tris HCl pH8.5, 2M $NH_4H_2PO_4$, 4°C
Spherulites	2	0.1M Glycine pH9.5, 16% PEG 8000, 0.2M LiCl, 4°C
Spherulites	7 – 10	0.1M Glycine pH9.5, 20% PEG 600, 0.2M LiCl, 4°C
Single 3D	2 – 6	0.1M Glycine pH9.5, 20% MPD, 5% PEG 8000, 4°C
Single 3D	10 – 18	0.1M Glycine pH9.5, 20% PEG 300, 0.2M LiCl, 4°C

Figure 2.4: *Sc*Exo70$_{\Delta 62}$ crystals

Photographs of several different forms of *Sc*Exo70$_{\Delta 62}$ crystals, each grown at 4°C unless otherwise noted.
A: Plate clusters grown in 100mM glycine pH9.5, 13% PEG 8000, and 200mM NaCl.
B: Plate clusters grown in 100mM glycine pH9.5, 13% PEG 8000, and 200mM $CaCl_2$.
C: Rod clusters grown in 100mM glycine pH9.5, 15% PEG 8000, and 200mM Li_2SO_4.
D: Rod clusters grown in 100mM tris pH8.5, 15% PEG 20000, and 200mM $CaCl_2$.
E: Irrepreoducible rod clusters grown in 100mM tris pH8.5, 16% PEG 8000, 200mM $CaCl_2$, and 100mM spermine·4HCl at 20°C.
F: Individual needles grown in 100mM tris pH8.5 and 2M $(NH_4)H_2PO_4$.
G: Three-dimensional trapezoids grown in 100mM glycine pH9.5, 20% PEG 300, and 200mM LiCl.

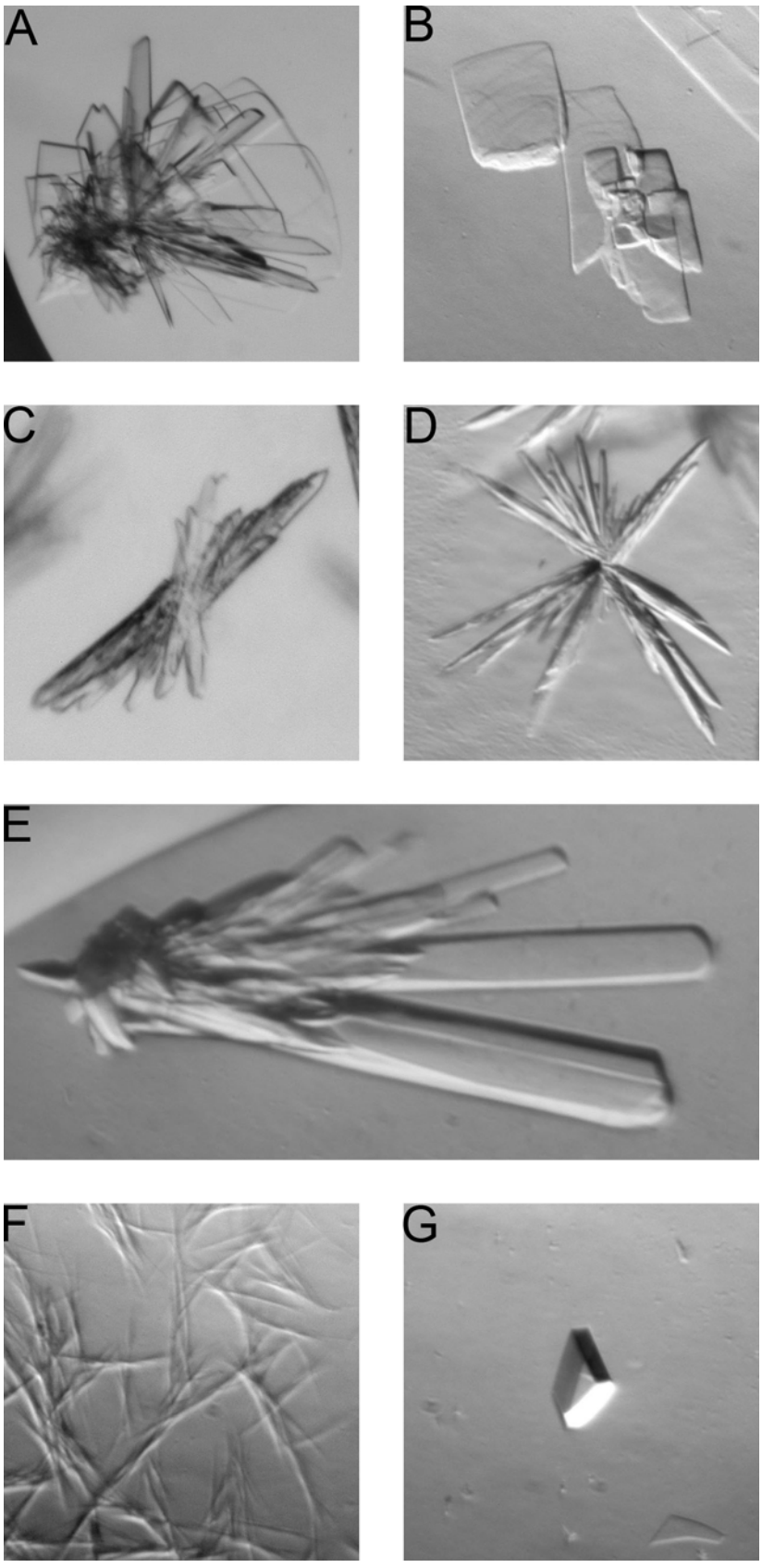
A
B
C
D
E
F
G

the screen similar to this condition produced spherulites that were a degenerate form of this three-dimensional crystal. Crystals were transferred into a cryo solution (100mM glycine pH9.5, 40% PEG 300, 200mM LiCl) and snap-frozen in liquid nitrogen.

X-ray diffraction, data collection, and processing of *Sc*Exo70$_{\Delta 62}$

Diffraction to a resolution of 2.3Å and a mosaicity of 0.3° was achieved at beamline 21 (Life Sciences CAT) at APS from the three-dimensional crystals of *Sc*Exo70$_{\Delta 62}$. The space group of the crystal was determined to be $P2_12_12_1$ with unit cell dimensions a = 45.54Å, b = 60.07Å, and c = 218.06Å ($\alpha = \beta = \gamma = 90°$) using d*TREK (Pflugrath, 1999). The asymmetric unit was calculated to contain one molecule.

Phase determination of *Sc*Exo70$_{\Delta 62}$

B834(DE3) *E. coli* containing the *Sc*Exo70$_{\Delta 62}$ pSJ7D construct was grown in a minimal MOPS media substituting SeMet for Met (see Appendix) and purified using a method identical to that used for native *Sc*Exo70$_{\Delta 62}$ with a yield of 4.2mg/L of culture. SeMet-substituted protein crystallized in the same form in the same condition, with optimal growth requiring 22% PEG 300. SeMet-substituted crystals grew faster than native crystals, appearing within three days and reaching full size in 5-10 days. These crystals were similarly prepared for diffraction. Howard Robinson, a staff scientist at NLS, achieved diffraction to a resolution of 2.1Å at beamline X29A at NLS. He collected data sets at the experimentally determined peak, inflection, and remote wavelengths of selenium in this protein. Data were processed using HKL2000 (Otwinowski and Minor, 1997), revealing the same $P2_12_12_1$ space group as the native protein with similar unit cell

dimensions a = 45.28Å, b = 58.78Å, and c = 222.73Å ($\alpha = \beta = \gamma = 90°$). All thirteen expected selenium sites in the asymmetric unit were located, and phases were calculated and refined, using SOLVE (Terwilliger and Berendzen, 1999). Although sufficient data were collected to use the MAD method (Hendrickson and Ogata, 1997), experimental phases were determined using the SAD method because the electron density map it produced had improved definition (Table 2.2).

Model building and refinement of the *Sc*Exo70$_{\Delta 62}$ structure

Solvent flattening was performed using RESOLVE (Terwilliger, 2000) and the initial model was built using ARP/wARP (Vonrhein *et al.*, 2006). The remainder of the model was built based on the known locations of selenium atoms using O (Jones *et al.*, 1991) and CNS (Brunger *et al.*, 1998) was used to refine the model and its B factors. Initial refinement consisted of several iterations of simulated annealing by the MLHL target function using amplitudes and phase probability distribution, grouped B factor refinement, and model rebuilding using O with data up to a resolution of 2.4Å. Later rounds of refinement consisted of iterations of simulated annealing by the MLF target function using amplitudes, individual B factor refinement, and model rebuilding using O with all data up to a resolution of 2.1Å. $3F_o$-$2F_c$ and F_o-F_c maps were calculated using CNS to aid model building and water placement. The final model consists of residues 67-223 and 232-623 and 111 water molecules. Residues 63-66, 224-231, two residues at the N-terminus left over from the TEV cleavage site, and a small number of side chains were not included in the final model due to missing or incomplete electron density. The final

Table 2.2: Data, phasing, and refinement statistics for *Sc*Exo70$_{\Delta 62}$

	***Sc*Exo70$_{\Delta 62}$**
Data collection	
Space group	$P2_12_12_1$
Cell dimensions [*a*, *b*, *c* (Å)]	45.54, 60.07, 222.73
Resolution (Å)	50.0-2.1 (2.18-2.10)
Wavelength (Å)	0.9792
Completeness (%)	95.4 (74.0)
Redundancy	6.3 (3.9)
$I/\sigma I$	26.5 (2.1)
R_{merge} (%)	8.6 (35.7)
Phasing	
Phasing power	
Acentric anomolous	1.792
Figure of Merit	
Centric	0.136
Acentric	0.331
After density modification	0.795
Refinement	
Resolution (Å)	50.0-2.1
No. reflections in working set	32281
No. reflections in test set	1632
R_{work}/R_{free} (%)	24.1/27.1
No. of atoms	
Protein	4304
Water	111
Average *B*-factors	
Protein	44.3
Water	40.1
Rms deviations from ideality	
Bond lengths (Å)	0.006
Bond angles (deg.)	1.1
Ramachandran plot	
% in most favored regions	93.3
% in additional allowed regions	5.9
% in generously allowed regions	0.8

Highest resolution shell shown in parentheses.

model and structure factors were deposited into the RCSB PDB with the PDB identified 2PFV. Refinement statistics can be found in Table 2.2.

REFERENCES

Ausubel, F. M., Brent, R., Kingston, R. E., Moore, D. D., Seidman, J. G., Smith, J. A., Struhl, K., Albright, L. M., Coen, D. M., and Varki, A., Eds. (1998). Current Protocols in Molecular Biology. Vol. 1. Current Protocols. Edited by Chanda, V. B. 4 vols: John Wiley & Sons, Inc.

Brunger, A. T., Adams, P. D., Clore, G. M., DeLano, W. L., Gros, P., Grosse-Kunstleve, R. W., Jiang, J. S., Kuszewski, J., Nilges, M., Pannu, N. S., Read, R. J., Rice, L. M., Simonson, T., and Warren, G. L. (1998). Crystallography & Nmr System: A New Software Suite for Macromolecular Structure Determination. *Acta crystallographica* **54**, 905-921.

Cherry, J. M., Adler, C., Ball, C., Chervitz, S. A., Dwight, S. S., Hester, E. T., Jia, Y., Juvik, G., Roe, T., Schroeder, M., Weng, S., and Botstein, D. (1998). Sgd: Saccharomyces Genome Database. *Nucleic acids research* **26**, 73-79.

Don, R. H., Cox, P. T., Wainwright, B. J., Baker, K., and Mattick, J. S. (1991). 'Touchdown' Pcr to Circumvent Spurious Priming During Gene Amplification. *Nucleic acids research* **19**, 4008.

Dujon, B. (2006). Yeasts Illustrate the Molecular Mechanisms of Eukaryotic Genome Evolution. *Trends Genet* **22**, 375-387.

Esnault, C., Maestre, J., and Heidmann, T. (2000). Human Line Retrotransposons Generate Processed Pseudogenes. *Nature genetics* **24**, 363-367.

Gasteiger, E., Hoogland, C., Gattiker, A., Duvaud, S., Wilkins, M. R., Appel, R. D., and Bairoch, A. (2005). Protein Identification and Analysis Tools on the Expasy Server. In *The Proteomics Protocols Handbook* (Walker, J. M., ed.), pp. 1016. Humana Press.

Gu, Z., Cavalcanti, A., Chen, F. C., Bouman, P., and Li, W. H. (2002). Extent of Gene Duplication in the Genomes of Drosophila, Nematode, and Yeast. *Molecular biology and evolution* **19**, 256-262.

Hendrickson, W. A. and Ogata, C. M. (1997). Phase Determination from Multiwavelength Anomalous Diffraction Measurements. *Methods in enzymology* **276**, 494-523.

Jones, T. A., Zou, J. Y., Cowan, S. W., and Kjeldgaard, M. (1991). Improved Methods for Building Protein Models in Electron Density Maps and the Location of Errors in These Models. *Acta Crystallogr A* **47 (Pt 2)**, 110-119.

Matsudaira, P. (1987). Sequence from Picomole Quantities of Proteins Electroblotted onto Polyvinylidene Difluoride Membranes. *The Journal of biological chemistry* **262**, 10035-10038.

Mewes, H. W., Frishman, D., Gruber, C., Geier, B., Haase, D., Kaps, A., Lemcke, K., Mannhaupt, G., Pfeiffer, F., Schuller, C., Stocker, S., and Weil, B. (2000). Mips: A Database for Genomes and Protein Sequences. *Nucleic acids research* **28**, 37-40.

Otwinowski, Z. and Minor, W. (1997). Processing of X-Ray Diffraction Data Collected in Oscillation Mode. *Methods in enzymology* **276**, 307-326.

Pflugrath, J. W. (1999). The Finer Things in X-Ray Diffraction Data Collection. *Acta crystallographica* **55**, 1718-1725.

Skoneczna, A. (2006). [Decade of Genomics--Methods for Genome Investigation in Yeast Saccharomyces Cerevisiae]. *Postepy biochemii* **52**, 435-447.

Spingola, M., Grate, L., Haussler, D., and Ares, M., Jr. (1999). Genome-Wide Bioinformatic and Molecular Analysis of Introns in Saccharomyces Cerevisiae. *RNA (New York, NY* **5**, 221-234.

Terwilliger, T. C. and Berendzen, J. (1999). Automated Mad and Mir Structure Solution. *Acta crystallographica* **55**, 849-861.

Terwilliger, T. C. (2000). Maximum-Likelihood Density Modification. *Acta crystallographica* **56**, 965-972.

Vonrhein, C., Blanc, E., Roversi, P., and Bricogne, G. (2006). Automated Structure Solution with Autosharp. *Methods in molecular biology (Clifton, NJ* **364**, 215-230.

Chapter 3

*Mm*Exo70 Expression, Purification, and X-ray Crystallography

ABSTRACT

In this chapter additional structural information is sought to investigate the structure and function relationship in mammalian Exo70, enabling a comparison with *Sc*Exo70$_{\Delta 62}$. In preparation for X-ray crystallographic data collection, several different mammalian Exo70 constructs are created, over-expressed, purified, and crystallized. The most successful mammalian construct contains a deletion of the N-terminal 84 residues of *Mus musculus* Exo70. It crystallized initially in eight conditions, one of which was optimized to yield a 2.25Å resolution data set.

INTRODUCTION

At the start of this work on mammalian Exo70 several publications had determined structural information for several exocyst subunits, and more details of the interactions between these and other cellular components had been revealed. Additional roles for Exo70 specific to mammals had been detected, increasing interest in this mammalian Exo70. None of the available structural information was from a mammalian exocyst subunit, and no orthologous structural comparisons had yet been made. The initial goal of this stage of the project was to explore the structure and function of

mammalian Exo70 using X-ray crystallographic techniques and compare and contrast it with the *Sc*Exo70$_{\Delta 62}$ structure.

Although many cellular processes are well conserved in eukaryotes, those in mammals tend to contain additional levels of complexity not present in *S. cerevisiae*. Multiple tissue types exist in animals that can each express different forms of the same molecule in order to perform various tissue-specific functions. The three different forms of Exo70 that have been identified in mouse are an example, with additional residues in Exo70 likely performing brain-specific functions. (Carninci *et al.*, 2005; Guo *et al.*, 1997; Strausberg *et al.*, 2002). The form of *Mm*Exo70 studied here is the shortest form and has only been identified in tissues other than the brain. Structural information of this shorter form can serve as a basis for the understanding of the basic conserved functions of all forms of Exo70.

MATERIALS & METHODS

Plasmids, *Escherichia coli* strains, and source DNA

The pSJ series of plasmids were employed in the constructs used in this work. pSJ3, pSJ5, pSJ6, and pSJ7 are used here and are described in Chapter 2. pSJ2 is based on pET21a (Novagen) and includes a His$_8$ tag and TEV protease cleavage site upstream of the BamHI restriction site. pSJ8 was created by inserting a PCR product containing the MalE gene from pMALC2 (New England Biolabs) between the NdeI and KpnI restriction sites and the His$_8$ tag and TEV protease cleavage site from pSJ6 between the KpnI and XhoI restriction sites. pSJ8 contains an MBP tag upstream of the His$_8$ tag. pSJ6D and pSJ7D are versions of pSJ6 and pSJ7, respectively, modified to include a shorter linker

sequence between the large protein tags and His_8 tags. pSJ2, pSJ7D, and pSJ8 contain an Ampicilin resistance gene and pSJ6D contains a Kanamycin resistance gene. The four strains of *Escherichia coli* described in Chapter 2 are used again in this chapter.

Alan Saltiel (University of Michigan) provided a plasmid containing the cDNA of Exo70 from *Mus musculus*. Wei Guo (University of Pennsylvania) provided a plasmid containing the cDNA of Exo70 from *Rattus norvegicus*. For primers used in this study, see Table A.1.

Amplification and cloning

Two methods of PCR were implemented to optimize amplification of genes and insert restriction sites at the start and end of genes. The thermocycling protocol for a standard method of PCR begins with 5min at 95°C; is followed by 30 cycles of 1min at 95°C, 1min at 55°C, and 3min at 72°C; and concludes with 10min at 72°C. The Touchdown method of PCR (Don *et al.*, 1991) uses a series of cycles in which the annealing temperature is slowly decreased in four stages and is described in Chapter 2. PCR products are stored at -20°C if necessary before purification using a PCR purification kit (Qiagen). Restriction digestions and ligations were performed as described in Chapter 2. Plasmids were isolated from culture by miniprep (Qiagen), test digested with the appropriate restriction enzymes, and DNA was sequenced as described in Chapter 2.

Protein expression and purification

Protein was expressed as described in Chapter 2. Protein was purified as described in Chapter 2 except slightly different buffer compositions were used. Buffer A contained 50mM Tris pH8.0, 10% glycerol, 300mM NaCl, 0-10mM imidazole·HCl, 0.07% β-me, 20μg/mL PMSF, and was filtered at 45μm. Buffer B contained 50mM Tris pH8.0, 10% glycerol, 300mM NaCl, 250mM imidazole·HCl, 0.07% β-me, 20μg/mL PMSF, and was filtered at 45μm. Buffer C contained 50mM Tris pH8.0, 100mM NaCl, 0.07% β-me, 20μg/mL PMSF, and was not filtered. Buffer D contained 50mM Tris pH8.0, 300mM NaCl, 0.07% β-me, 20μg/mL PMSF, and was filtered at 45μm. Buffer E contained 50mM Tris pH8.0, 1mM DTT, 1mM EDTA, and was filtered at 20μm. Buffer F contained 50mM Tris pH8.0, 1M NaCl, 1mM DTT, 1mM EDTA, and was filtered at 20μm. Buffer G contained 50mM Tris pH8.0, 100mM NaCl, 1mM DTT, 1mM EDTA, filtered at 20μm. Crystallization buffer contained 50mM Tris pH8.0, 100mM NaCl, 1mM TCEP, and was filtered at 20μm.

Limited proteolysis, N-terminal sequencing, crystallization, and streak seeding

Limited proteolysis, N-terminal sequencing, and protein crystallization were each performed as described in Chapter 2. Streak seeding is a technique useful for increasing nucleation rate, the first and often limiting step of crystal growth. Microcrystals were created by crushing several small crystals of the desired crystal form in crystallization buffer using the mortar and pestle from a Reacti-ware micro tissue grinder kit (Pierce). A Chinese human head hair or house cat whisker was used to distribute the microcrystals to freshly set-up crystallization drops by gently dragging the hair dipped in the microcrystal solution across the drop surface immediately before sealing the well.

RESULTS AND DISCUSSION

Preparation, Purification and crystallization of *Mm*Exo70

The Exo70 genes from the rat *Rattus norvegicus* and the mouse *M. musculus* were amplified by PCR from cDNA. *Rn*Exo70 was not found to express while *Mm*Exo70 expressed weakly in pSJ5. The poor expression of *Mm*Exo70 was compounded by its weak binding to a Ni^{2+}-NTA column, as it eluted over a wide, low peak. Overnight dialysis at 4°C with TEV protease was sufficient to cleave >98% of protein and >95% of the tag was removed by two passages over another Ni^{2+}-NTA column. Some TEV-digested *Mm*Exo70 was retained on the column, resulting in a further loss of protein. Finally, *Mm*Exo70 was passed over a Source Q ion exchange column and was eluted with NaCl over a wide, low peak with a lagging shoulder containing 50-70kDa contaminants. Further passage of contaminated fractions over a Mono Q ion exchange column shifted the protein away from the shoulder, increasing yield. Final yield was approximately 1mg/L of culture, and protein was placed in crystallization buffer at a concentration of 9.62mg/mL. Due to poor yield, only the X screen was used at 4°C to search for crystallization conditions. Most conditions precipitated quickly, suggesting that full-length *Mm*Exo70 is not a good candidate for crystallization.

Limited proteolysis of *Mm*Exo70

*Mm*Exo70 was digested with subtilisin, trypsin or chymotrypsin in a concentration course experiment. All proteases produced stable fragments at approximately 65kDa, 46kDa, 31kDa, and 25kDa at increasing concentrations of

protease. The 65kDa fragment was of the greatest interest, as it was the largest and similar in relative size to *Sc*Exo70$_{\Delta 62}$. The band produced by subtilisin was the easiest to separate from undigested *Mm*Exo70 (Figure 3.1) and was excised for N-terminal sequencing, which identified Asp85 as the N-terminal residue of this fragment (*Mm*Exo70$_{\Delta 84}$). A second construct lacking the first 75 residues (*Mm*Exo70$_{\Delta 75}$) corresponds to the successfully crystallized *Sc*Exo70$_{\Delta 62}$ construct (see Chapter 2). This was based on an early alignment of Exo70 that was validated by the presence of a short stretch of conserved residues in this region. Expression of *Mm*Exo70$_{\Delta 75}$ in pSJ5 at 16°C was soluble and of greater quantity than *Mm*Exo70 and it was purified to low yield, but no useful crystallization conditions were identified.

Preparation and purification of *Mm*Exo70$_{\Delta 84}$

The *Mm*Exo70$_{\Delta 84}$ gene was amplified by PCR. A pSJ5 construct expressed a moderate quantity of protein that was greater than both *Mm*Exo70 and *Mm*Exo70$_{\Delta 75}$ at 16°C. Expression from a pSJ2 construct was soluble and of an even greater quantity. The protein eluted from a Ni^{2+}-NTA column with 115mM imidazole (Figure 3.2). Overnight dialysis at 4°C with TEV protease was sufficient to cleave >98% of the protein. The digested product was passed over a second Ni^{2+}-NTA column for removal of >95% of the tag and TEV protease. Finally, *Mm*Exo70$_{\Delta 84}$ eluted from a Source Q ion exchange column with 55mM NaCl. Final yield was estimated at 13.0mg/L of culture. Protein was stored in crystallization buffer at a concentration of 14.5mg/mL and stored at -80°C.

Crystallization and diffraction screening of *Mm*Exo70$_{\Delta 84}$

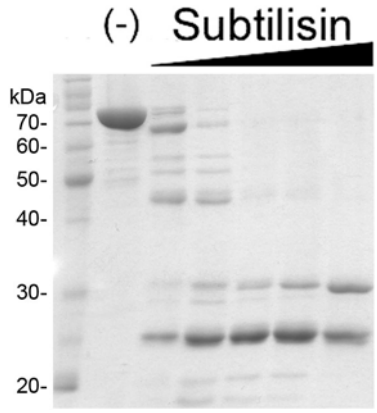

Figure 3.1: Limited proteolysis of *Mm*Exo70

A photograph of a 12% SDS-PAGE gel stained with Coomassie blue.
Left lane: Benchmark standard (Invitrogen) with 20-70kDa bands labeled.
(-): Purified *Mm*Exo70 treated with no subtilisin protease.
Subtilisin lanes: From left to right, *Mm*Exo70 treated with a 1:289, 1:86, 1:29, 1:9, or 1:3 molar ratio of subtilisin:*Mm*Exo70.

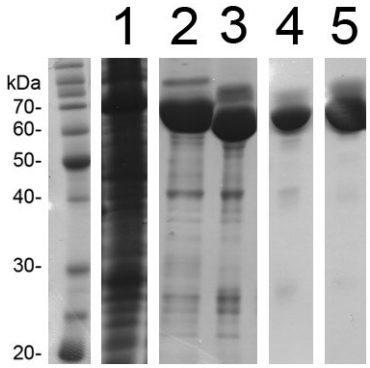

Figure 3.2: Purification of *Mm*Exo70$_{\Delta 84}$

A photograph of a 12% SDS-PAGE gel stained with Coomassie blue. 70kDa bands represent His$_8$-tagged *Mm*Exo70$_{\Delta 84}$ and 60kDa bands represent untagged *Mm*Exo70$_{\Delta 84}$.
Left lane: Benchmark standard (Invitrogen) with 20-70kDa bands labeled.
1: Soluble protein from sonicated *E. coli*, diluted 1:2 in buffer A (see text).
2: Protein after passage over a Ni^{2+}-NTA affinity column.
3: Protein after overnight digestion with TEV protease.
4: Protein after passage over a second Ni^{2+}-NTA column.
5: Final purified *Mm*Exo70$_{\Delta 84}$ after passage over a SourceQ ion exchange column.

*Mm*Exo70$_{\Delta 84}$ was screened for crystal formation with the Hampton Crystal Screens I and II and the X screen at 4°C and 20°C using the sitting drop method. The Hampton screens produced crystals in two conditions at 20°C that appeared within 24 hours and the X screen yielded six conditions at 4°C (Table 3.1). The X screen produced clustered rods or needles in 1-6 days, but no conditions could be found to improve size and prevent clustering of these crystals. The Hampton screens produced hexagonal plates at 20°C that formed within 24 hours, but optimization only increased the size of the plate and not its thickness. In addition, the diffraction of these crystals was found to only reach a resolution of about 8Å. The Hampton screens also produced small three-dimensional crystals at 20°C that formed within 24 hours and were only sometimes found in clusters. Optimization was able to improve size, and an additive screen revealed a number of potentially useful additives, including $MgCl_2$, urea, Cys, EDTA sodium salt, spermidine, trimethylamine hydrochloride, and NDSB 195. Some of these had an effect on the size and/or shape of the crystal while most had no visible effect (Figure 3.3). These crystals were difficult to duplicate, so two different techniques were employed to improve reproducibility. First, the composition of the precipitant added to the protein drop was changed from that of the well solution to alter crystal growth kinetics. Second, streak seeding was employed to improve the nucleation rate. While these crystals appeared within 24 hours, they continued to grow for up to 14 days. A sticky film would form on all surfaces during and after crystal growth, and after about fourteen days the film would begin to impede crystal harvesting by adhering the crystals to surfaces, resulting in increased crystal breakage and leaving sticky film on the surface of crystals. Ultimately, crystals were harvested between 10-13 days to maximize growth and minimize the effect

Table 3.1: *Mm*Exo70$_{\Delta 84}$ crystals produced by initial screening

Crystal Type	Appearance Time (days)	Screen Condition
Clustered rods	4 – 6	0.1M HEPES pH7.5, 16% PEG 8000, 0.2M LiCl, 4°C
Clustered rods	1 – 3	0.1M HEPES pH7.5, 10% 2-propanol, 4°C
Clustered rods	4 – 6	0.1M glycine pH9.5, 8% PEG 2000, 10% ethanol, 4°C
Clustered rods	4 – 6	0.1M glycine pH9.5, 20% MPD, 4°C
Clustered rods	1 – 3	0.1M glycine pH.5, 10% 2-propanol, 4°C
Clustered rods	4 – 6	1.5M sodium tartrate pH7.0, 4°C
Single 3D	1	0.1M MES pH6.5, 12% PEG 20000, 20°C
Single 3D	1	0.1M HEPES pH7.5, 10% PEG 8000, 8% ethylene glycol, 4°C

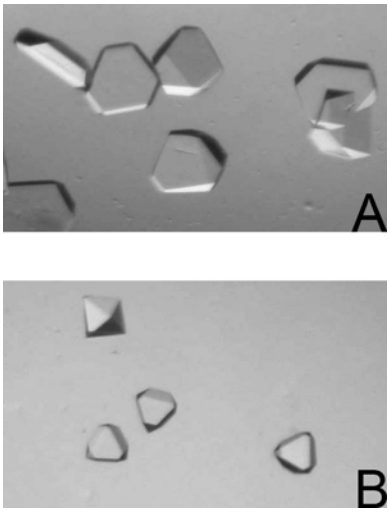

Figure 3.3: *Mm*Exo70$_{\Delta 84}$ crystals

Photographs of two different forms of *Mm*Exo70$_{\Delta 84}$ crystals, both grown at 20°C.
A: Hexagonal three-dimensional crystals grown in 100mM hepes pH7.5, 9% PEG 8000, 10% ethylene glycol, and 100mM EDTA sodium salt. Crystals grown without EDTA sodium salt look identical and also grow flat, on edge, individually, and in clusters as shown.
B: Octahedral three-dimensional crystals grown in 100mM hepes pH7.5, 9% PEG 8000, 7% ethylene glycol, and 100mM $MgCl_2 \cdot 6H_20$.

of the film. For crystal harvesting, cryo solution was added directly to the drop, the film was removed from the surface of the drop using microtools, crystals were removed from clusters and surfaces as intact as possible, and crystals were soaked in cryo solution for more than 1min before snap-freezing in liquid nitrogen on a nylon loop. Except for snap-freezing, crystals were moved by pipette because some crystals were believed to have cracked as a result of exposure to air during transfer on a nylon loop. The optimized *Mm*Exo70$_{\Delta 84}$ condition used a well solution containing 8.5% PEG 8000, 10% ethylene glycol, and 100mM HEPES pH7.5 and a drop precipitant (mixed 1:1 with protein) containing 5.5% PEG 8000, 10% ethylene glycol, 10mM $MgCl_2$, and 100mM HEPES pH7.5. The cryo solution was optimized to contain 100mM HEPES pH7.5, 10% PEG 8000, 30% ethylene glycol, 10mM $MgCl_2$, and was filtered at 0.22μm.

X-ray diffraction, data collection, and processing of *Mm*Exo70$_{\Delta 84}$

X-ray diffraction screening on beamline 23-ID-D (General Medicine and Cancer Institutes CAT) at APS revealed that *Mm*Exo70$_{\Delta 84}$ crystals grown in the presence of PEG 8000 and ethylene glycol without additives diffract to a resolution of about 3.5Å. Similar crystals grown with the additive trimethylamine hydrochloride diffracted to a resolution of about 9Å. The addition of EDTA sodium salt, spermidine, or NDSB 195 improved diffraction to a resolution of 2.8-3.5Å, and the addition of $MgCl_2$ was found to further improve diffraction to a resolution of 2.25-2.7Å. The best data set from a native crystal, which was ultimately used to refine the final model, was harvested from a small cluster of sharp-edged crystals and had a usable resolution limit of 2.25Å and mosaicity less than 0.2°. 95° of data were collected in 0.5° increments. The diffraction images also contain a

second crystal lattice, possibly the result of twinning, but it was offset by a large enough angle to be ignored during processing using HKL2000 (Otwinowski and Minor, 1997). The space group of the crystal was determined to be $P3_221$ with unit cell dimensions of a = b = 61.52Å and c = 294.73Å ($\alpha = \beta = 90°$, $\gamma = 120°$). The asymmetric unit was calculated to contain one molecule. Data collection statistics can be found in Table 3.2.

Phase determination of *Mm*Exo70$_{\Delta 84}$

Attempts were made to solve the structure of *Mm*Exo70$_{\Delta 84}$ using molecular replacement with *Sc*Exo70$_{\Delta 62}$ as a search model using Phaser (McCoy *et al.*, 2005) or CNS (Brunger *et al.*, 1998). Many variations of the *Sc*Exo70$_{\Delta 62}$ model were used, including combinations of domains, with or without loops present, and with or without trimming of side chains to serine or alanine. No statistically significant solution was identified.

B834(DE3) *E. coli* containing the *Mm*Exo70$_{\Delta 84}$ pSJ2 construct was grown in a minimal MOPS media substituting SeMet for Met (see Appendix) and purified using a method identical to that used for native *Mm*Exo70$_{\Delta 84}$ with a yield of 10.1mg/L of culture. SeMet-substituted protein crystallized in the same crystal form under the same condition, with optimal growth requiring 7.5% ethylene glycol in the well solution and 4.5% in the drop precipitant. They grew at about the same rate as native crystals and were harvested and prepared for diffraction in a similar manner. Diffraction to a resolution of 2.5Å was achieved at beamline 23-ID-D (General Medicine and Cancer Institutes CAT) at APS and data sets were collected at the experimentally determined peak, inflection, high remote, and low remote wavelengths. Data were processed using HKL2000, revealing the same

Table 3.2: Data, phasing, and refinement statistics for *Mm*Exo70$_{\Delta 84}$

	***Mm*Exo70 Native**	***Mm*Exo70 SeMet substituted**		
Data collection				
Space group	$P3_221$	$P3_221$		
Cell dimensions [*a*, *b*, *c* (Å)]	61.52, 61.52, 294.73	61.64, 61.64, 294.68		
Resolution (Å)	50.0-2.25 (2.33-2.25)	50.0-2.5 (2.59-2.50)		
		Peak	Inflection	Remote
Wavelength (Å)	0.97926	0.97926	0.97942	0.95660
Completeness (%)	93.7 (77.7)	98.6 (89.2)	97.1 (77.5)	93.4 (59.2)
Redundancy	4.2 (3.1)	6.2 (4.6)	5.7 (3.0)	5.4 (2.3)
$I/\sigma I$	24.6 (3.0)	34.0 (4.7)	32.0 (2.8)	29.8 (1.8)
R_{merge} (%)	5.4 (41.6)	7.9 (29.7)	6.9 (36.5)	6.9 (42.3)
Phasing				
Phasing power				
Centric isomorphous		---	1.275	1.011
Acentric isomorphous		---	1.354	1.097
Acentric anomolous		2.415	1.361	1.032
Figure of Merit				
Centric		0.387		
Acentric		0.563		
After density modification		0.865		
Refinement				
Resolution (Å)	50.0-2.25			
No. reflections in working set	27369			
No. reflections in test set	1435			
R_{work}/R_{free} (%)	23.5/28.5			
No. of atoms				
Protein	4099			
Water	170			
Average *B*-factors				
Protein	54.4			
Water	54.8			
Rms deviations from ideality				
Bond lengths (Å)	0.006			
Bond angles (deg.)	1.1			
Ramachandran plot				
% in most favored regions	92.8			
% in addl. allowed regions	6.5			
% in gen. allowed regions	0.6			

Highest resolution shell shown in parentheses.

space group as the native protein with unit cell dimensions of a = b = 61.64Å and c = 294.68Å ($\alpha = \beta = 90°$, $\gamma = 120°$). Initial heavy atom sites were found using CNS and Table 3.2. Crystallographic data, phasing, and refinement statistics for *Mm*Exo70 were confirmed using Shake-N-Bake (Weeks and Miller, 1999). Refinement of the heavy atom sites was carried out using autoSHARP (Vonrhein *et al.*, 2006), and ten of the expected eleven selenium sites in the monomer were found (the missing selenium site was later determined to be located in a disordered portion of the molecule). Phases were calculated using the MAD method (Hendrickson and Ogata, 1997) and refined using the peak, inflection, and high remote data sets using autoSHARP. Data collection statistics can be found in Table 3.2.

Model building and refinement of the *Mm*Exo70$_{\Delta 84}$ structure

Solvent flattening was performed using autoSHARP and the initial model was built using ARP/wARP (Vonrhein *et al.*, 2006). The remainder of the model was built based on the known locations of selenium atoms using O (Jones *et al.*, 1991), and all refinement procedures were performed using CNS. Initial refinement consisted of several iterations of simulated annealing using the MLHL target function with amplitudes and phase probability distribution, grouped B factor refinement, and model rebuilding using O utilizing data from the peak wavelength of the MAD data set to a resolution of 2.7Å and later 2.5Å. Further refinement was done against the native data set to a resolution of 2.2Å. This consisted of iterations of simulated annealing by the MLF target function using amplitudes, individual B factor refinement, and model building using O. Final refinement was done to a resolution of 2.25Å to improve statistics. $3F_o$-$2F_c$ and F_o-F_c

maps were calculated using CNS to aid model building and water placement. The final model consists of residues 85-179, 188-241, 275-446, and 455-652, and 170 water molecules. Residues 180-187, 242-274, 447-454, 653, two residues at the N-terminus left over from the TEV cleavage site, and a small number of side chains were not included in the final model due to missing or incomplete electron density. The final model and structure factors were deposited into the RCSB PDB with the PDB identifier 2PFT. Refinement statistics can be found in Table 3.2.

REFERENCES

Brunger, A. T., Adams, P. D., Clore, G. M., DeLano, W. L., Gros, P., Grosse-Kunstleve, R. W., Jiang, J. S., Kuszewski, J., Nilges, M., Pannu, N. S., Read, R. J., Rice, L. M., Simonson, T., and Warren, G. L. (1998). Crystallography & Nmr System: A New Software Suite for Macromolecular Structure Determination. *Acta crystallographica* **54**, 905-921.

Carninci, P. and Kasukawa, T. and Katayama, S. and Gough, J. and Frith, M. C. and Maeda, N. and Oyama, R. and Ravasi, T. and Lenhard, B. and Wells, C. and Kodzius, R. and Shimokawa, K. and Bajic, V. B. and Brenner, S. E. and Batalov, S. and Forrest, A. R. and Zavolan, M. and Davis, M. J. and Wilming, L. G. and Aidinis, V. and Allen, J. E. and Ambesi-Impiombato, A. and Apweiler, R. and Aturaliya, R. N. and Bailey, T. L. and Bansal, M. and Baxter, L. and Beisel, K. W. and Bersano, T. and Bono, H. and Chalk, A. M. and Chiu, K. P. and Choudhary, V. and Christoffels, A. and Clutterbuck, D. R. and Crowe, M. L. and Dalla, E. and Dalrymple, B. P. and de Bono, B. and Della Gatta, G. and di Bernardo, D. and Down, T. and Engstrom, P. and Fagiolini, M. and Faulkner, G. and Fletcher, C. F. and Fukushima, T. and Furuno, M. and Futaki, S. and Gariboldi, M. and Georgii-Hemming, P. and Gingeras, T. R. and Gojobori, T. and Green, R. E. and Gustincich, S. and Harbers, M. and Hayashi, Y. and Hensch, T. K. and Hirokawa, N. and Hill, D. and Huminiecki, L. and Iacono, M. and Ikeo, K. and Iwama, A. and Ishikawa, T. and Jakt, M. and Kanapin, A. and Katoh, M. and Kawasawa, Y. and Kelso, J. and Kitamura, H. and Kitano, H. and Kollias, G. and Krishnan, S. P. and Kruger, A. and Kummerfeld, S. K. and Kurochkin, I. V. and Lareau, L. F. and Lazarevic, D. and Lipovich, L. and Liu, J. and Liuni, S. and McWilliam, S. and Madan Babu, M. and Madera, M. and Marchionni, L. and Matsuda, H. and Matsuzawa, S. and Miki, H. and Mignone, F. and Miyake, S. and Morris, K. and Mottagui-Tabar, S. and Mulder, N. and Nakano, N. and Nakauchi, H. and Ng, P. and Nilsson, R. and Nishiguchi, S. and Nishikawa, S., *et al.* (2005). The Transcriptional Landscape of the Mammalian Genome. *Science (New York, NY* **309**, 1559-1563.

Don, R. H., Cox, P. T., Wainwright, B. J., Baker, K., and Mattick, J. S. (1991). 'Touchdown' PCR to Circumvent Spurious Priming During Gene Amplification. *Nucleic acids research* **19**, 4008.

Guo, W., Roth, D., Gatti, E., De Camilli, P., and Novick, P. (1997). Identification and Characterization of Homologues of the Exocyst Component Sec10p. *FEBS letters* **404**, 135-139.

Hendrickson, W. A. and Ogata, C. M. (1997). Phase Determination from Multiwavelength Anomalous Diffraction Measurements. *Methods in enzymology* **276**, 494-523.

Jones, T. A., Zou, J. Y., Cowan, S. W., and Kjeldgaard, M. (1991). Improved Methods for Building Protein Models in Electron Density Maps and the Location of Errors in These Models. *Acta Crystallogr A* **47 (Pt 2)**, 110-119.

McCoy, A. J., Grosse-Kunstleve, R. W., Storoni, L. C., and Read, R. J. (2005). Likelihood-Enhanced Fast Translation Functions. *Acta crystallographica* **61**, 458-464.

Otwinowski, Z. and Minor, W. (1997). Processing of X-Ray Diffraction Data Collected in Oscillation Mode. *Methods in enzymology* **276**, 307-326.

Strausberg, R. L., Feingold, E. A., Grouse, L. H., Derge, J. G., Klausner, R. D., Collins, F. S., Wagner, L., Shenmen, C. M., Schuler, G. D., Altschul, S. F., Zeeberg, B., Buetow, K. H., Schaefer, C. F., Bhat, N. K., Hopkins, R. F., Jordan, H., Moore, T., Max, S. I., Wang, J., Hsieh, F., Diatchenko, L., Marusina, K., Farmer, A. A., Rubin, G. M., Hong, L., Stapleton, M., Soares, M. B., Bonaldo, M. F., Casavant, T. L., Scheetz, T. E., Brownstein, M. J., Usdin, T. B., Toshiyuki, S., Carninci, P., Prange, C., Raha, S. S., Loquellano, N. A., Peters, G. J., Abramson, R. D., Mullahy, S. J., Bosak, S. A., McEwan, P. J., McKernan, K. J., Malek, J. A., Gunaratne, P. H., Richards, S., Worley, K. C., Hale, S., Garcia, A. M., Gay, L. J., Hulyk, S. W., Villalon, D. K., Muzny, D. M., Sodergren, E. J., Lu, X., Gibbs, R. A., Fahey, J., Helton, E., Ketteman, M., Madan, A., Rodrigues, S., Sanchez, A., Whiting, M., Madan, A., Young, A. C., Shevchenko, Y., Bouffard, G. G., Blakesley, R. W., Touchman, J. W., Green, E. D., Dickson, M. C., Rodriguez, A. C., Grimwood, J., Schmutz, J., Myers, R. M., Butterfield, Y. S., Krzywinski, M. I., Skalska, U., Smailus, D. E., Schnerch, A., Schein, J. E., Jones, S. J., and Marra, M. A. (2002). Generation and Initial Analysis of More Than 15,000 Full-Length Human and Mouse Cdna Sequences. *Proceedings of the National Academy of Sciences of the United States of America* **99**, 16899-16903.

Vonrhein, C., Blanc, E., Roversi, P., and Bricogne, G. (2006). Automated Structure Solution with Autosharp. *Methods in molecular biology (Clifton, NJ* **364**, 215-230.

Weeks, C. M. and Miller, R. (1999). Optimizing Shake-and-Bake for Proteins. *Acta crystallographica* **55**, 492-500.

Chapter 4

The Structures of *Sc*Exo70$_{\Delta 62}$ and *Mm*Exo70$_{\Delta 84}$

ABSTRACT

The expression, purification, crystallization, and data collection for the structures of *Sc*Exo70$_{\Delta 62}$ and *Mm*Exo70$_{\Delta 84}$ was performed in Chapters 2 and 3, respectively. The structures of these molecules are presented in this chapter. Both structures share a common architecture of 19 α-helices organized into three domains forming a long rod. These structures permit the creation of a structure-based primary sequence alignment, which is significantly more accurate than previous sequence-based primary sequence alignment due to the misalignment of more than 100 residues in three sections as a result of the low degree of sequence conservation in Exo70. This alignment reveals two significant patches of conserved residues on the surface of the crystallized fragments. The largest patch is at least partly involved in Arpc1 interaction while the smaller patch has not been studied but probably maintains the structure of an interesting loop structure. In addition, the N domain shows similarity to several other exocyst subunits and the unconventional myosin *Sc*Myo2. The differences between these two structures include the orientation of the C domain, the organization of the domain boundaries, the organization of several loop structures, and the surface properties of the molecule. The data presented in this chapter reveal features of Exo70 that provide information helpful to the study of several known Exo70 interactions and provide evidence for the function of

the molecule, both conserved and species-specific. Analysis of this structural information suggests the prsence of several potential mechanisms that may be important for the function of Exo70, including reorientation of the C domain and flexibility at the N-M domain interface.

MATERIALS AND METHODS

Structure-based primary sequence alignment

The primary sequence alignment of Exo70 as calculated by Clustal W (Thompson *et al.*, 1994) contains errors stemming from the low sequence identity among Exo70 molecules in distantly related species. In order to improve the accuracy of this alignment, overlapping three-helix sections of the *Sc*Exo70$_{\Delta 62}$ structure were aligned with corresponding sections of the *Mm*Exo70$_{\Delta 84}$ structure by the Dali server's DaliLite Pairwise comparison tool (Holm and Park, 2000). Residues in similar positions were aligned within the overall structure-based primary sequence alignment. Sequences from *Candida albicans*, *Schizosaccharomyces pombe*, *Caenorhabditis elegans*, *Drosophila melanogaster*, and *Homo sapiens* were then added. Plants such as *Arabidopsis thaliana* and *Oryza sativa* were not included due to the presence of multiple Exo70 genes (Synek *et al.*, 2006). These sequences were aligned by Clustal W and then adjusted to align with the structure-based alignment with preference given to α-helical regions and conserved residues. Completely conserved residues are defined as those that always contain the same amino acid at a particular position in at least six of these seven species. Partially conserved residues always contain an amino acid that is always hydrophobic (alanine, isoleucine, leucine, methionine, phenylalanine, or valine), aromatic (phenylalanine,

tryptophan, or tyrosine), polar (asparagine, aspartic acid, glutamine, or glutamic acid), or basic (arginine or lysine). Selections identified only as conserved contain both completely and partially conserved residues.

Identification of similar structural motifs

The Dali Server's Database Search tool (Holm and Sander, 1995) was used to search the RCSB PDB (Berman *et al.*, 2000) for proteins with structures similar to individual domains or combinations of those domains from *Sc*Exo70$_{\Delta 62}$ or *Mm*Exo70$_{\Delta 84}$. The top 30 results of each search were evaluated for overall structural similarity.

Structural alignment of molecules

The Dali Server's DaliLite Pairwise comparison tool (Holm and Park, 2000) was used to align molecules. The alignment with the greatest Z score was selected for use. For full-molecule alignments based on a particular subset, PDB files were edited to contain only the residues of interest and aligned using the DaliLite tool. The full-length molecules were then aligned to these fragments.

Calculation of surface electrostatic potentials

The APBS Tools plug-in for PyMOL (www.umich.edu/~mlerner/Pymol) was used in combination with MacPyMol (http://www.pymol.org) to calculate the surface electrostatic potential of each molecule. Molecules used in this calculation had all missing side chains added to the model in a standard rotamer position.

RESULTS AND DISCUSSION

Overall structure of *Sc*Exo70$_{\Delta 62}$

*Sc*Exo70$_{\Delta 62}$ is composed of 561 residues (native *Sc*Exo70 contains 623 residues) that compose nineteen α-helices (H1-H19) connected by loops of varying lengths (L_{1-2}-L_{18-19}; subscript numbers identify α-helices connected by the loop). These structures are organized into a series of right-handed helix-turn-helix motifs (Figure 4.1). The overall shape of the molecule is that of a bent and twisted rod with approximate dimensions of 165Å × 35Å × 35Å and can be divided into three distinct domains: the N (N-terminal) domain, the M (Middle) domain, and the C (C-terminal) domain. Contacts between domains are relatively few and do not exhibit extensive packing as observed among α-helices within a domain. A long α-helix with a kink at the domain boundary links each consecutive pair of domains.

N domain of *Sc*Exo70$_{\Delta 62}$

The N domain is composed of residues 1-344, which make up 55% of the molecule. It includes H1-H9 and the first half of H10. The right-handed helix-turn-helix motifs that compose the domain pack against one another with a slight right-handed super-helical twist. H4 is unusually short, containing only seven residues, and is perpendicular to other α-helices within the domain. The first four residues of the crystallized construct, Asn63-Ser66, are not present in the structure and are presumably disordered within the crystal. Most loops in this domain contain between 1-9 residues. The longest loop of the domain, L_{6-7}, is adjacent to H4 and contains 16 residues, nine of which are disordered. The interface between H2 and H4 and bisecting H3 buries 644Å^2

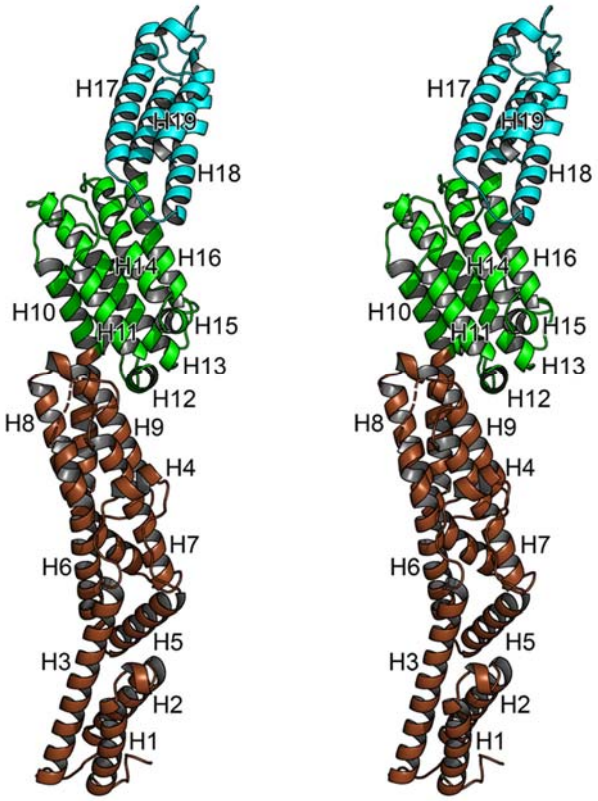

Figure 4.1: Structure of *Sc*Exo70$_{\Delta 62}$

A stereo cartoon diagram of *Sc*Exo70$_{\Delta 62}$. α-helices are labeled H1-H19 with the N domain colored brown, the M domain colored green, and the C domain colored cyan. A dashed line indicates residues not present in the structure.

of surface area, which is more area than the N and M domain interface but less area than the M and C domain interface. It has been described as a domain boundary (Dong *et al.*, 2005), but here it is not because there is no organizational change here as there is at other domain boundaries (Hamburger *et al.*, 2006). Another notable interface within the N domain is between a four-helix bundle, composed of H1-H3 and H5, and a five-helix bundle, composed of H6-H10 (Hamburger *et al.*, 2006). These bundles are defined by a significant change in angle between H5 and H7, although the overall organization of α-helices here is not disrupted. This feature gives a slight curve to the overall shape of the domain.

M domain of *Sc*Exo70$_{\Delta 62}$

The M domain is composed of residues 345-516, which make up 28% of the molecule. It includes the second half of H10, H11-H15, and the first half of H16. H10, H11, H13, H14, and H16 compose a five-helix bundle that is tilted approximately 40° from the long axis of the complete structure. H13 is located at the center of the domain and is surrounded by H10, H11, H14, H16, $L_{10\text{-}11}$, and $L_{11\text{-}12}$. H12 and H15 are unusually short at eight and six residues, respectively, and both are found at one end of the helical bundle perpendicular to all other α-helices. $L_{11\text{-}12}$, $L_{14\text{-}15}$ and $L_{15\text{-}16}$ contain only 1-2 residues each while the other loops in the domain are much longer. $L_{12\text{-}13}$ and $L_{13\text{-}14}$ are 29 and 18 residues long, respectively, and pack against the surface formed by H10, H13, and H16. These loops form a hydrogen bond between the side chains of Lys409 and Asp457. This domain is known to interact with Rho3 (Dong *et al.*, 2005), but it is not obvious from the structure what portion of this domain is involved.

C domain of *Sc*Exo70$_{\Delta 62}$

The C domain is composed of residues 517-623, which make up 17% of the molecule. It includes the second half of H16 and H17-H19. These α-helices are organized into a four-helix bundle that is angled away from the long axis of the complete structure, adding a slight twist to it. The hydrophobic core contains a high concentration of aromatic residues, especially near the tip of the molecule. Arpc1 interacts with *Sc*Exo70 by yeast-two-hybrid, and probably interacts with the C domain (Zuo *et al.*, 2006). $L_{13\text{-}14}$ and $L_{15\text{-}16}$ are eight and thirteen residues long, respectively, and are adjacent to one another at the tip of the molecule. $L_{14\text{-}15}$ is five residues long and is near the interface with the M domain.

N-M domain interface of *Sc*Exo70$_{\Delta 62}$

The N-M domain interface in *Sc*Exo70 buries 580Å^2 of surface area and forms a constricted "waist" at the midsection of the molecule. The interaction between these domains is composed only of the linking H10 and a small hydrophobic patch composed of five aromatic residues that will be discussed later. This interface is may be flexible, as each of the four molecules in the asymmetric unit of the C2 crystal form structure is identical except for the angle of the kink in H10 that varies by up to 14.6° (Hamburger *et al.*, 2006). No hydrogen bonds are present in this structure.

M-C domain interface of *Sc*Exo70$_{\Delta 62}$

The M-C domain interface in *Sc*Exo70$_{\Delta 62}$ buries a surface area of 772Å^2 that also appears somewhat constricted, although not as much as at the N-M domain interface. It is

primarily composed of a significant number of poorly conserved hydrophobic residues participating in the hydrophobic core. Two direct hydrogen bonds are found in the M-C domain interface. Several water-mediated hydrogen bonds are also found at this interface. In contrast to the N-M domain interface, this interface appears to be rigid, as all structures of *Sc*Exo70 share an identical M-C domain interface organization (Dong *et al.*, 2005; Hamburger *et al.*, 2006).

Overall structure of *Mm*Exo70$_{\Delta 84}$

*Mm*Exo70$_{\Delta 84}$ contains 569 residues of 653 found in full-length *Mm*Exo70 and is composed of nineteen α-helices connected by loops of varying lengths organized into a series of right-handed helix-turn-helix motifs (Figure 4.2). The molecule takes the shape of a slightly bent and twisted rod with approximate dimensions of 170Å × 35Å × 35Å. Like the structure of *Sc*Exo70$_{\Delta 62}$, it can be divided into three distinct domains (the N, M, and C domains) and contacts between domains are relatively weak and do not exhibit the same extent of packing as found within a domain. A single long α-helix links each consecutive pair of domains and a kink in H16 exists at the M-C domain boundary.

N domain of *Mm*Exo70$_{\Delta 84}$

The N domain is composed of residues 1-393, which make up 60% of the molecule. It includes H1-H9 and the first half of H10, and the right-handed helix-turn-helix motifs pack against one another with a slight right-handed super-helical twist. H4 is unusually short, containing only ten residues, and is perpendicular to other α-helices of the domain. Most loops in this domain contain between 2-5 residues, but two loops, $L_{4\text{-}5}$

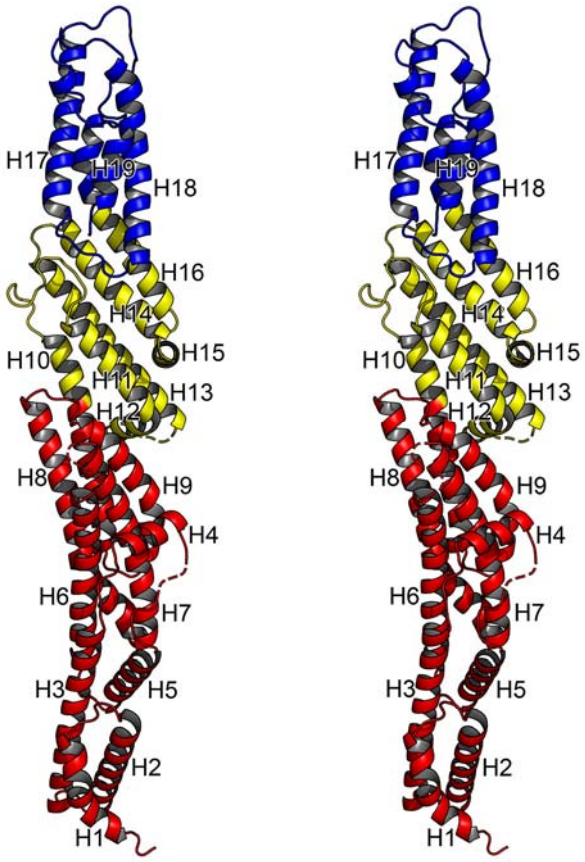

Figure 4.2: Structure of *Mm*Exo70$_{\Delta 84}$

A stereo cartoon diagram of *Mm*Exo70$_{\Delta 84}$. α-helices are labeled H1-H19 with the N domain colored red, the M domain colored yellow, and the C domain colored blue. The orientation of this molecule is aligned with *Sc*Exo70$_{\Delta 62}$ in Figure 4.1. Dashed lines indicate residues not present in the structure.

and L_{6-7}, are considerably longer. L_{4-5} is composed of sixteen residues, nine of which are disordered. L_{6-7}, the longest loop of the domain, is located between H4 and L_{4-5} and contains 33 residues, all of which are also disordered. H6 leads into, and H7 exits from the disordered region without loss of α-helical structure, making it unclear at exactly what point these α-helices end and L_{6-7} begins. All of the disordered residues are predicted by jnet (Cuff and Barton, 2000) to be unstructured, which is consistent with the definition of all disordered residues as a part of L_{6-7}. The forms of Exo70 found in the brain contain an additional 31 residues at the end of this loop (Carninci *et al.*, 2005; Guo *et al.*, 1997; Strausberg *et al.*, 2002) that are predicted by jnet to form a single α-helix and extend H7. The interface between H2 and H4 and bisecting H3 buries 621Å^2 of surface area, which is less area than either of the domain interfaces. Although this interface has been described as a domain boundary in *Sc*Exo70 (Dong *et al.*, 2005), it is not considered a domain boundary here because it does not result in any change in overall organization. The N domain can also be divided into a pair of α-helical bundles. A four-helix bundle, composed of H1-H3 and H5, and a five-helix bundle, composed of H6-H10 are defined by a change in angle between H5 and H7, although the overall organization of α-helices here is not disrupted (Hamburger *et al.*, 2006). Finally, the Rho-family GTPase TC10 is known to interact with this domain in *Homo sapiens* (Inoue *et al.*, 2003).

M domain of *Mm*Exo70$_{\Delta 84}$

The M domain is composed of residues 394-538, which make up 22% of the molecule. It includes the second half of H10, H11-H15, and the first half of H16. H10, H11, H13, H14, and H16 are organized into a five-helix bundle that is tilted

approximately 40° from the long axis of the complete structure. H12 and H15 are unusually short at eleven and eight residues, respectively, and both are found at one end of the helical bundle perpendicular to all other α-helices in the domain. Most loop structures in this domain are short, containing only 1-5 residues each, while $L_{10\text{-}11}$ contains 15 residues and $L_{12\text{-}13}$ contains ten residues, eight of which are disordered. Thirteen additional residues are inserted at the beginning of this loop in the longest form of Exo70 found in brain.

C domain of *Mm*Exo70$_{\Delta 84}$

The C domain is composed of residues 539-653, which make up 18% of the molecule. It includes the second half of H16 and H17-H19, which are organized into a four-helix bundle. In *R. norvegicus*, deletion of Lys571-Glu572 or Lys628-Pro630 prevented direct interaction with Arpc1 of the Arp2/3 actin-branching complex, although it is not clear if this phenotype is the result of structural disruption or the removal of important residues (Zuo *et al.*, 2006). $L_{13\text{-}14}$ and $L_{15\text{-}16}$ are both fifteen residues long and are adjacent to one another at the tip of the molecule. $L_{14\text{-}15}$ is six residues long and interacts with the M domain.

N-M domain interface of *Mm*Exo70$_{\Delta 84}$

The N-M domain interface in *Mm*Exo70$_{\Delta 84}$ buries 741Å^2 of surface area and appears as a constricted "waist" at the midsection of the molecule. The interface between these domains contains the linking H10, two small, mostly aromatic hydrophobic patches, and several water-mediated hydrogen bonds. The hydrophobic patches at this interface

will be discussed later. Water-mediated hydrogen bonds exist between the carbonyl of Ile339 on H8, the side chain of His342 on L_{8-9}, and the side chain of Asn400 on H10; the η amine of Arg355 on H9 and the carbonyl of Asp433 on H11; and the side chain of Glu436 on H12, the side chain of Glu387 on H10, and the side chain of Gln445 on H12.

M-C domain interface of *Mm*Exo70$_{\Delta 84}$

The M-C domain interface in *Mm*Exo70$_{\Delta 84}$ also appears somewhat constricted, burying a surface area of 754Å^2. It is primarily composed of a significant number of poorly conserved hydrophobic residues participating in the hydrophobic core of the molecule. Six direct and several water-mediated hydrogen bonds strengthen this interface.

Comparison of the N domain

The N domain of *Sc*Exo70 and *Mm*Exo70 share several common features. Both are composed of a similar set of α-helices, no α-helix or loop deviates by more than six residues, and each α-helix or loop is found in a similar position, except in the case of two loops (Figure 4.3 and Figure 4.4). L_{6-7} contains disordered residues in both structures, suggesting an inherent flexibility in this loop. The truncated residues at the N-terminus of the molecule contains several completely conserved residues and is predicted by jnet (Cuff and Barton, 2000) to form two α-helices, possibly continuing the particular style of right-handed helix-turn-helix motif found throughout the rest of this domain. The *Sc*Exo70$_{\Delta 62}$ structure begins with a loop that turns 180° (Thr67-Ser74), which is also consistent with this prediction. In addition, the site of truncation may be flexible as it is

Figure 4.3: Structural alignment of Exo70

An alignment of the primary sequences of Exo70 in five species, *M. musculus*, *H. sapiens*, *D. melanogaster*, *S. pombe*, and *S. cerevisiae*. This alignment was constructed by first aligning the structures of *Sc*Exo70$_{\Delta 62}$ and *Mm*Exo70$_{\Delta 84}$ using the DALI server in overlapping three-helix chunks and second aligning the Clustal W-aligned primary sequences of *Candida albicans*, *S. pombe*, *Caenorhabditis elegans*, *D. melanogaster*, and *H. sapiens* with the structural alignment. Adjustments were made to minimize breaks within α-helices. Residue numbers are indicated at the beginning of each line of sequence alignment. Secondary structural elements are indicated above the sequence block for *Mm*Exo70$_{\Delta 84}$ and below for *Sc*Exo70$_{\Delta 62}$. α-helices are indicated by rectangles, loops are indicated by lines, no β-strands are present in the structure, and residues not found in the structure are indicated by dashed lines. Domains are indicated by secondary structure coloration. In *Mm*Exo70$_{\Delta 84}$ the N domain is red, the M domain is yellow, and the C domain is blue. In *Sc*Exo70$_{\Delta 62}$, the N domain is brown, the M domain is green, and the C domain is cyan. Residues invariable in six of these seven species were considered completely conserved and are highlighted in purple. Residues that always appear as a particular residue type in six of these seven species were considered similarly conserved and are highlighted in pink. For clarity, sequences lacking homology have been replaced wit7h bracketed numbers indicating the number of residues omitted.

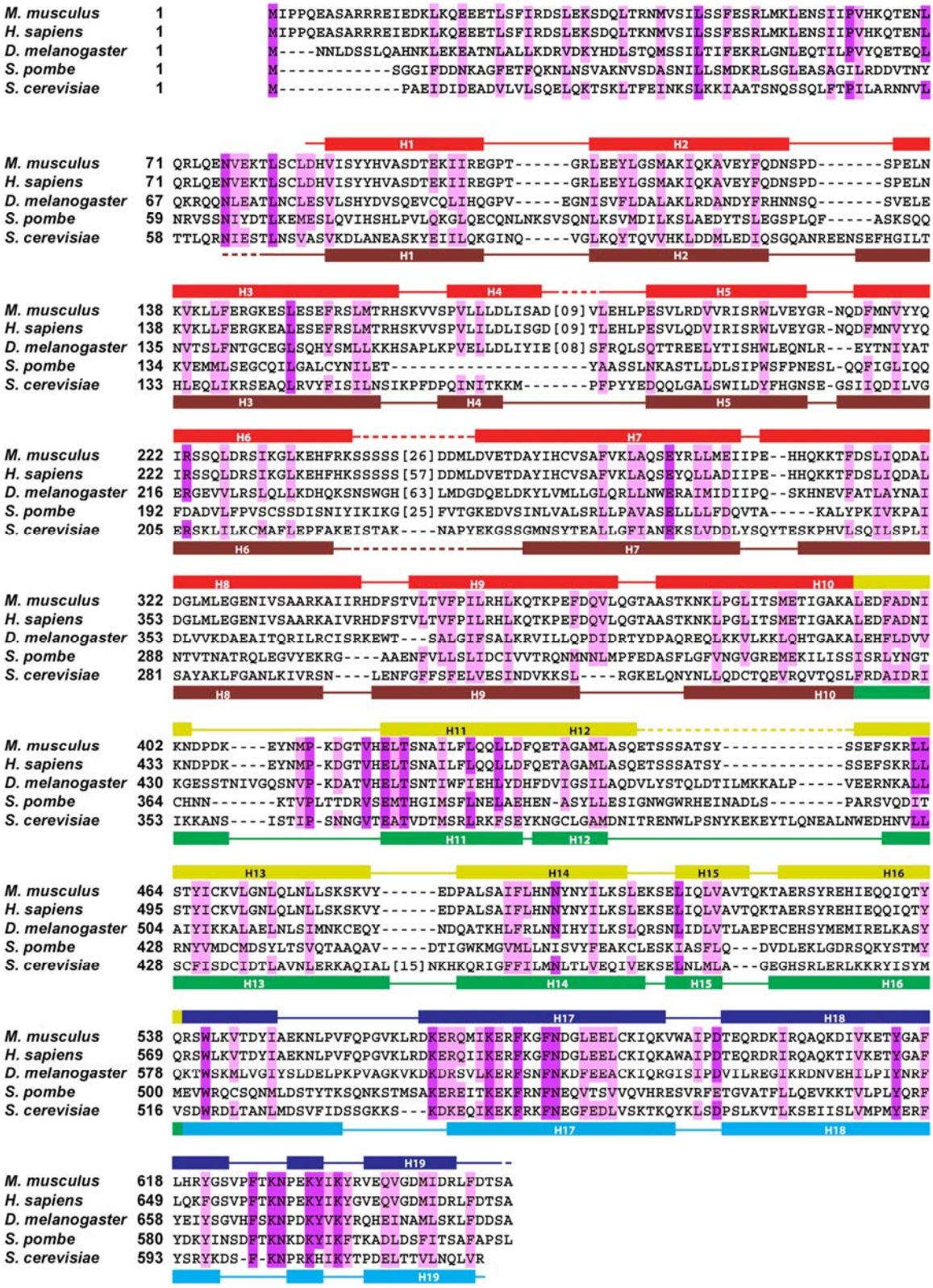
M. musculus 1 MIPPQEASARRREIEDKLKQEEETLSFIRDSLEKSDQLTRNMVSILSSFESRLMKLENSIIPVHKQTENL
H. sapiens 1 MIPPQEASARRREIEDKLKQEEETLSFIRDSLEKSDQLTKNMVSILSSFESRLMKLENSIIPVHKQTENL
D. melanogaster 1 M----NNLDSSLQAHNKLEKEATNLALLKDRVDKYHDLSTQMSSILTIFEKRLGNLEQTILPVYQETEQL
S. pombe 1 M------------SGGIFDDNKAGFETFQKNLNSVAKNVSDASNILLSMDKRLSGLEASAGILRDDVTNY
S. cerevisiae 1 M-------------PAEIDIDEADVLVLSQELQKTSKLTFEINKSLKKIAATSNQSSQLFTPILARNNVL
H1 H2
M. musculus 71 QRLQENVEKTLSCLDHVISYYHVASDTEKIIREGPT------GRLEEYLGSMAKIQKAVEYFQDNSPD-------SPELN
H. sapiens 71 QRLQENVEKTLSCLDHVISYYHVASDTEKIIREGPT------GRLEEYLGSMAKIQKAVEYFQDNSPD-------SPELN
D. melanogaster 67 QKRQQNLEATLNCLESVLSHYDVSQEVCQLIHQGPV-----EGNISVFLDALAKLRDANDYFRHNNSQ-------SVELE
S. pombe 59 NRVSSNIYDTLKEMESLQVIHSHLPVLQKGLQECQNLNKSVSQNLKSVMDILKSLAEDYTSLEGSPLQF-----ASKSQQ
S. cerevisiae 58 TTLQRNIESTLNSVASVKDLANEASKYEIILQKGINQ-----VGLKQYTQVVHKLDDMLEDIQSGQANREENSEFHGILT
H1 H2
H3 H4 H5
M. musculus 138 KVKLLFERGKESLESEFRSLMTRHSKVVSPVLLLDLISAD[09]VLEHLPESVLRDVVRISRWLVEYGR-NQDFMNVYYQ
H. sapiens 138 KVKLLFERGKEALESEFRSLMTRHSKVVSPVLILDLISGD[09]TLEHLPESVLQDVIRISRWLVEYGR-NQDFMNVYYQ
D. melanogaster 135 NVTSLFNTGCEGLSQHYSMLLKKHSAPLKPVELLDLIYIE[08]SFRQLSQTTREELYTISHWLEQNLR---EYTNIYAT
S. pombe 134 KVEMMLSEGCQILGALCYNILET----------YAASSLNKASTLLDLSIPWSFPNESL-QQFIGLIQQ
S. cerevisiae 133 HLEQLIKRSEAQLRVYFISILNSIKPFDPQINITKKM-------PFPYYEDQQLGALSWILDYFHGNSE-GSIIQDILVG
H3 H4 H5
H6 H7
M. musculus 222 IRSSQLDRSIKGLKEHFRKSSSSS[26]DDMLDVETDAYIHCVSAFVKLAQSEYRLLMEIIPE--HHQKKTFDSLIQDAL
H. sapiens 222 IRSSQLDRSIKGLKEHFHKSSSSS[57]DDMLDVETDAYIHCVSAFVKLAQSEYQLLADIIPE--HHQKKTFDSLIQDAL
D. melanogaster 216 ERGEVVLRSLQLLKDHQKSNSWGH[63]LMDGDQELDKYLVMLLGLQRLLNWERAIMDIIPQ--SKHNEVFATLAYNAI
S. pombe 192 FDADVLFPVSCSSDISNIYIKIKG[25]FVTGKEDVSINLVALSRLLPAVASELLLLFDQVTA-----KALYPKIVKPAI
S. cerevisiae 205 ERSKLILKCMAFLEPFAKEISTAK----NAPYEKGSSGMNSYTEALLGFIANEKSLVDDLYSQYTESKPHVLSQILSPLI
H6 H7
H8 H9 H10
M. musculus 322 DGLMLEGENIVSAARKAIIRHDFSTVLTVFPILRHLKQTKPEFDQVLQGTAASTKNKLPGLITSMETIGAKALEDFADNI
H. sapiens 353 DGLMLEGENIVSAARKAIVRHDFSTVLTVFPILRHLKQTKPEFDQVLQGTAASTKNKLPGLITSMETIGAKALEDFADNI
D. melanogaster 353 DLVVKDAEAITQRILRCISRKEWT---SALGIFSALKRVILLQPDIDRTYDPAQREQLKKVLKKLQHTGAKALEHFLDVV
S. pombe 288 NTVTNATRQLEGVYEKRG----AAENFVLLSLIDCIVVTRQNMNNLMPFEDASFLGFVNGVGREMEKILISSISRLYNGT
S. cerevisiae 281 SAYAKLFGANLKIVRSN----LENFGFFSFELVESINDVKKSL----RGKELQNYNLLQDCTQEVRQVTQSLFRDAIDRI
H8 H9 H10
H11 H12
M. musculus 402 KNDPDK----EYNMP-KDGTVHELTSNAILFLQQLLDFQETAGAMLASQETSSSATSY-------------SSEFSKRLL
H. sapiens 433 KNDPDK----EYNMP-KDGTVHELTSNAILFLQQLLDFQETAGAMLASQETSSSATSY-------------SSEFSKRLL
D. melanogaster 430 KGESSTNIVGQSNVP-KDATVHELTSNTIWFIEHLYDHFDVIGSILAQDVLYSTQLDTILMKKALP-----VEERNKALL
S. pombe 364 CHNN-------KTVPLTTDRVSEMTHGIMSFLNELAEHEN-ASYLLESIGNWGWRHEINADLS--------PARSVQDIT
S. cerevisiae 353 IKKANS----ISTIP-SNNGVTEATVDTMSRLRKFSEYKNGCLGAMDNITRENWLPSNYKEKEYTLQNEALNWEDHNVLL
H11 H12
H13 H14 H15 H16
M. musculus 464 STYICKVLGNLQLNLLSKSKVY------EDPALSAIFLHNNYNYILKSLEKSELIQLVAVTQKTAERSYREHIEQQIQTY
H. sapiens 495 STYICKVLGNLQLNLLSKSKVY------EDPALSAIFLHNNYNYILKSLEKSELIQLVAVTQKTAERSYREHIEQQIQTY
D. melanogaster 504 AIYIKKALAELNLSIMNKCEQY------NDQATKHLFRLNNIHYILKSLQRSNLIDLVTLAEPECEHSYMEMIRELKASY
S. pombe 428 RNYVMDCMDSYLTSVQTAAQAV-----DTIGWKMGVMLLNISVYFEAKCLESKIASFLQ---DVDLEKLGDRSQKYSTMY
S. cerevisiae 428 SCFISDCIDTLAVNLERKAQIAL[15]NKHKQRIGFFILMNLTLVEQIVEKSELNLMLA---GEGHSRLERLKKRYISYM
H13 H14 H15 H16
H17 H18
M. musculus 538 QRSWLKVTDYIAEKNLPVFQPGVKLRDKERQMIKERFKGFNDGLEELCKIQKVWAIPDTEQRDKIRQAQKDIVKETVGAF
H. sapiens 569 QRSWLKVTDYIAEKNLPVFQPGVKLRDKERQIIKERFKGFNDGLEELCKIQKAWAIPDTEQRDRIRQAQKTIVKETVGAF
D. melanogaster 578 QKTWSKMLVGIYSLDELPKPVAGKVKDKDRSVLKERFSNFNKDFEEACKIQRGISIPDVILREGIKRDNVEHILPIYNRF
S. pombe 500 MEVWRQCSQNMLDSTYTKSQNKSTMSAKEREITKEKFRNFNEQVTSVVQVHRESVRFETGVATFLLQEVKKTVLPLYQRF
S. cerevisiae 516 VSDWRDLTANLMDSVFIDSSGKKS---KDKEQIKEKFRKFNEGFEDLVSKTKQYKLSDPSLKVTLKSEIISLVMPMYERF
H17 H18
H19
M. musculus 618 LHRYGSVPFTKNPEKYIKYRVEQVGDMIDRLFDTSA
H. sapiens 649 LQKFGSVPFTKNPEKYIKYGVEQVGDMIDRLFDTSA
D. melanogaster 658 YEIYSGVHFSKNPDKYVKYRQHEINAMLSKLFDDSA
S. pombe 580 YDKYINSDFTKNKDKYIKFTKADLDSFITSAFAPSL
S. cerevisiae 593 YSRYKDS-F-KNPRKHIKYTPDELTTVLNQLVR
H19

Figure 4.4: Structural organization of the N domain

A cartoon diagram of the N domain of *Sc*Exo70$_{\Delta 62}$ (top) and *Mm*Exo70$_{\Delta 84}$ (bottom). Left panels are in the same orientation as in Figures 4.1 and 4.2 and right panels are related to the left panel by a rotation of -90° about the long axis of the molecule. α-helices are labeled H1-H10. H1-H5 form a four-helix bundle and are colored raspberry in *Sc*Exo70$_{\Delta 62}$ and ruby in *Mm*Exo70$_{\Delta 84}$. H6-H10 form a five-helix bundle and are colored brown in *Sc*Exo70$_{\Delta 62}$ and red in *Mm*Exo70$_{\Delta 84}$. The side chains of three completely conserved residues found in this domain are shown as stick models with oxygen colored red, nitrogen colored blue, and carbon colored purple. These residues are Leu145/150 on H3, Arg206/223 on H6, and Glu253/296 on H7 (*Sc*Exo70$_{\Delta 62}$/*Mm*Exo70$_{\Delta 84}$). Red lines indicate hydrogen bonds. Dashed lines indicate residues not present in the structure.

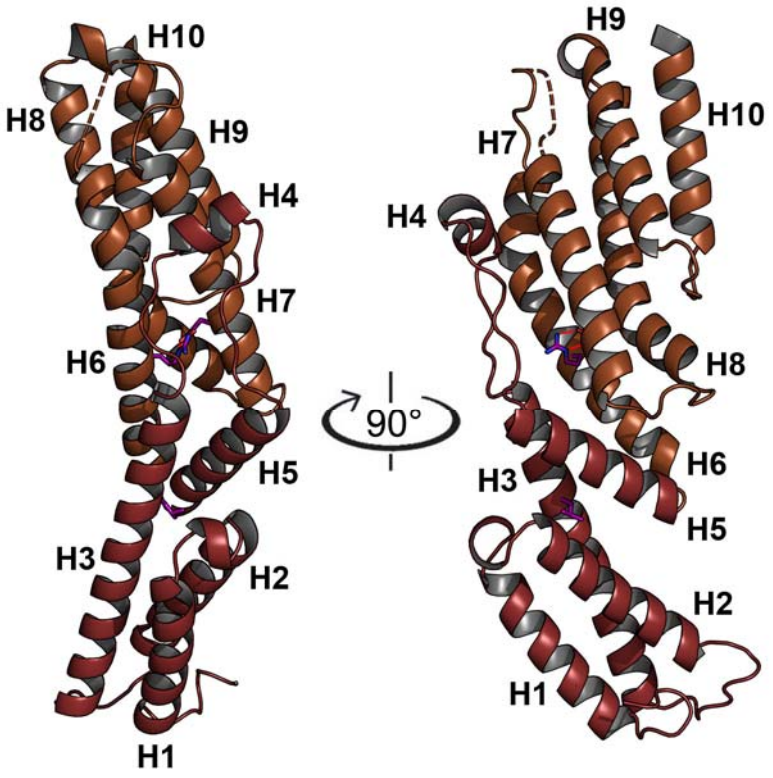
H10
H8
H9
H4
H7
H6
H5
H3
H2
H1
90°
H9
H7
H10
H4
H8
H6
H3
H5
H2
H1

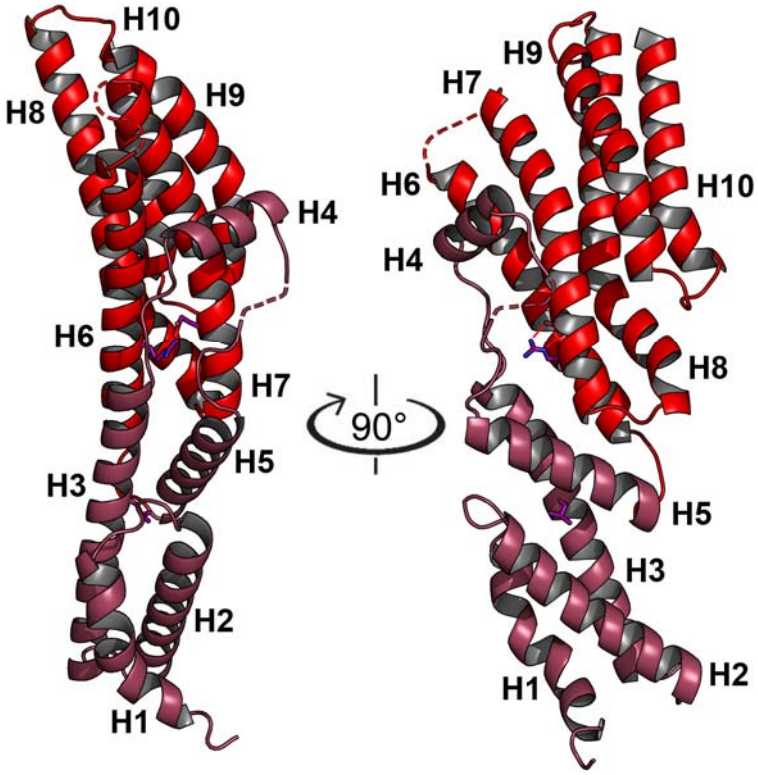
H10
H8
H9
H4
H6
H7
H5
H3
H2
H1
90°
H9
H7
H6
H10
H4
H8
H5
H3
H2
H1

succeptible to proteolysis in both species and *Sc*Exo70$_{\Delta 62}$ and *Mm*Exo70$_{\Delta 84}$ are stable and crystallizable while full-length Exo70 is not.

Of the residues found in each crystallized construct, 17.7/17.8% (*Sc*Exo70$_{\Delta 62}$/*Mm*Exo70$_{\Delta 84}$) of those in the N domain are conserved while only 1.0/1.0% are completely conserved. Of these conserved residues, 88.0/83.6% are hydrophobic and 12.0/16.4% are hydrophilic. The majority of these conserved residues participate in the hydrophobic core of the domain. The three completely conserved residues, Leu145/150 on H3, Arg206/223 on H6, and Glu296/253 on H7, are presumed to be important for the structure of the domain (Figure 4.4). Leu145/150 participates in hydrophobic interactions with several similarly conserved residues from H2 and H4. Arg206/223 and Glu296/253 form two hydrogen bonds between the two carboxylic oxygens of glutamic acid and the ε and η amines of arginine. This interaction is surrounded by hydrophobic residues, about half of which are similarly conserved, and is located beneath $L_{3\text{-}4}$ and $L_{4\text{-}5}$. Arg206/223 also forms a third hydrogen bond with Tyr174 at the end of $L_{4\text{-}5}$ in *S. cerevisiae* or Ser162 at the start of $L_{3\text{-}4}$ in *M. musculus*.

The N domain also exhibits several major differences between *Sc*Exo70 and *Mm*Exo70. First, the truncated N terminus contains thirteen more residues in *Mm*Exo70 than in *Sc*Exo70. Second, $L_{4\text{-}5}$ is eight residues longer in *Mm*Exo70$_{\Delta 84}$. Although nine residues of this loop are disordered and the position of H4 is shifted, there is little effect on the rest of the structure. Lastly, $L_{6\text{-}7}$ contains up to nineteen more residues in *Mm*Exo70 than in *Sc*Exo70. Although the complete disorder of $L_{6\text{-}7}$ limits what can be learned from this region, it is clear that this is a generally unstructured region of the molecule. In addition, its significantly increased length and further extended form in

brain *Mm*Exo70 suggests a species-specific and possibly tissue-specific function may be associated with this loop in *Mm*Exo70.

*Sc*Exo70$_{\Delta 62}$ has a greater angle between the four-helix bundle and the five-helix bundle than in *Mm*Exo70$_{\Delta 84}$, resulting in greater curvature of the N domain in *Sc*Exo70$_{\Delta 62}$ and a more linear domain in *Mm*Exo70$_{\Delta 84}$ (Figure 4.4). Despite this difference, there is no evidence for flexibility within the N domain, as other *Sc*Exo70 structures exhibit no variability in this region (Dong *et al.*, 2005; Hamburger *et al.*, 2006).

Finally, several α-helices contain kinks that are not conserved (Figure 4.4). *Mm*Exo70$_{\Delta 84}$ H1 contains a kink near its middle for which the effect and function is difficult to determine due to its proximity to, and possible interaction with, truncated residues. This kink could have an effect on the organization of preceding residues. Alternatively, this kink could also be an artifact of truncation. *Sc*Exo70$_{\Delta 62}$ H6 contains a kink near its C-terminal end, possibly positioning the partially disordered region of $L_{6\text{-}7}$ along the body of the molecule over H8 and H9. In contrast, *Mm*Exo70$_{\Delta 84}$ H6 is not kinked and points into solution where the disordered residues of $L_{6\text{-}7}$ may exist, away from the body of the molecule. *Mm*Exo70$_{\Delta 84}$ H9 also contains a kink not found in *Sc*Exo70$_{\Delta 62}$, bringing a portion of this α-helix closer to H12 in the M domain, possibly contributing to the increased interaction between these domains.

Comparison of the M domain

The M domain of *Sc*Exo70$_{\Delta 62}$ and *Mm*Exo70$_{\Delta 84}$ share several common features. Both are composed of a similar set of α-helices, no α-helix or loop deviates by more than

four residues, and each α-helix or loop is found in a similar position, except in the case of two loops (Figure 4.5).

Of the residues found in each construct, 19.8/24.8% (*Sc*Exo70$_{\Delta 62}$/*Mm*Exo70$_{\Delta 84}$) are conserved while 5.2/4.1% are completely conserved. Of all conserved residues, 82.4/83.3% are hydrophobic and 17.6/16.7% are hydrophilic. The majority of these conserved residues participate in the hydrophobic core of the domain. There are nine completely conserved residues within the M domain of *Sc*Exo70 and ten in *Mm*Exo70. These are Pro363/412 and Val368/417 on $L_{10\text{-}11}$; Glu370/419, Thr372/421, Leu379/428 and *Mm*Leu431 on H11; Leu426/462 and Leu427/463 on H13, Asn372/421 on H14, and Leu385/434 on H15 (Figure 4.5). Most of these residues probably participate in the maintenance of conserved structural features. The first three completely conserved residues of the M domain form a patch on its surface and may maintain the conserved structure of $L_{10\text{-}11}$. Pro363/412 is found at the start of a conserved sharp bend in $L_{10\text{-}11}$. The similarly conserved and solvent exposed Asn365/Asp414 is found at the other end of this bend, and its side chain forms a hydrogen bond with the main chain amide of Gly367/Thr416. Val368/417 is found at the end of a linear stretch of residues that began with Asn365/Asp414, and its side chain is both solvent exposed and positioned over a hydrophobic patch of residues. Ile362/Met411 and Ala371/Leu420 are somewhat conserved residues that interact are positioned so that they could possibly stabilize the ends of this conserved loop structure by interacting with the hydrophobic core of the domain. Glu370/419 is the first residue of H11 and its side chain is completely solvent exposed. Although it is common for completely conserved surface exposed residues to be involved in a conserved interaction, only the few other conserved residues just mentioned

Figure 4.5: Structural organization of the M domain

A cartoon diagram of the M domain of *Sc*Exo70$_{\Delta 62}$ (top) and *Mm*Exo70$_{\Delta 84}$ (bottom). Left panels are in the same orientation as in Figures 4.1 and 4.2 and right panels are related to the left panel by a rotation of -90° about the long axis of the molecule. α-helices are labeled H10-H16, and H10 is located behind H13 and is not labeled in the right panel. H10-H13 align with the N domain and are colored green in *Sc*Exo70$_{\Delta 62}$ and yellow in *Mm*Exo70$_{\Delta 84}$. H14-H16 align with the C domain and are colored splitpea in *Sc*Exo70$_{\Delta 62}$ and wheat in *Mm*Exo70$_{\Delta 84}$. The side chains of ten completely conserved residues and one similarly conserved residue found in this domain are shown as stick models with oxygen colored red, nitrogen colored blue, and carbon colored purple in completely conserved residues and pink in the similarly conserved residue. These residues are Pro363/412 and Val368/417 on L$_{10\text{-}11}$; Glu370/419, Thr372/421, Leu379/428, and *Mm*Leu431 on H11; Leu426/462 and Leu427/463 on H13; Asn479/498 on H14; Leu492/511 on H15; and Asn365/Asp414 on L$_{10\text{-}11}$ (*Sc*Exo70$_{\Delta 62}$/*Mm*Exo70$_{\Delta 84}$). Red lines indicate hydrogen bonds. Dashed lines indicate residues not present in the structure.

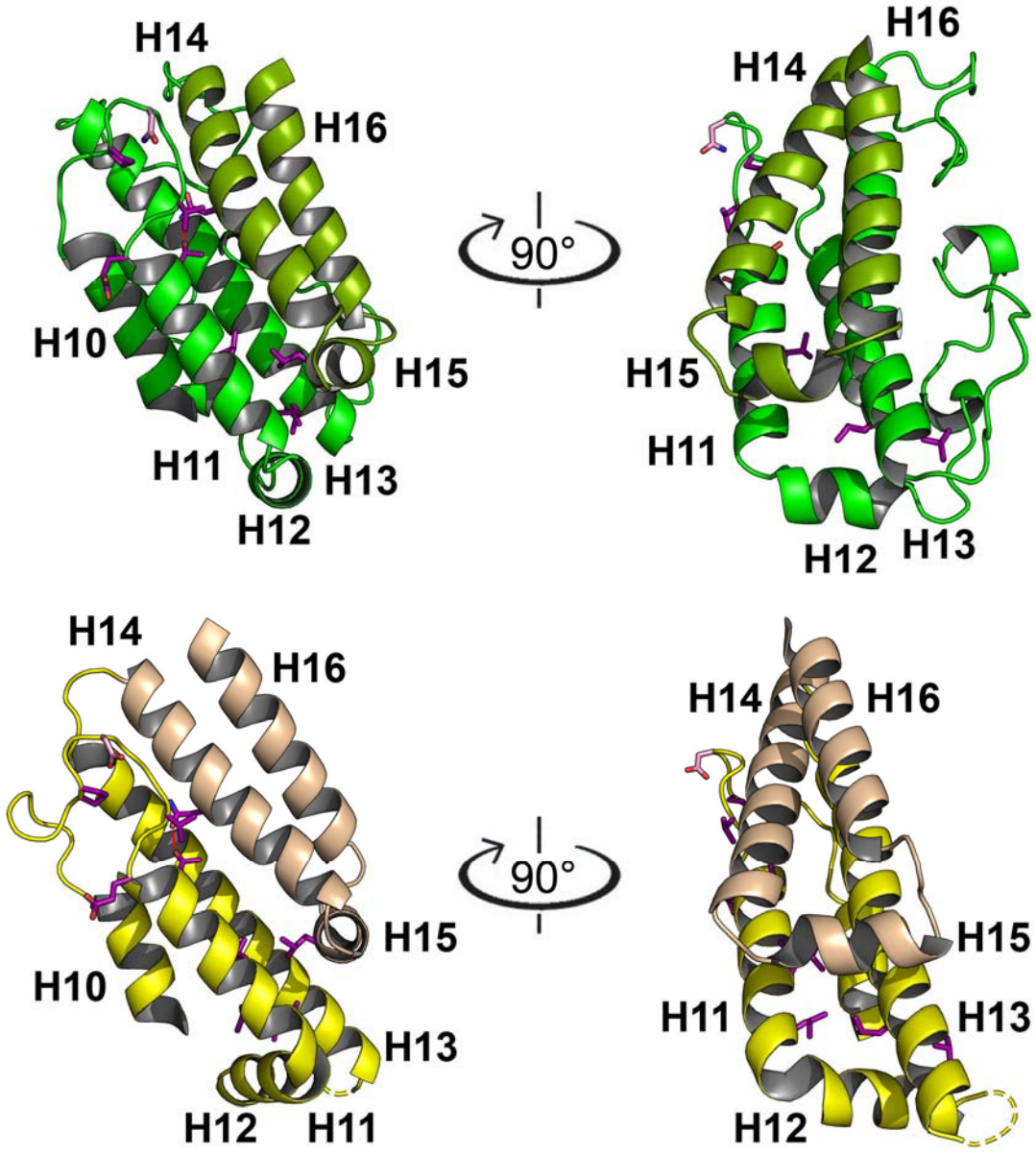
H14
H16
H10
H15
H11
H13
H12
90°
H16
H14
H15
H11
H12
H13
H14
H16
H10
H15
H13
H12
H11
90°
H14
H16
H15
H11
H13
H12

are nearby on the surface of the molecule. Thr372/421 follows Ala371/Leu420 and forms a hydrogen bond inside the domain with the other completely conserved residue Asn479/498. Leu379/428, *Mm*Leu431, Leu426/462, and Leu385/434 are completely conserved and are clustered together in the hydrophobic core of the domain.

There are several features within the M domain that differ by more than four residues between *Sc*Exo70$_{\Delta 62}$ and *Mm*Exo70$_{\Delta 84}$. In *Mm*Exo70$_{\Delta 84}$ $L_{12\text{-}13}$ and $L_{13\text{-}14}$ are ten and three residues long, respectively. In *Sc*Exo70$_{\Delta 62}$ $L_{12\text{-}13}$ and $L_{13\text{-}14}$ are 29 and eighteen residues long, respectively, forming two meandering horseshoe-shaped loops that mostly lay along the surface created by H10, H13, and H16. These loops share a hydrogen bond between the side chains of Lys407 and Asp457. The length of $L_{12\text{-}13}$ is variable among species, being longest in budding yeast and shortest in some mammalian forms. The length of $L_{13\text{-}14}$, however, is long in budding yeast and uniformly short in other organisms.

Despite several conserved residues in the M domain that appear to stabilize its internal packing, the interface between H11-H13 and H14-H16 exhibits two different organizations that are related by a rotation of H14-H16 by approximately 20° on the surface of H11-H13 (Figure 4.6). The C domain is rigidly associated with H14-H16 and it also rotates similarly. Alignment of H1-H13 reveals that the conserved hydrogen bonding pair, Thr372/421 and Asn479/498, is located at what may be a pivot point around which H14-H19 rotates. This conserved interaction, therefore, may play an important role in this interface. There is no evidence for flexibility at this location, as all structures of *Sc*Exo70 (Dong *et al.*, 2005; Hamburger *et al.*, 2006) have identical M domain and M-C domain

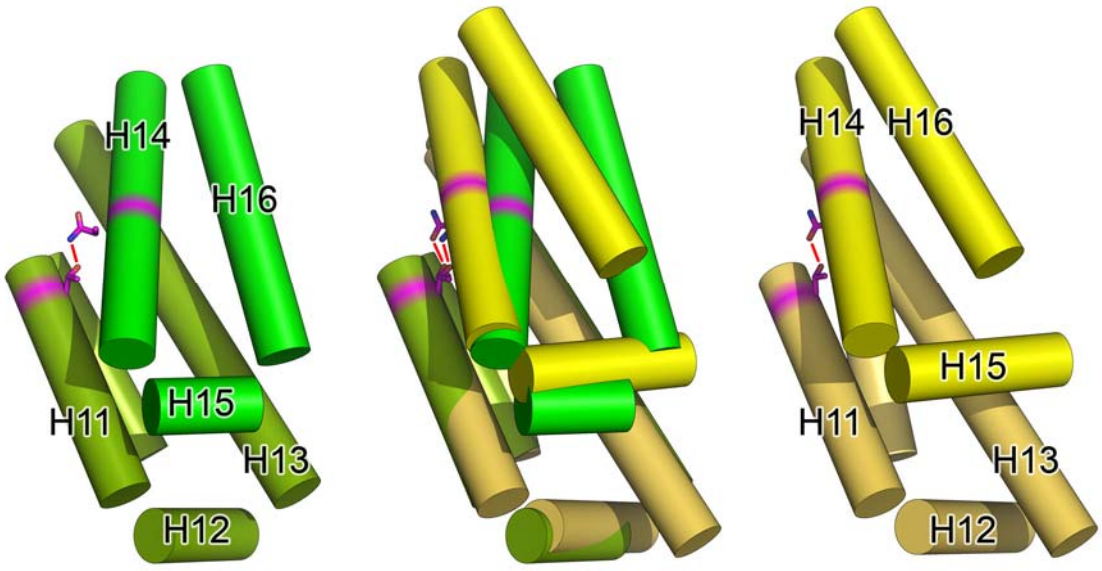

Figure 4.6: Conserved surface residues of the M and C domain interface

A cartoon diagram of the M and C domain interface of *Sc*Exo70$_{\Delta 62}$ (left) and *Mm*Exo70$_{\Delta 84}$ (right). Both panels are in the same orientation as in Figures 4.1 and 4.2. Several relevant structural features are labeled in red. The M domain is colored green in *Sc*Exo70$_{\Delta 62}$ and yellow in *Mm*Exo70$_{\Delta 84}$, and the C domain is colored cyan in *Sc*Exo70$_{\Delta 62}$ and blue in *Mm*Exo70$_{\Delta 84}$. The main chains of important sections of $L_{10\text{-}11}$, $L_{17\text{-}18}$, and H18 are shown as sticks with oxygen colored red and nitrogen colored blue. The side chains of surface exposed conserved residues are shown as sticks with oxygen colored red, nitrogen colored blue, and carbon colored purple in completely conserved residues and pink in the similarly conserved residue. Red lines indicate hydrogen bonds. H13-H16 and H19 are faded to emphasize other α-helices and loops.

interface structures, and this organizational difference may be explainable by several structural features that stabilize these two interfaces.

There are two structural features of *Sc*Exo70$_{\Delta 62}$ that stabilize its internal M domain packing. First, $L_{13\text{-}14}$ connects H1-H13 to H14-H19, restricting the possible positions that H14-H19 can take in relation to H1-H13 through its length. This loop is composed of eighteen residues in *Sc*Exo70$_{\Delta 62}$, giving freedom for a wide range of possible positions. This organization is the same in all *Sc*Exo70 structures, suggesting that $L_{13\text{-}14}$ does not actually provide flexibility to the region, but does allow for the observed packing. Second, $L_{12\text{-}13}$ and $L_{13\text{-}14}$ both interact with H10, H13, and H16 through five direct hydrogen bonds and several water-mediated hydrogen bonds. The interactions of these loops with H16 may have an effect on the organization of this interface.

*Mm*Exo70$_{\Delta 84}$ also exhibits two structural features that stabilize the conformation of the interface between H1-H13 and H14-H19. First, $L_{13\text{-}14}$ is only three residues long in *Mm*Exo70$_{\Delta 84}$, restricting the possible positions that H14-H19 can take in relation to H1-H13. Alignment reveals that all animals and possibly other organisms probably have a similar $L_{13\text{-}14}$. This would impose similar restrictions on this organization in these organisms, suggesting that the *Mm*Exo70$_{\Delta 84}$ orientation is more common than the *Sc*Exo70$_{\Delta 62}$ orientation. Second, $L_{10\text{-}11}$ interacts with $L_{17\text{-}18}$ through a hydrogen bond between the main chain carbonyl of Asp414 and the main chain amide of Ala592 (Figure 4.7). As mentioned above, $L_{10\text{-}11}$ contains a number of conserved residues that may maintain the structure of the loop. Here, the linear portion of the loop is parallel to a similarly linear section of $L_{17\text{-}18}$, which has a conserved structure but only one completely

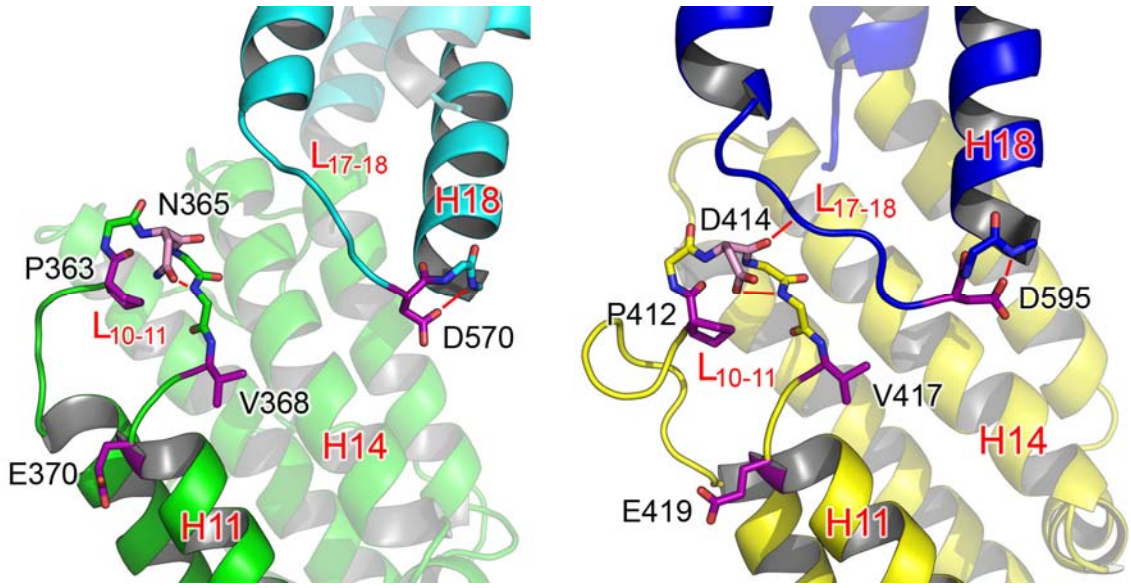

Figure 4.7: α-helical packing of the M domain

A cartoon diagram of the M domain in *Sc*Exo70$_{\Delta 62}$ (left), *Mm*Exo70$_{\Delta 84}$ (right), and both aligned using PyMOL (center) with α-helices shown as cylinders and loops omitted for clarity. H11-H16 are labeled, and H10 appears behind H11 and H14. H10-H13 align with the N domain and are colored splitpea in *Sc*Exo70$_{\Delta 62}$ and wheat in *Mm*Exo70$_{\Delta 84}$. H14-H16 align with the C domain and are colored green in *Sc*Exo70$_{\Delta 62}$ and yellow in *Mm*Exo70$_{\Delta 84}$. The side chains of completely conserved residues located at a proposed pivot point, Thr372/421 and Asn479/498 (*Sc*Exo70$_{\Delta 62}$/*Mm*Exo70$_{\Delta 84}$), are shown as sticks with carbon colored purple, oxygen colored red, and nitrogen colored blue. Red lines indicate hydrogen bonds.

conserved residue, Asp570/Asp595 (*Sc*Exo70$_{\Delta 62}$/*Mm*Exo70$_{\Delta 84}$), at the end of the loop. The interaction between these loops may stabilize the conformation of the H1-H13 and H14-H19 interface in *Mm*Exo70$_{\Delta 84}$. The conservation of these structures does not have an obvious function in *Sc*Exo70$_{\Delta 62}$, raising the possibility that, although it lacks any evidence, rotation at this interface may indeed be possible in *Sc*Exo70 in order to bring these two conserved structures together under certain circumstances.

Comparison of the C domain

The C domain of *Sc*Exo70$_{\Delta 62}$ and *Mm*Exo70$_{\Delta 84}$ are highly similar. Both are composed of a similar set of α-helices, no α-helix or loop deviates by more than three residues, and each α-helix or loop is found in a similar position, except in the case of H16 and L$_{16\text{-}17}$. The overall shape of each α-helix and loop is conserved, although L$_{16\text{-}17}$ and L$_{18\text{-}19}$ exhibit some flexibility in position that appears to be affected by crystal packing.

This domain contains the highest number and percentage of conserved residues in the molecule. Of the residues found in each construct, 32.7/31.3% (*Sc*Exo70$_{\Delta 62}$/*Mm*Exo70$_{\Delta 84}$) are conserved while 12.1/12.2% are completely conserved. Of these conserved residues, 57.1/58.3% are hydrophobic and 42.9/41.7% are hydrophilic, the greatest percentage of conserved hydrophilic residues in any domain of Exo70. Most of these conserved hydrophobic residues participate in packing within the hydrophobic core of the domain. 40.0/47.6% of these residues are aromatic and most of these are concentrated near the tip of the molecule, suggesting that the internal structure of this domain is important. The conserved hydrophilic residues are mostly concentrated in a large surface exposed patch (Figure 4.8). These residues are Lys540/565, *Sc*Asp541,

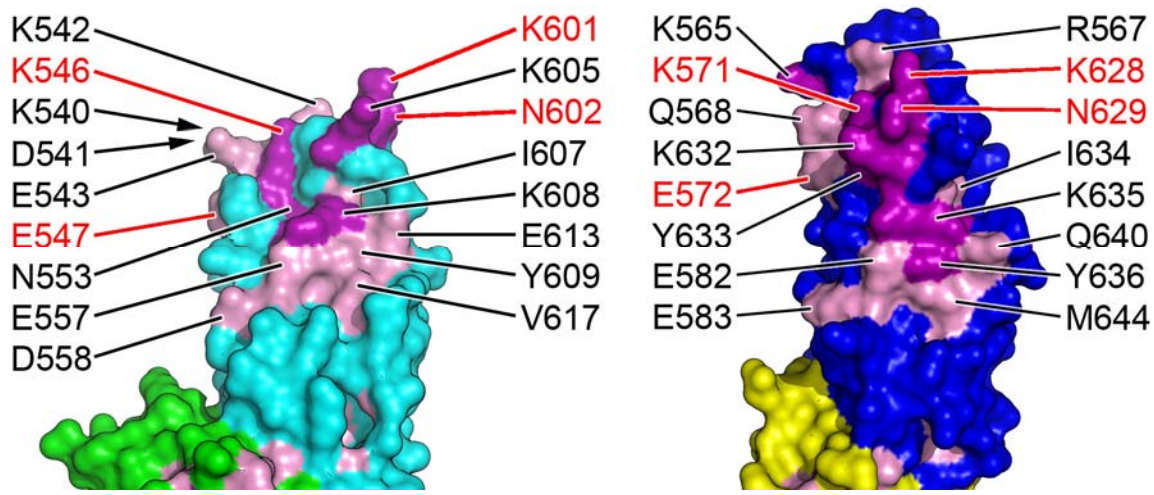

Figure 4.8: Surface exposed conserved residues of the C domain

A molecular surface diagram of the C domain of *Sc*Exo70$_{\Delta 62}$ (left) and *Mm*Exo70$_{\Delta 84}$ (right). The left and right panels are rotated 45° about the long axis of the molecule with respect to Figure 4.1 and 4.2, respectively. The M domain is colored green in *Sc*Exo70$_{\Delta 62}$ and yellow in *Mm*Exo70$_{\Delta 84}$, and the C domain is colored cyan in *Sc*Exo70$_{\Delta 62}$ and blue in *Mm*Exo70$_{\Delta 84}$. Completely conserved residues are colored purple and similarly conserved residues are colored pink. Lines indicate residues contributing to the large conserved surface patch on the C domain. Arrows indicate conserved residues on the back of the molecule. Residues highlighted in red are homologous to residues required for Arpc1 binding in *R. norvegicus*.

Lys542/Arg567, Glu543/Gln568, Lys546/571, Glu547/572, *Sc*Asn553, Glu557/582, and Asp558/Glu583 on H17; Lys601/628, Asn602/629, Lys605/632, *Mm*Tyr633, Ile607/634, Lys608/635, and Tyr609/636 on $L_{18\text{-}19}$; and Glu613/Gln640 and Val617/Met644 on H19. Lys571-Glu572 and Lys628-Pro630, residues found to be important for Arpc1 interaction in *R. norvegicus* (Zuo *et al.*, 2006), are included in this patch except for Pro630, implicating this patch in the Arpc1 interaction. However, mutation of Lys565, found on the edge of this patch, has no effect on Arpc1 binding (Zuo *et al.*, 2006). This suggests that at least one of the conserved residues in this patch are redundant or not required for this interaction. It is also possible that Lys565 could participate under circumstances other the experimental conditions applied, or that a second interaction could occur at this site that requires this residue. Despite the strong conservation of residues both on the surface of the molecule and within the hydrophobic core, the surface topology of this patch does not appear to be well conserved between species due to variations in the positions of $L_{16\text{-}17}$ and $L_{18\text{-}19}$ among all structures. This suggests that these loops may be inherently flexible and may be stabilized by interaction with other proteins. These loops form intermolecular interactions within the crystal lattice except for $L_{16\text{-}17}$ in the C2 crystal form, where it is disordered (Hamburger *et al.*, 2006). Thus, it is possible that the surface topology of this domain can reorganize when interacting with a binding partner such as Arpc1.

A second difference between the C domains of *Sc*Exo70$_{\Delta 62}$ and *Mm*Exo70$_{\Delta 84}$ is found in the length of H16 and $L_{16\text{-}17}$. H16 is eight residues shorter and $L_{16\text{-}17}$ is seven residues longer in *Mm*Exo70$_{\Delta 84}$ than in *Sc*Exo70$_{\Delta 62}$. This apparent exchange of residues from H16 to $L_{16\text{-}17}$ may result from a partial unwinding of H16, which could theoretically

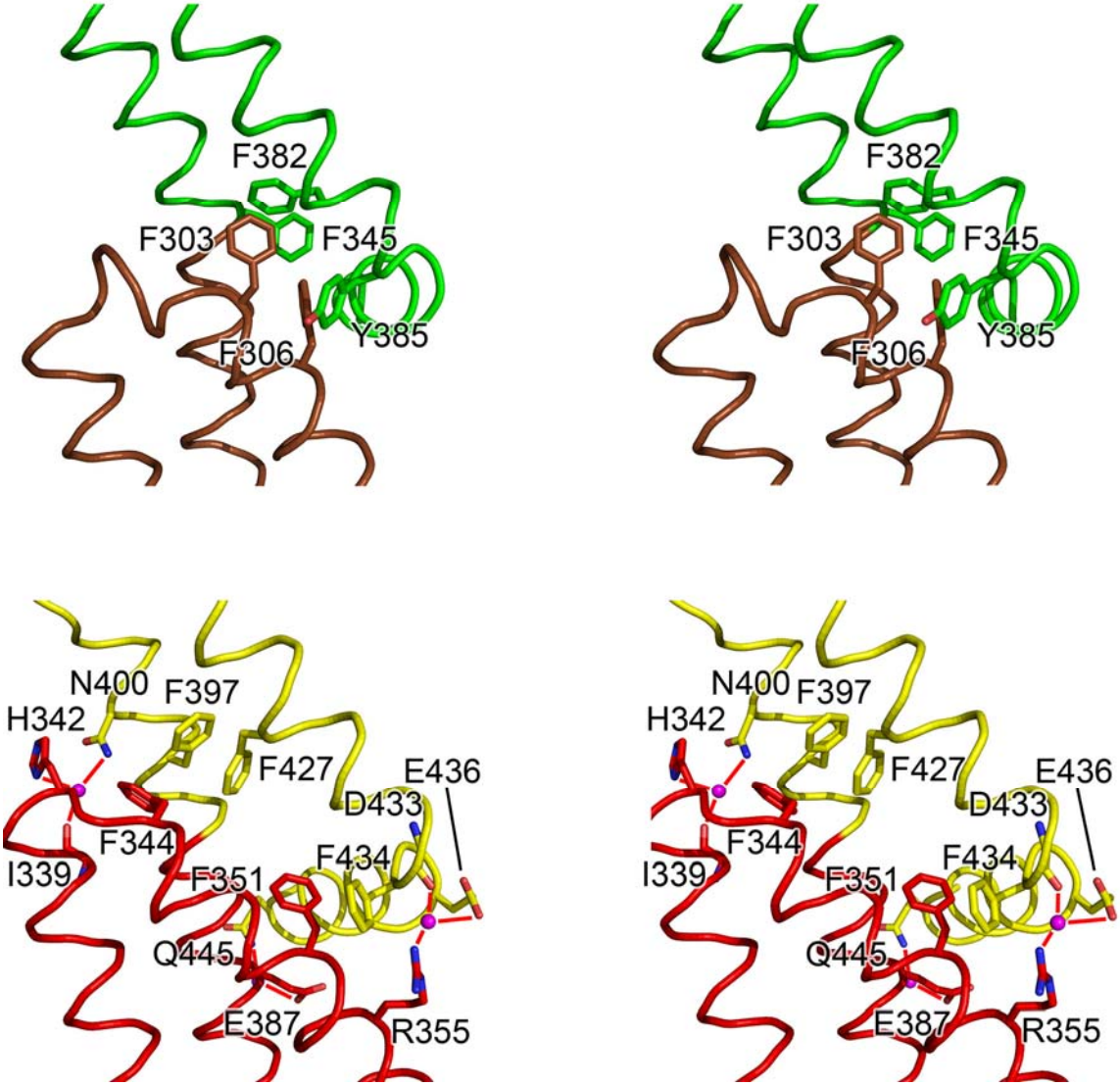

Figure 4.9: Residues involved in the N and M domain interface

A stereo cartoon diagram of the N and M domain interface of *Sc*Exo70$_{\Delta 62}$ (top) and *Mm*Exo70$_{\Delta 84}$ (bottom). H8-H12 are shown as ribbons with the N domain colored brown in *Sc*Exo70$_{\Delta 62}$ and red in *Mm*Exo70$_{\Delta 84}$ and the M domain colored green in *Sc*Exo70$_{\Delta 62}$ and yellow in *Mm*Exo70$_{\Delta 84}$. These sections were aligned using the DALI server. The side chains or main chains of residues that participate in the interface between the N and M domains are labeled and shown as sticks with oxygen colored red and nitrogen colored blue. Relevant water molecules are shown as magenta spheres. Red lines depict hydrogen bonds.

be the result of a pulling force exerted by the intermolecular contacts. It is also possible that this difference in H16 and $L_{16\text{-}17}$ lengths could be a true representation of the molecule. It is unclear if this feature has any effect on the conserved regions of the domain, whether it is naturally occurring or an artifact of crystallization.

Comparison of the N-M domain interface

The N-M domain interface in *Sc*Exo70$_{\Delta 62}$ is composed of H10, which is kinked at the domain boundary, and a single patch of hydrophobic residues composed of Phe303 and Phe306 on H9, Leu344 and Phe345 on H10, Phe382 on H11, and Tyr385 on $L_{11\text{-}12}$ (Figure 4.9). All of these residues except Tyr385 are conserved hydrophobic residues. The interface between these two domains buries only 580Å^2, the smallest interface of any Exo70 molecule.

The N-M domain interface in *Mm*Exo70$_{\Delta 84}$ is composed of H10, which is not kinked, two small hydrophobic patches, and several water-mediated hydrogen bonds (Figure 4.9). The first hydrophobic patch is composed of Phe344 on H9, Phe397 on H10, and Phe427 on H11. These residues correspond to *Sc*Exo70$_{\Delta 62}$ Phe303, Phe345 and Phe382, respectively. The second hydrophobic patch, which is separated from the first by a space of 6Å, is composed of Phe351 and Leu354 on H9, Leu394 on H10, and Phe434 and Met441 on H12. Phe351, Leu394, and Phe434 correspond to *Sc*Exo70$_{\Delta 62}$ Phe306, Leu344, and Tyr385, respectively. All of these residues except Phe344, Phe427, and Phe434 are conserved hydrophobic residues. The *Mm*Exo70$_{\Delta 84}$ N-M domain interface buries an area of 741Å^2, which is 27.8% greater than the interface in *Sc*Exo70$_{\Delta 62}$. Water-mediated hydrogen bonds that participate in this interface exist between the carbonyl of

Ile339 on H8, the side chain of His342 on $L_{8\text{-}9}$, and the side chain of Asn400 on H10; the side chain of Arg355 on H9 and the carbonyl of Asp433 on H11; and the side chain of Glu387 on H10 and the side chains of Glu436 and Gln445 on H12.

The N-M domain interface in *Sc*Exo70 is composed of only H10 and a single hydrophobic patch. The C2 crystal form contains four molecules in the asymmetric unit, each of which has a different angle in the kink of H10 that differs by up to 14.6° (Hamburger *et al.*, 2006). This observation, combined with the presence of only a single small patch of residues adjacent to H10 at this interface, suggests that this interface is flexible. It is unclear what the actual range of motion is for this feature or what function could be associated with it. The N-M domain interface in *Mm*Exo70$_{\Delta 84}$ is unlikely to be as flexible as in *Sc*Exo70$_{\Delta 62}$ as a result of the increased buried surface area and the water-mediated hydrogen bonds. These features are predicted to have a stabilizing effect on this interface, although flexibility at this location has not been ruled out.

Comparison of the M-C domain interface

The overall organization of the M-C domain interface is conserved, as each feature that is involved appears in a similar location and position. The residues participating in this interface, however, are not well conserved. The interface is composed of a large hydrophobic core surrounded by hydrogen bonds. The only notable feature of this interface is the hydrogen bond that is formed between the carbonyl of Asp414 on $L_{10\text{-}11}$ and the amide of Ala592 on $L_{17\text{-}18}$, as described previously.

Comparison of overall surface electrostatic potentials

*Sc*Exo70$_{\Delta 62}$ has been noted for the polarity of its surface electrostatic potential (Dong *et al.*, 2005; Hamburger *et al.*, 2006). Its N-terminus is strongly electronegative, resulting from a patch of residues found on H2, H3 and H5 (Figure 4.10). Its C-terminus is primarily electropositive, resulting primarily from residues on $L_{10\text{-}11}$, H11, $L_{13\text{-}14}$, H14, and H16-H19. This polarity is not observed in *Mm*Exo70$_{\Delta 84}$ (Figure 4.10). Its N-terminus lacks a strong electronegative patch, and the C-terminus retains only a small electropositive patch at the extreme tip of the molecule that is primarily composed of Lys561, Arg563, Lys565, Arg567, Lys571, Lys575, Lys628, Lys632, and Lys635. All of these residues except Lys561, Arg563, and Lys575 are conserved, and Lys571 and Lys628 have been implicated in Arpc1 interaction (Zuo *et al.*, 2006). The middle of *Mm*Exo70$_{\Delta 84}$ has an overall electronegative potential that contrasts with the mixed potential found in this region of *Sc*Exo70$_{\Delta 62}$. Residues found primarily on H4, $L_{4\text{-}5}$, H7, H9-H12, H14-H15, $L_{17\text{-}18}$ and H18 contribute to this feature of *Mm*Exo70$_{\Delta 84}$. Only a few small regions have the same electrostatic potential in both structures. In addition to the C-terminal electropositive patch, residues on H6 form a second electropositive patch that is opposite the strong N-terminal electronegative patch on *Sc*Exo70$_{\Delta 62}$. Two electronegative pockets are composed of residues found on H7 and H9, and H14-H15. Thus, Exo70 has highly variable surface electrostatic properties, suggesting great variability in any electrostatic requirements for Exo70-mediated protein-protein interactions.

Comparison to other molecules

The overall organization of Exo70 is novel. The Dali Server's Database Search tool (Holm and Sander, 1995) was used to search the RCSB PDB (Berman *et al.*, 2000)

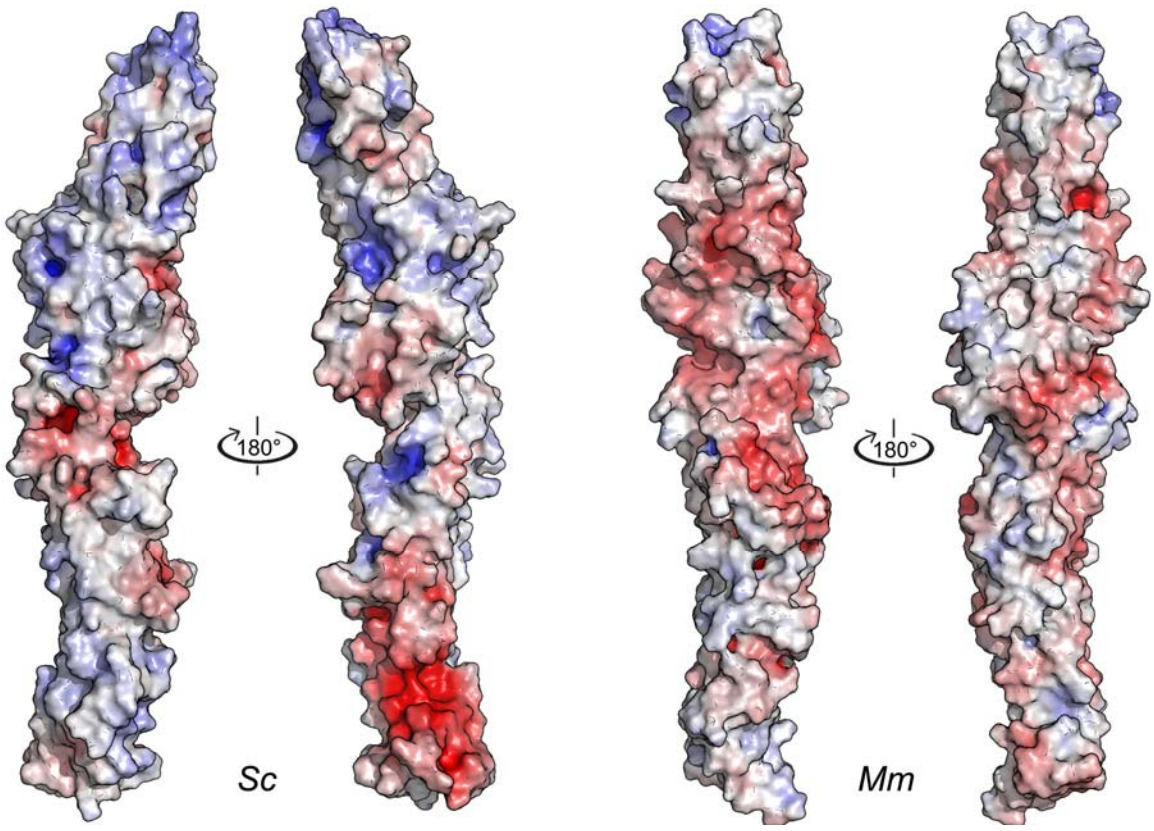

Figure 4.10: Surface electrostatic potential

The molecular surfaces of *Sc*Exo70$_{\Delta 62}$ (left two panels) and *Mm*Exo70$_{\Delta 84}$ (right two panels). The left panel of each pair is oriented as in Figures 4.1 and 4.2, respectively. The right panel of each pair is rotated 180° about the long axis of the molecule with respect to the left panel. The surfaces are colored on the basis of the solvent-accessible electrostatic potential of the molecules. Blue and red depict positive and negative electrostatic potential, respectively, with a range of $\pm 10 k_B T/e$. White depicts neutral electrostatic potential. All missing side chains, but not completely missing residues, were modeled in a rotamer allowed by the surrounding structure for this calculation.Electrostatic potentials were produced using the adaptive Poisson-Boltzmann solver in the APBS Tools plug-in for PyMOL (www.umich.edu/~mlerner/Pymol).

for proteins with structures similar to each domain or pair of adjoining domains of *Sc*Exo70$_{\Delta 62}$ or *Mm*Exo70$_{\Delta 84}$. No strong matches were detected except with the N domain. High-scoring matches for all queries found helix-turn-helix motifs from various proteins that overlapped for only one or two motifs, even when multiple motifs were present, suggesting that the arrangement of helix-turn-helix motifs found in Exo70 is unique among structures in the PDB. Good matches with extensive similarity to the N domain include the N domain of the opposite Exo70 molecule, the C-terminus of *Sc*Exo84 (Dong *et al.*, 2005), the C-terminus of *D. melanogaster* Sec15 (Sivaram *et al.*, 2006; Wu *et al.*, 2005), the C-terminus of *Sc*Sec6 (Sivaram *et al.*, 2006), and the C-terminal cargo-binding domain of *Sc*Myo2 (Pashkova *et al.*, 2006). Each of these molecules is primarily composed of a domain that corresponds well to the N domain of Exo70, including a corresponding α-helix for each α-helix of the domain (Figure 4.11). *Sc*Myo2 is an unconventional Myosin V motor protein involved in the transport of exocytic vesicles and other organelles along actin filaments (Govindan *et al.*, 1995; Johnston *et al.*, 1991). Like *Sc*Exo70, it interacts with Rho3, although this domain is probably not involved in both cases (Robinson *et al.*, 1999). Each of these crystal structures begins with the same corresponding α-helix, suggesting that there is a common property associated with the N-terminus of this domain that disfavors crystallization. This could possibly be a flexible loop immediately prior to H1. So far, Exo70 is the only molecule known to contain this domain near its N-terminus.

The function of this fold remains unclear despite its presence in these structures. It has been speculated that other exocyst subunits may also contain this fold (Munson and Novick, 2006), and it is possible that it plays a general role in protein-protein

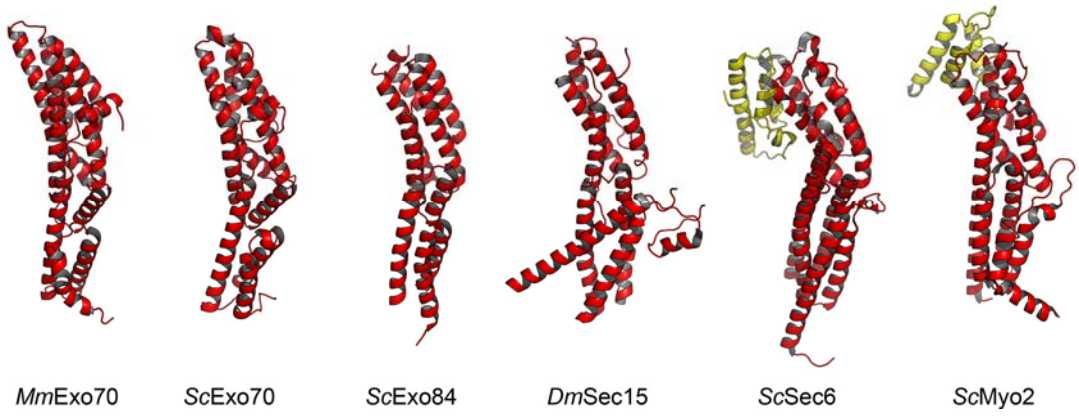

Figure 4.11: Similarity of the N domain to other molecules

A cartoon diagram of structures with similarity to the N domain of Exo70. From left to right the structures shown are the N domain of *Mm*Exo70$_{\Delta 84}$, the N domain of *Sc*Exo70$_{\Delta 62}$, a C terminal portion of *S. cerevisiae* Exo84, a C-terminal portion of *D. melanogaster* Sec15, a C-terminal portion of *S. cerevisiae* Sec6, and the C-terminal cargo binding domain of *S. cerevisiae* Myo2. All structures were aligned using the DALI server to *Sc*Exo70$_{\Delta 62}$ and *Mm*Exo70$_{\Delta 84}$ in orientations similar to Figures 4.1 and 4.2, respectively. Except for *Sc*Exo70$_{\Delta 62}$ and *Mm*Exo70$_{\Delta 84}$, the entirety of these structures are shown. Portions of these structures that correspond to H1-H10 of *Sc*Exo70$_{\Delta 62}$ and *Mm*Exo70$_{\Delta 84}$ are colored red, and additional residues are colored yellow.

interactions, as these are a common feature among exocyst subunits and *Sc*Myo2. A large number of interactions have been identified among exocyst subunits (Munson and Novick, 2006). In *S. cerevisiae* Exo70 interacts with Sec6, Sec8 and Sec10 in a manner that may require at least a portion of its N domain in each case (Dong *et al.*, 2005), and the C-terminus of Sec6 interacts with Exo70 and Sec10 (Sivaram *et al.*, 2006). Also, in *H. sapiens* Exo70, the N domain is required for interaction with TC10 (Inoue *et al.*, 2003). In *D. melanogaster* Sec15, the C-terminal half of this domain is required for its interaction with Rab11 (Wu *et al.*, 2005; Zhang, 2003). The cargo-binding domain of *Sc*Myo2 is capable of binding to multiple protein targets, including *Sc*Vac17 and an unidentified protein required for secretory vesicle binding at two separate sites (Catlett and Weisman, 1998; Catlett *et al.*, 2000; Pashkova *et al.*, 2005; Pashkova *et al.*, 2006; Schott *et al.*, 1999). Taken together, these findings are consistent with a general function of protein-protein interaction for this domain. Given the relationship between these molecules and the rarity of this fold, it is also possible that this fold plays a specific role in exocytosis.

REFERENCES

Berman, H. M., Westbrook, J., Feng, Z., Gilliland, G., Bhat, T. N., Weissig, H., Shindyalov, I. N., and Bourne, P. E. (2000). The Protein Data Bank. *Nucleic acids research* **28**, 235-242.

Carninci, P. and Kasukawa, T. and Katayama, S. and Gough, J. and Frith, M. C. and Maeda, N. and Oyama, R. and Ravasi, T. and Lenhard, B. and Wells, C. and Kodzius, R. and Shimokawa, K. and Bajic, V. B. and Brenner, S. E. and Batalov, S. and Forrest, A. R. and Zavolan, M. and Davis, M. J. and Wilming, L. G. and Aidinis, V. and Allen, J. E. and Ambesi-Impiombato, A. and Apweiler, R. and Aturaliya, R. N. and Bailey, T. L. and Bansal, M. and Baxter, L. and Beisel, K. W. and Bersano, T. and Bono, H. and Chalk, A. M. and Chiu, K. P. and Choudhary, V. and Christoffels, A. and Clutterbuck, D. R. and Crowe, M. L. and Dalla, E. and Dalrymple, B. P. and de Bono, B. and Della Gatta, G. and di Bernardo, D. and Down, T. and Engstrom, P. and Fagiolini, M. and Faulkner, G. and Fletcher, C. F. and Fukushima, T. and Furuno, M. and Futaki, S. and Gariboldi, M. and Georgii-Hemming, P. and Gingeras, T. R. and Gojobori, T. and Green, R. E. and Gustincich, S. and Harbers, M. and Hayashi, Y. and Hensch, T. K. and Hirokawa, N. and Hill, D. and Huminiecki, L. and Iacono, M. and Ikeo, K. and Iwama, A. and Ishikawa, T. and Jakt, M. and Kanapin, A. and Katoh, M. and Kawasawa, Y. and Kelso, J. and Kitamura, H. and Kitano, H. and Kollias, G. and Krishnan, S. P. and Kruger, A. and Kummerfeld, S. K. and Kurochkin, I. V. and Lareau, L. F. and Lazarevic, D. and Lipovich, L. and Liu, J. and Liuni, S. and McWilliam, S. and Madan Babu, M. and Madera, M. and Marchionni, L. and Matsuda, H. and Matsuzawa, S. and Miki, H. and Mignone, F. and Miyake, S. and Morris, K. and Mottagui-Tabar, S. and Mulder, N. and Nakano, N. and Nakauchi, H. and Ng, P. and Nilsson, R. and Nishiguchi, S. and Nishikawa, S.*, et al.* (2005). The Transcriptional Landscape of the Mammalian Genome. *Science (New York, NY* **309**, 1559-1563.

Catlett, N. L. and Weisman, L. S. (1998). The Terminal Tail Region of a Yeast Myosin-V Mediates Its Attachment to Vacuole Membranes and Sites of Polarized Growth. *Proceedings of the National Academy of Sciences of the United States of America* **95**, 14799-14804.

Catlett, N. L., Duex, J. E., Tang, F., and Weisman, L. S. (2000). Two Distinct Regions in a Yeast Myosin-V Tail Domain Are Required for the Movement of Different Cargoes. *The Journal of cell biology* **150**, 513-526.

Cuff, J. A. and Barton, G. J. (2000). Application of Multiple Sequence Alignment Profiles to Improve Protein Secondary Structure Prediction. *Proteins* **40**, 502-511.

Dong, G., Hutagalung, A. H., Fu, C., Novick, P., and Reinisch, K. M. (2005). The Structures of Exocyst Subunit Exo70p and the Exo84p C-Terminal Domains Reveal a Common Motif. *Nat Struct Mol Biol* **12**, 1094-1100.

Govindan, B., Bowser, R., and Novick, P. (1995). The Role of Myo2, a Yeast Class V Myosin, in Vesicular Transport. *The Journal of cell biology* **128**, 1055-1068.

Guo, W., Roth, D., Gatti, E., De Camilli, P., and Novick, P. (1997). Identification and Characterization of Homologues of the Exocyst Component Sec10p. *FEBS letters* **404**, 135-139.

Hamburger, Z. A., Hamburger, A. E., West, A. P., Jr., and Weis, W. I. (2006). Crystal Structure of the S.Cerevisiae Exocyst Component Exo70p. *Journal of molecular biology* **356**, 9-21.

Holm, L. and Sander, C. (1995). Dali: A Network Tool for Protein Structure Comparison. *Trends in biochemical sciences* **20**, 478-480.

Holm, L. and Park, J. (2000). Dalilite Workbench for Protein Structure Comparison. *Bioinformatics* **16**, 566-567.

Inoue, M., Chang, L., Hwang, J., Chiang, S. H., and Saltiel, A. R. (2003). The Exocyst Complex Is Required for Targeting of Glut4 to the Plasma Membrane by Insulin. *Nature* **422**, 629-633.

Johnston, G. C., Prendergast, J. A., and Singer, R. A. (1991). The Saccharomyces Cerevisiae Myo2 Gene Encodes an Essential Myosin for Vectorial Transport of Vesicles. *The Journal of cell biology* **113**, 539-551.

Munson, M. and Novick, P. (2006). The Exocyst Defrocked, a Framework of Rods Revealed. *Nat Struct Mol Biol* **13**, 577-581.

Pashkova, N., Catlett, N. L., Novak, J. L., Wu, G., Lu, R., Cohen, R. E., and Weisman, L. S. (2005). Myosin V Attachment to Cargo Requires the Tight Association of Two Functional Subdomains. *The Journal of cell biology* **168**, 359-364.

Pashkova, N., Jin, Y., Ramaswamy, S., and Weisman, L. S. (2006). Structural Basis for Myosin V Discrimination between Distinct Cargoes. *The EMBO journal* **25**, 693-700.

Robinson, N. G., Guo, L., Imai, J., Toh, E. A., Matsui, Y., and Tamanoi, F. (1999). Rho3 of Saccharomyces Cerevisiae, Which Regulates the Actin Cytoskeleton and Exocytosis, Is a Gtpase Which Interacts with Myo2 and Exo70. *Molecular and cellular biology* **19**, 3580-3587.

Schott, D., Ho, J., Pruyne, D., and Bretscher, A. (1999). The Cooh-Terminal Domain of Myo2p, a Yeast Myosin V, Has a Direct Role in Secretory Vesicle Targeting. *The Journal of cell biology* **147**, 791-808.

Sivaram, M. V., Furgason, M. L., Brewer, D. N., and Munson, M. (2006). The Structure of the Exocyst Subunit Sec6p Defines a Conserved Architecture with Diverse Roles. *Nat Struct Mol Biol* **13**, 555-556.

Strausberg, R. L., Feingold, E. A., Grouse, L. H., Derge, J. G., Klausner, R. D., Collins, F. S., Wagner, L., Shenmen, C. M., Schuler, G. D., Altschul, S. F., Zeeberg, B., Buetow, K. H., Schaefer, C. F., Bhat, N. K., Hopkins, R. F., Jordan, H., Moore, T., Max, S. I., Wang, J., Hsieh, F., Diatchenko, L., Marusina, K., Farmer, A. A., Rubin, G. M., Hong, L., Stapleton, M., Soares, M. B., Bonaldo, M. F., Casavant, T. L., Scheetz, T. E., Brownstein, M. J., Usdin, T. B., Toshiyuki, S., Carninci, P., Prange, C., Raha, S. S., Loquellano, N. A., Peters, G. J., Abramson, R. D., Mullahy, S. J., Bosak, S. A., McEwan, P. J., McKernan, K. J., Malek, J. A., Gunaratne, P. H., Richards, S., Worley, K. C., Hale, S., Garcia, A. M., Gay, L. J., Hulyk, S. W., Villalon, D. K., Muzny, D. M., Sodergren, E. J., Lu, X., Gibbs, R. A., Fahey, J., Helton, E., Ketteman, M., Madan, A., Rodrigues, S., Sanchez, A., Whiting, M., Madan, A., Young, A. C., Shevchenko, Y., Bouffard, G. G., Blakesley, R. W., Touchman, J. W., Green, E. D., Dickson, M. C., Rodriguez, A. C., Grimwood, J., Schmutz, J., Myers, R. M., Butterfield, Y. S., Krzywinski, M. I., Skalska, U., Smailus, D. E., Schnerch, A., Schein, J. E., Jones, S. J., and Marra, M. A. (2002). Generation and Initial Analysis of More Than 15,000 Full-Length Human and Mouse Cdna Sequences. *Proceedings of the National Academy of Sciences of the United States of America* **99**, 16899-16903.

Synek, L., Schlager, N., Elias, M., Quentin, M., Hauser, M. T., and Zarsky, V. (2006). Atexo70a1, a Member of a Family of Putative Exocyst Subunits Specifically Expanded in Land Plants, Is Important for Polar Growth and Plant Development. *Plant J* **48**, 54-72.

Thompson, J. D., Higgins, D. G., and Gibson, T. J. (1994). Clustal W: Improving the Sensitivity of Progressive Multiple Sequence Alignment through Sequence Weighting, Position-Specific Gap Penalties and Weight Matrix Choice. *Nucleic acids research* **22**, 4673-4680.

Wu, S., Mehta, S. Q., Pichaud, F., Bellen, H. J., and Quiocho, F. A. (2005). Sec15 Interacts with Rab11 Via a Novel Domain and Affects Rab11 Localization in Vivo. *Nat Struct Mol Biol* **12**, 879-885.

Zhang, B. (2003). Genetic and Molecular Analysis of Synaptic Vesicle Recycling in Drosophila. *J Neurocytol* **32**, 567-589.

Zuo, X., Zhang, J., Zhang, Y., Hsu, S. C., Zhou, D., and Guo, W. (2006). Exo70 Interacts with the Arp2/3 Complex and Regulates Cell Migration. *Nature cell biology* **8**, 1383-1388.

Chapter 5

Discussion of the Structures of *Sc*Exo70$_{\Delta 62}$ and *Mm*Exo70$_{\Delta 84}$

Introduction

The examination of the structures of *Sc*Exo70$_{\Delta 62}$ and *Mm*Exo70$_{\Delta 84}$ reveal several interesting features that deserve further study. The interaction of a GTPase with Exo70 is conserved only as far as the family of that GTPase is concerned. Rho3 and TC10, both Rho family GTPases, interact with Exo70 at different locations in the respective species they are found (Inoue *et al.*, 2003; Robinson *et al.*, 1999). Arpc1, in contrast, interacts with Exo70 at a highly conserved location. At least one of the conserved residues in this region is not involved in Arpc1 interaction, making a complete understanding of this interaction desirable (Zuo *et al.*, 2006).

The overall architecture of Exo70 is relatively well conserved between *S. cerevisiae* and *M. musculus* despite low sequence similarity (12% identity and 35% similarity) between these two species. A truncation deleting approximately 10% of the residues from the N-terminus of the molecule leaves questions about the function, organization, and conservation of these residues. In addition, differences in $L_{4\text{-}5}$ and $L_{6\text{-}7}$ reveal the potential for a functional association. The N-M domain interface appears to be stabilized in *Mm*Exo70$_{\Delta 84}$ in comparison to the flexible interface ovserved in *Sc*Exo70$_{\Delta 62}$ and could serve to prevent an undetermined *Sc*Exo70-specific function from occurring in mammalian Exo70. Lastly, observations and comparisons between the M and C domains

of these structures suggest the possibility of a functional reorganization within the M domain, resulting in the reorientation of the C domain.

GTPase interactions

It is not clear how *Sc*Rho3 and mammalian TC10, both Rho GTPases, have evolved to interact with Exo70 on two separate domains (Inoue *et al.*, 2003; Robinson *et al.*, 1999). It would be useful to understand how these two different binding sites offer species-specific interactions important for their functions. *Sc*Rho3 interacts with the M domain, a central location that could allow the interaction to affect a large part of the structure within the molecule. Mammalian TC10 is known to interact with the N domain, probably near its N-terminus. This location presents a different electrostatic environment and probably a different topological organization for GTPase interactions. Neither of these interaction sites is well conserved, which is not surprising given the inconsistency of the GTPase interaction site. In the following sections more will be discussed concerning the possible effects of GTPase binding on each structural feature.

N-terminal truncation

The N-terminal 62 and 84 residues are truncated in *Sc*Exo70$_{\Delta 62}$ and *Mm*Exo70$_{\Delta 84}$, respectively. Both of these constructs begin with a portion of the loop preceding H1. Each of the structures containing a fold similar to the N domain, *Sc*Exo84 (Dong *et al.*, 2005), *Dm*Sec15 (Wu *et al.*, 2005), *Sc*Sec6 (Sivaram *et al.*, 2006), and *Sc*Myo2 (Pashkova *et al.*, 2006), has a variable number of residues N-terminal of H1. Each of these constructs was identified by limited proteolysis or, in one case, domain prediction

by BLAST (Marchler-Bauer *et al.*, 2003). The fact that many of these similar constructs were identified by limited proteolysis suggests that this beginning region is commonly accessible and susceptible to general proteolysis, and therefore likely to be unstructured and flexible. The *Mm*Exo70$_{\Delta 75}$ construct was created based on the *Sc*Exo70$_{\Delta 62}$ construct by beginning at the same relative location. Its failure to crystallize is consistent with the idea that this region is flexible, although the successful crystallization of the similar *Sc*Exo70$_{\Delta 62}$ construct suggests that this flexibility may not be identical in all molecules. This is not unexpected due to the low sequence homology among these molecules (*Mm*Exo70 is composed of 5.1% completely conserved residues and 23.1% partially conserved residues based on Figure 4.3).

Exo70 contains a cluster of conserved residues among the 28 residues preceding H1, including four of nine completely conserved residues in the N domain. There are also seven similarly conserved residues, including two hydrophilic residues. Although there are only a few, other conserved residues in the structures of Exo70 appear to play a role in either conservation of structure or protein interaction. A few of these N-terminal conserved residues are present in the structures, including Leu68, Val71, and Val74 in *Sc*Exo70$_{\Delta 62}$ and Val87 in *Mm*Exo70$_{\Delta 84}$. Asp85 is also present but lacks side chain density. Val74/87 packs against $L_{2\text{-}3}$, and *Sc*Leu68 and *Sc*Val71 are solvent exposed. It is unusual to have solvent exposed, conserved hydrophobic residues unless they have a specific function usually involved in protein-protein interaction, but it is not clear if these residues are actually solvent exposed in the full-length protein. The truncated residues are predicted by jnet (Cuff and Barton, 2000) to form two α-helices, and these could be organized in the style of right-handed helix-turn-helix motif found throughout the rest of

this domain. The positions of these solvent exposed hydrophobic residues could be artificial due to the proximity of the truncation, or they could be involved in packing with the α-helices formed by the truncated residues. Currently there is not enough data to determine the role that any of these residues might play in the structure and function of Exo70. If some of these conserved residues did indeed form a surface exposed patch, this would suggest a conserved interaction at this site. The only known interaction in this region would be TC10 in mammals, although this raises the additional question of why TC10-interacting residues would be conserved in *Sc*Exo70 since this interaction does not exist in *S. cerevisiae*.

$L_{4\text{-}5}$ and $L_{6\text{-}7}$

$L_{4\text{-}5}$ and $L_{6\text{-}7}$ are both significantly longer in *Mm*Exo70$_{\Delta 84}$ than in *Sc*Exo70$_{\Delta 62}$. *Mm*Exo70$_{\Delta 84}$ H4 also contains three extra residues and lays flat across H6 and H7, while *Sc*Exo70$_{\Delta 62}$ H4 projects out and away from the surface of these α-helices. This is not too surprising, as the interactions between $L_{3\text{-}4}$ and H6 are not conserved and may affect the organization of this region. The skewed angle of *Sc*Exo70$_{\Delta 62}$ H4 increases the distance traveled by $L_{4\text{-}5}$, causing it to traverse a relatively linear path along H7. The position and length of *Mm*Exo70$_{\Delta 84}$ H4 puts the start of $L_{4\text{-}5}$ on a different face of H7. *Mm*Exo70$_{\Delta 84}$ $L_{4\text{-}5}$ contains additional residues and covers less distance than *Sc*Exo70$_{\Delta 62}$ $L_{4\text{-}5}$, resulting in a meandering, non-linear path for this loop. Nine residues are missing from the structure of this loop, making it unclear how exactly these residues interact with the rest of the molecule, but it could also suggest that they are flexible. In addition, of the molecules with structural similarity to the N domain mentioned above, only one, *Sc*Sec6,

contains an α-helix corresponding to H4, although with a different conformation. Thus, H4 may have a specific function in Exo70 and *Sc*Sec6, and its position is not important to this function. *Sc*Exo84, *Dm*Sec15, and *Sc*Myo2 structures each have a short loop connecting the α-helices equivalent to H3 and H5, demonstrating that H4 and its adjoining loops are not necessary for the general function of this domain.

$L_{6\text{-}7}$ has the most variable length of any region in Exo70 and has no obvious correlation between length and species complexity. For example, *Schizosaccharomyces pombe* $L_{6\text{-}7}$ contains more residues than either *Caenorhabditis elegans* or *S. cerevisiae*. *Sc*Exo70$_{\Delta 62}$ $L_{6\text{-}7}$ is composed of 16 residues and *Mm*Exo70$_{\Delta 84}$ has 33. There are also several forms of *Mm*Exo70 found in different tissues, including two longer forms in brain (Carninci *et al.*, 2005; Guo *et al.*, 1997). These include an additional insert at the end of this loop that is predicted by jnet (Cuff and Barton, 2000) to contain an additional α-helix and an extension of H7. The specific function of this insert has not been studied to date, and its absence from the structure prevents any direct conclusions from being drawn. Comparison to other molecules with structural similarity to the N domain reveals that $L_{6\text{-}7}$ is always partially disordered, except in *Sc*Sec6, which contains a short loop interrupted by a small α-helix. This again suggests that some amount of variability is inherent in this region, and that a function not necessary for the general function of the domain may be associated with this flexible region. *Mm*Exo70$_{\Delta 84}$ is unique among similar structures both for the long length of $L_{6\text{-}7}$ and the high number of disordered residues present. Also, it is conceivable that some secondary structure may form within $L_{6\text{-}7}$, although it predicted to be unstructured.

N-M domain interface

The N and M domain interface is flexible in *Sc*Exo70$_{\Delta 62}$ (Hamburger *et al.*, 2006). One possible reason for this feature could be that the association between the vesicle and the plasma membrane as mediated by the exocyst is not rigid, and some flexibility is required within the exocyst in order to properly maintain this dynamic interaction. Alternatively, the conformation of this interface could be stabilized by interactions with other exocyst components, making innate stability unnecessary. Conversely, the conformation of this interface may be part of an important function of *Sc*Exo70. This could be modulated by interaction with another factor, usch as Arpc1 (Zuo *et al.*, 2006), GTPases (Inoue *et al.*, 2003; Robinson *et al.*, 1999), other exocyst subunits (Munson and Novick, 2006), and potentially other factors that could modify the interactions made by *Sc*Exo70, possibly affecting the function of the complex. As an example, the interaction of Rho3 with the M domain of *Sc*Exo70 could dictate a particular organization at this interface, which could potentially affect the organization and interactions between Exo70 and exocyst subunits.

If some flexibility is required for a dynamic interaction between the vesicle and the plasma membrane in *Sc*Exo70$_{\Delta 62}$, the structure of the *Mm*Exo70$_{\Delta 84}$ N and M domain interface suggests that this motion is either diminished or prevented in this molecule (see Chapter 4) and must either be relegated to another part of the exocyst or is otherwise not a necessary feature. Another possibility could be that the flexibility of this interface is required for Rho3 to affect exocyst function, but not for TC10, which could account for the lack of flexibility found in *Mm*Exo70$_{\Delta 84}$. Finally, Arpc1 probably does not have a

functional association with the N and M domain interface because its interaction is presumed to be important and conserved while the flexibility of this interface is not.

M domain packing and C domain orientation

The internal packing of the M domain between H11-H13 and H14-H16 may be intrinsically linked to the orientation of the C domain (see Chapter 4). Although it appears that the orientation of the C domain is stable in both *Sc*Exo70$_{\Delta 62}$ and *Mm*Exo70$_{\Delta 84}$, the apparent conservation of the $L_{10\text{-}11}$ and $L_{17\text{-}18}$ structures is conspicuous in *Sc*Exo70$_{\Delta 62}$ where they do not interact. Rho3 could possibly interact with $L_{12\text{-}13}$ or $L_{13\text{-}14}$, and the loss of a lengthy $L_{13\text{-}14}$ in more complex organisms would correlate with the loss of this function. If Rho3 does interact with one or both of these loops, this interaction could possibly affect the organization of the M domain and the orientation of the C domain, allowing it to be repositioned, possibly like that observed in *Mm*Exo70$_{\Delta 84}$. If movement is actually possible here, then a conserved function is likely to be associated with it based on the conservation of these structures. The conserved interaction of Exo70 with Arpc1 occurs on the C domain, and if the *Mm*Exo70$_{\Delta 84}$ orientation is active for Arpc1 interaction while the *Sc*Exo70$_{\Delta 62}$ orientation is not, Rho3 binding could potentially control the interaction between *Sc*Exo70 and Arpc1.

The only completely conserved interaction at the interface between H11-H13 and H14-H16 is a hydrogen bond found between the side chains of Thr372/421 and Asn479/498 (*Sc*Exo70$_{\Delta 62}$/*Mm*Exo70$_{\Delta 84}$). A hypothetical rotation from one of the two observed interfaces to the other could pivot about this interaction, which otherwise appears only to have a limited role in stabilization of the M domain. This rotation is

consistent with the hypothesis that this region can be reoriented, and it provides a clear path for this rotation to the other position. In addition, if a conserved pivot point does exist here, then it also exists in *Mm*Exo70$_{\Delta 84}$, which does not obviously require any reorientation. This could suggest the possibility of a similar movement in *Mm*Exo70, and although the available structural data do not support these theories of movement at this position, they do not preclude this possibility. Finally, the interaction of Arpc1 with the C domain could function through these loops. Different control mechanisms may be in place in different organisms, and separate proteins in mammals could effectively play the role of this feature in budding yeasts.

C domain conservation and interaction

The C domain contains a large, mostly basic conserved surface patch at the tip of the molecule and an underlying conserved core of aromatic hydrophobic residues (see Chapter 4). Arpc1 interacts with Exo70 in *S. cerevisiae* and *Rattus norvegicus*, and at least a portion of this conserved basic surface patch is involved in *R. norvegicus* (Zuo *et al.*, 2006). It is assumed that similar residues are involved in the *S. cerevisiae* interaction because these residues are conserved. It has also been found that at least one of these conserved residues, Lys565, is not required for Arpc1 interaction, and the effect of mutations on a large section of this patch has not been published. The fact that not all conserved residues of this patch are required for Arpc1 interaction raises interest in what conserved role they may actually be involved in. It is possible that Lys565 is involved in Arpc1 interaction, but in a manner that is more complex or difficult to detect. It is also possible that it, and other residues in the patch, are involved in interaction with other

proteins, although there are no known candidates at this time. It has also been proposed that this basic patch may be associated with the membrane (Dong *et al.*, 2005). This is based on the ideas that large basic patches can be associated with phospholipids, the exocyst is known to be closely associated with vesicles and the plasma membrane (Guo *et al.*, 1999b), and Exo70 is possibly involved in the localization of the exocyst and could serve as a spatial marker for its assembly in mammals (Boyd *et al.*, 2004; Inoue *et al.*, 2003). While this idea was proposed before the publication of the Arpc1 interaction data, this idea is not yet invalid, although the larger basic patch is found in *S. cerevisiae* where Exo70 has not been shown to be directly important for localization of the exocyst, which would require a specific link to the PM. In any case, it remains possible that this conserved site on Exo70 can support multiple interactions, either simultaneously or individually.

Future directions

The solution of the crystal structures of *Sc*Exo70$_{\Delta 62}$ and *Mm*Exo70$_{\Delta 84}$ has answered a few questions, such as questions about the shape, organization, and conservation of Exo70. These structures, however, raise many more questions that need to be answered before the function of Exo70 can be completely understood. The general lack of conservation and comparability to other existing protein structures contributes to the shortage of conclusions that can immediately be drawn from these structures. This section focuses on several questions that have been raised by these structures as hypothesized above.

It has been known for several years that Exo70 interacts with a different Rho family GTPase in *S. cerevisiae* than in mammals, and that these interactions occur through two separate domains. However, the details of these interactions have never been characterized in the published literature. As the interaction with GTPases is critical to the role of Exo70, it is important to gain a full understanding of how these interactions result in function, and several hypotheses posited above could explain the regulation of these important GTPases. It would also be of interest to understand how these two different binding sites are similar and different in order to further understand the function of the exocyst across species once these sites of interaction have been identified.

One of the curiosities found in comparing Exo70 to other similar structures was the corresponding start position of all N-domain-like structures with an α-helix corresponding to H1. This consistency raises interest in this feature. Additionally, the structure and function of the whole truncated portion of Exo70 is not yet understood, although it is likely to play some role in TC10 interaction in mammals. A study of this region might also determine if these truncated residues should indeed be classified as a part of the N domain or if they actually form an independent domain. The presence of a cluster of conserved residues within this truncated region suggests an important function, and further experiments are necessary to understand the full role of this region.

$L_{4\text{-}5}$ is the first of several loops in the crystallized Exo70 fragments to exhibit significant variability in length across species. The purpose of this variation is not clear, and further study needs to be done to determine if there is a function associated with this feature and what it may be. Similarly, of the structures similar to the N domain of Exo70, all except Exo70 and *Sc*Sec6 have a short loop in place $L_{3\text{-}4}$, H4, and $L_{4\text{-}5}$. This suggests

that H4 and possibly the surrounding loops may be present in these molecules in order to play some role, although more investigation is needed to determine the role of H4 and its surrounding features, and if a similar feature is associated with the corresponding region of *Sc*Sec6.

$L_{6\text{-}7}$ is also noteworthy due to its extreme variability in length between distantly related species. Mammals seem to have multiple forms with varying lengths of this loop, and both forms are of interest. This entire loop is disordered in *Mm*Exo70$_{\Delta 84}$, making it a portion of the molecule in need of further study in order to understand its role in the structure and function of Exo70 and the exocyst. It is possible that an interaction with another molecule here could stabilize the structure of this loop. Although a comprehensive study has not yet been made, the longer forms of Exo70 are expressed in the brain while the shorter form is expressed elsewhere. This suggests that the longer form may have a brain-specific function that could be tied to the presence of these additional residues. It would be useful to understand the expression patterns of different forms of Exo70 in different tissues and how exactly these different forms function.

The N and M domain interface appears to be flexible in *Sc*Exo70$_{\Delta 62}$ but not in *Mm*Exo70$_{\Delta 84}$. The functional implication of this conclusion is not clear and further study is needed to determine if flexibility at this interface is required for *Sc*Exo70$_{\Delta 62}$ function and if it is actually possible in *Mm*Exo70$_{\Delta 84}$. In addition, its possible association with GTPase functions should be examined. Further work is needed to determine not only the role of this interface but also with what various control elements it is associated with.

The packing within the M domain and the orientation of the C domain are probably the most interesting observations to result from this study, as they suggest a

possible mechanism in *Sc*Exo70. Although present structural data does not support motion of the C domain, the conservation of several residues at the interface of H11-H13 and H14-H16 could suggest otherwise. There are several facets here that are worth investigating under the hypothesis of movement at this location. First, several conserved surface exposed residues appear in $L_{10\text{-}11}$ that may be stabilizing the conformation of the loop in such a way as to maintain an orientation parallel to $L_{17\text{-}18}$, even in *Sc*Exo70$_{\Delta 62}$ where these loops do not interact directly. The function of these residues needs to be investigated in order to understand the exact role they play in these structures, in this interaction in *Mm*Exo70, and to determine if a similar interaction can occur in *Sc*Exo70 and what its role may be. Additionally, the fact that these conserved residues are surface exposed could suggest a conserved interaction, although the likelihood of this is diminished by the lack of strong surface conservation. Second, the function of the conserved hydrogen bond between Thr372/421 and Asn479/498 (*Sc*Exo70$_{\Delta 62}$/*Mm*Exo70$_{\Delta 84}$) is conspicuous and should also be investigated, as it may play an important role in the hypothesized motion. Third, *Sc*Exo70$_{\Delta 62}$ $L_{12\text{-}13}$ and $L_{13\text{-}14}$ may stabilize the C domain orientation observed in crystal structures by interacting directly with H16. These loops are only long enough to interact with H16 in budding yeast. Fission yeasts also have Rho3 that interacts with Exo70, but $L_{12\text{-}13}$ and $L_{13\text{-}14}$ are not as lengthy as they are in budding yeast, suggesting that Rho3 may not have a conserved interaction in all yeast. At least the interaction of these loops with H16 should be investigated, especially in relation to the possible movement of the C domain mentioned above, and any possible interaction with Rho3 should also be considered here. Finally, $L_{13\text{-}14}$ has a short length that appears to be conserved in all organisms other than budding

yeast. It is possible that this short loop restricts the position of the C domain in these Exo70 molecules from moving into a position similar to that observed in the *Sc*Exo70$_{\Delta 62}$ structure. An investigation of the role of this loop could reveal more about the possibility of movement in this region and the relationship of this loop to the function of Exo70 in most organisms.

The C domain is known to contain a conserved basic surface patch, of which at least part of it interacts with Arpc1. This patch is rather large, and at least one residue is not required for this interaction. The role of this residue and its conservation are therefore curious, and the deletion method used to identify the necessary residues could have had unintended effects. Further study is necessary to determine the exact nature of this interaction and to what extent this conserved patch is involved. If not all conserved residues are involved in Arpc1 interaction, then the role of these residues should be further investigated and possibly other interactions should be sought.

Conclusion

The goal of this project was to gain an understanding of the structure and function of Exo70 and to make a comparison across distantly related species in order to gain further insight into its static and variable features and functions. In this work X-ray crystallographic methods were used to determine the structures of *Sc*Exo70$_{\Delta 62}$ and *Mm*Exo70$_{\Delta 84}$. It was revealed that Exo70 is a long, rod-shaped molecule that lacks strong sequence conservation and contains a unique fold found only in a few other molecules also involved in exocytosis. The overall fold and organization of the molecule is strikingly similar across such distantly related species despite low primary sequence

conservation, although there are several notable differences in this organization. The unusual architecture of Exo70 makes it difficult to draw strong conclusions about its functions, but the plethora of new questions raised by these structures may lead to a more detailed understanding of the interplay between structure and function in Exo70.

REFERENCES

Boyd, C., Hughes, T., Pypaert, M., and Novick, P. (2004). Vesicles Carry Most Exocyst Subunits to Exocytic Sites Marked by the Remaining Two Subunits, Sec3p and Exo70p. *The Journal of cell biology* **167**, 889-901.

Carninci, P. and Kasukawa, T. and Katayama, S. and Gough, J. and Frith, M. C. and Maeda, N. and Oyama, R. and Ravasi, T. and Lenhard, B. and Wells, C. and Kodzius, R. and Shimokawa, K. and Bajic, V. B. and Brenner, S. E. and Batalov, S. and Forrest, A. R. and Zavolan, M. and Davis, M. J. and Wilming, L. G. and Aidinis, V. and Allen, J. E. and Ambesi-Impiombato, A. and Apweiler, R. and Aturaliya, R. N. and Bailey, T. L. and Bansal, M. and Baxter, L. and Beisel, K. W. and Bersano, T. and Bono, H. and Chalk, A. M. and Chiu, K. P. and Choudhary, V. and Christoffels, A. and Clutterbuck, D. R. and Crowe, M. L. and Dalla, E. and Dalrymple, B. P. and de Bono, B. and Della Gatta, G. and di Bernardo, D. and Down, T. and Engstrom, P. and Fagiolini, M. and Faulkner, G. and Fletcher, C. F. and Fukushima, T. and Furuno, M. and Futaki, S. and Gariboldi, M. and Georgii-Hemming, P. and Gingeras, T. R. and Gojobori, T. and Green, R. E. and Gustincich, S. and Harbers, M. and Hayashi, Y. and Hensch, T. K. and Hirokawa, N. and Hill, D. and Huminiecki, L. and Iacono, M. and Ikeo, K. and Iwama, A. and Ishikawa, T. and Jakt, M. and Kanapin, A. and Katoh, M. and Kawasawa, Y. and Kelso, J. and Kitamura, H. and Kitano, H. and Kollias, G. and Krishnan, S. P. and Kruger, A. and Kummerfeld, S. K. and Kurochkin, I. V. and Lareau, L. F. and Lazarevic, D. and Lipovich, L. and Liu, J. and Liuni, S. and McWilliam, S. and Madan Babu, M. and Madera, M. and Marchionni, L. and Matsuda, H. and Matsuzawa, S. and Miki, H. and Mignone, F. and Miyake, S. and Morris, K. and Mottagui-Tabar, S. and Mulder, N. and Nakano, N. and Nakauchi, H. and Ng, P. and Nilsson, R. and Nishiguchi, S. and Nishikawa, S.*, et al.* (2005). The Transcriptional Landscape of the Mammalian Genome. *Science (New York, NY* **309**, 1559-1563.

Dong, G., Hutagalung, A. H., Fu, C., Novick, P., and Reinisch, K. M. (2005). The Structures of Exocyst Subunit Exo70p and the Exo84p C-Terminal Domains Reveal a Common Motif. *Nat Struct Mol Biol* **12**, 1094-1100.

Guo, W., Roth, D., Gatti, E., De Camilli, P., and Novick, P. (1997). Identification and Characterization of Homologues of the Exocyst Component Sec10p. *FEBS letters* **404**, 135-139.

Guo, W., Roth, D., Walch-Solimena, C., and Novick, P. (1999b). The Exocyst Is an Effector for Sec4p, Targeting Secretory Vesicles to Sites of Exocytosis. *The EMBO journal* **18**, 1071-1080.

Hamburger, Z. A., Hamburger, A. E., West, A. P., Jr., and Weis, W. I. (2006). Crystal Structure of the S.Cerevisiae Exocyst Component Exo70p. *Journal of molecular biology* **356**, 9-21.

Inoue, M., Chang, L., Hwang, J., Chiang, S. H., and Saltiel, A. R. (2003). The Exocyst Complex Is Required for Targeting of Glut4 to the Plasma Membrane by Insulin. *Nature* **422**, 629-633.

Marchler-Bauer, A., Anderson, J. B., DeWeese-Scott, C., Fedorova, N. D., Geer, L. Y., He, S., Hurwitz, D. I., Jackson, J. D., Jacobs, A. R., Lanczycki, C. J., Liebert, C. A., Liu, C., Madej, T., Marchler, G. H., Mazumder, R., Nikolskaya, A. N., Panchenko, A. R., Rao, B. S., Shoemaker, B. A., Simonyan, V., Song, J. S., Thiessen, P. A., Vasudevan, S., Wang, Y., Yamashita, R. A., Yin, J. J., and Bryant, S. H. (2003). Cdd: A Curated Entrez Database of Conserved Domain Alignments. *Nucleic acids research* **31**, 383-387.

Munson, M. and Novick, P. (2006). The Exocyst Defrocked, a Framework of Rods Revealed. *Nat Struct Mol Biol* **13**, 577-581.

Pashkova, N., Jin, Y., Ramaswamy, S., and Weisman, L. S. (2006). Structural Basis for Myosin V Discrimination between Distinct Cargoes. *The EMBO journal* **25**, 693-700.

Robinson, N. G., Guo, L., Imai, J., Toh, E. A., Matsui, Y., and Tamanoi, F. (1999). Rho3 of Saccharomyces Cerevisiae, Which Regulates the Actin Cytoskeleton and Exocytosis, Is a Gtpase Which Interacts with Myo2 and Exo70. *Molecular and cellular biology* **19**, 3580-3587.

Sivaram, M. V., Furgason, M. L., Brewer, D. N., and Munson, M. (2006). The Structure of the Exocyst Subunit Sec6p Defines a Conserved Architecture with Diverse Roles. *Nat Struct Mol Biol* **13**, 555-556.

Wu, S., Mehta, S. Q., Pichaud, F., Bellen, H. J., and Quiocho, F. A. (2005). Sec15 Interacts with Rab11 Via a Novel Domain and Affects Rab11 Localization in Vivo. *Nat Struct Mol Biol* **12**, 879-885.

Zuo, X., Zhang, J., Zhang, Y., Hsu, S. C., Zhou, D., and Guo, W. (2006). Exo70 Interacts with the Arp2/3 Complex and Regulates Cell Migration. *Nature cell biology* **8**, 1383-1388.

Appendix

Contained in this appendix are protocols necessary for the complete and exact reproduction of this work. Most of these are variations on standard protocols (Ausubel *et al.*, 1998) that have proven to be more successful in the hands of the Xu lab.

Preparation of competent cells

A desired strain of *Escherichia coli* is streaked onto an agar LB plate (0.5% yeast extract, 1% tryptone, 1.5% agar (BD Biosciences) 10mM NaCl, 1mM NaOH) from a frozen stock. A colony is grown overnight at 37°C and a single colony is used to inoculate 3mL of sterile LB media (0.5% yeast extract, 1% tryptone, 10mM NaCl, 1mM NaOH) in an autoclave tube. The culture is grown overnight at 37°C and 1mL is used to inoculate 20mL of sterile LB media in a 125mL Erlenmeyer flask. The culture is grown at 37°C and shaken at 250rpm to an optical density at 595nm of 0.2. The culture is chilled on ice for 5min before centrifugation in a chilled Oakridge tube in an SS-34 rotor (Sorvall) at 10000rpm and 4°C for 2min. Cells are resuspended in 2.5mL chilled 50mM $CaCl_2$ and chilled on ice for 15min before centrifugation as above. Cells are resuspended in 2.5mL chilled TCM buffer (10mM Tris pH8.6, 50mM $CaCl_2$, 50mM $MgCl_2$) and aliquoted into Eppendorf tubes. Aliquots are snap-frozen in liquid nitrogen before storage at -80°C.

Preparation of ultracompetent cells

The DH5α strain of *Escherichia coli* is streaked onto an agar LB plate from a frozen stock. A colony is grown overnight at 37°C and a single colony is used to inoculate 250mL of sterile SOB media (0.5% yeast extract, 2% tryptone, 8.6mM NaCl, 2.5mM KCl, 10mM $MgCl_2$) in a 2L flask. The culture is grown at 20°C and shaken at 250rpm to an optical density at 600nm of 0.6. The culture is chilled on ice for 10min before centrifugation in 500mL Sorvall bottles in a GS-3 rotor (Sorvall) at 2500×g and 4°C for 10min. Cells are resuspended in 80mL ice-cold TB media (10mM PIPES pH6.7, 55mM $MnCl_2$, 15mM $CaCl_2$, 250mM KCl) and chilled on ice for 10min before centrifugation as above. Cells are resuspended in 20mL ice-cold TB media and DMSO is added to a final concentration of 7%. Cells were chilled on ice for 10min and aliquoted into Eppendorf tubes. Aliquots are snap-frozen in liquid nitrogen before storage at -80°C.

Preparation of TEV protease

TEV protease is used in the removal of tags from over-expressed proteins in the pSJ series of plasmids. 1μL of pET21d-TEV-NIa plasmid containing the oligo-histidine tagged TEV protease gene was added to 100μL competent BL21(DE3)pLysS *E. coli* and put on ice for 10min. The cells were then heat shocked for 2min in a 42°C water bath and 1mL LB media was added. After incubation for 1hr in a 37°C water bath 200μL cells were plated on LB-agar culture plates containing 100μg/mL ampcillin and 34ng/mL chloramphenicol and incubated overnight at 37°C. A single colony is used to inoculate 100mL LB media containing 100μg/mL ampcillin and 34ng/mL chloramphenicol. The culture is grown overnight at 30°C and shaken at 250rpm and 6×10mL culture is used to

inoculate 6×1L LB media containing 100μg/mL ampcillin and 34ng/mL chloramphenicol. These cultures are grown at 37°C to an optical density at 595nm of 0.4 and the temperature is reduced to 20°C. At an optical density at 595nm of 0.8 IPTG (Calbiochem) is added to a concentration of 100nM to induce protein expression for 8hr at 20°C. Cell pellets are collected by centrifugation in a GS-3 rotor at 6500rpm and 4°C for 15min and stored at -80°C.

Cell pellets are resuspended in buffer A (25mM Tris·HCl pH8.0, 300mM NaCl, 5mM β-me, 10% glycerol) and sonicated six times on ice for 30sec at power 8 on a Branson Sonifier 450 with 30sec breaks between pulses. Sonicated cells are centrifuged in an SS-34 rotor at 18000rpm and 4°C for 1hr and the supernatant is collected. The supernatant is passed over a Ni^{2+}-NTA Superflow column washed in buffer A. Material not bound to the column is washed away with 3×15mL buffer A before elution with 4×15mL buffer B (25mM Tris·HCl pH8.0, 300mM NaCl, 5mM β-me, 10% glycerol, 250mM imidazole·HCl). Column flow-through is analyzed by SDS-PAGE. Fractions containing an appropriate concentration and purity of the desired protein were collected and concentrated by centrifugation at 2750 × g in a Centriprep YM-10 concentrator (Amicon). Concentrated protein is then aliquoted into 500μL aliquots, snap-frozen in liquid nitrogen, and stored at -80°C.

Primer design

Many primers were used in this study for gene amplification and insertion of restriction sites using PCR (Table A.1). In general, primers were designed to contain three elements. The 5' element contains six or seven nucleotides that do not form

Table A.1: Primers used in this study

Name	Sequence
Exo70 5' BamHI	ATCGTAA GGA TCC ATG CCC GCT GAA ATT GAC ATT G
Exo70 3' SalI	ATCGTAA GT CGA CTA TCT CAC TAA TTG GTT AAG AAC
Exo84 5' NdeI	ATCGTAA CAT ATG GTT GAG TTT TCT TTG AAG AAG
Exo84 3' HindIII	ATCGT A AGC TTA GCG AAT TTT ATC ACT GTT CTT
Sec3 5' BamHI	ATCGTAT GGA TCC ATG AGG TCC TCG AAG TCT CC
Sec3 3' XhoI	ATCGTAA CTC GAG TTA GGC ATT CTT GTA TTC CTC
Sec5 5' BamHI	ATCGTAA GGA TCC ATG GAT AGG TTT CAA ATT GGC G
Sec5 3' XhoI	AACGTAT CTC GAG CTA GCT GAA GGC GGC GAA TTG
Sec6 5' BamHI	ATCGTAT GGA TCC ATG TCT TCA GAC CCC TTG CAG C
Sec6 3' XhoI	ATCGTAA CTC GAG TTA TTG CTT TTC GAA TTC TAA TAC A
Sec8 5' BamHI	ATCGTAA GGA TCC ATG GAT TAC CTA AAA CCA GCG
Sec8 3' SalI	ATCGTAA GTC GAC TCA TTT TTC GTT TGC AGT ATG GAC
Sec10 5' BamHI	ATCGTAA GGA TCC ATG AAC TCA TTA TAT GAA CTC GA
Sec10 3' XhoI	ATCGTAA CTC GAG CTA TCT AAA ATT CAA TTT AAC GCT
Sec15 5' BamHI	ATCGTAA GGA TCC ATG GAC CAA GAA GGC CAG CC
Sec15 3' XhoI	ATCGTAA CTC GAG TTA ACG TCT ATT AAA AAA TTT GGC
Exo70d168 5' BamHI	AGCTTAA GGA TCC ATG CCA TTT CCA TAC TAC GAG
Exo70d294 5' BamHI	ATCCTAA GGA TCC CGA AGC AAC CTC GAG AAC TTT G
Exo70d62 5' BamHI	ATCCTAA GGA TCC AAT ATT GAA AGT ACA TTG AAT TCC G
mExo70 5' EcoRI	ATCGTAA GAA TCC ATG ATT CCC CCG CAG GAG G
mExo70 3' XhoI	ATGGTAA CTC GAG TCA AGC AGA GGT GTC GAA AAG
RnExo70 5' EcoRI	ATCGTAA GAA TTC ATG ATT CCC CCG CAG GAG GC
RnExo70 3' XhoI	TAGGTAA CTC GAG TTA AGC AGA GGT GTC GAA GAG G
MmExo70d75 5' EcoRI	ATGCTAA GAA TTC AAC GTG GAG AAG ACG TTA TCC
MmExo70d84 5' EcoRI	AAGCTA GAA TCC GAC CAC GTT ATC AGC TAC TAC C

Restriction sites are underlined
Gene codons are separated by spaces

significant interactions with other nucleotides of the primer and are present to facilitate restriction digestion of the final PCR product. The central element contains a six-nucleotide restriction site that is unique to the target plasmid and not present in the amplified gene. The 3' element contains 17-24 nucleotides specific to the gene or gene fragment to be amplified. For a 5' primer this sequence matches the start sense strand of the desired amplification product. For a 3' primer this sequence matches the reverse compliment of the end of the sense strand of the desired amplification product. In order to ensure a strong enough interaction between primer and source DNA the following formula is applied: $2A + B \geq 30$, where A is the total number of cytosine-guanine pairs and B is the total number of adenine-thymine pairs formed between the primer and the source DNA strands. Primers containing high concentrations of adenosine and thymidine pairs often require a longer primer in order to achieve a score of 30 than primers containing high concentrations of cytidine and guanosine pairs, which can often use a shorter primer and still achieve a score of 30. It is also beneficial in choosing these sequences to end them with a cytidine or guanosine pair to improve the stability of the interaction. As a final check, the primer sequence is entered into the PrimerSelect program in the Lasergene package (DNA*) to detect the formation of any problematic primer dimers or hairpins. If any are detected the interacting sequences can be modified. If the problem exists in the 5' element, any change can be made to this sequence to prevent the formation of secondary structure. A problem in the restriction site can only be solved if another restriction site can be substituted. A problem in the 3' element can be solved if a wobble codon mutation will disrupt it. This type of mutation has no effect on

protein sequence but does require an extension of the primer to accommodate the mismatch between the primer and source DNA.

Crystal screening

A variety of conditions must be tested in order to identify those that promote protein crystal formation. Two screens were employed in this work in order to identify initial crystallization conditions. The Hampton crystal screens I and II (Hampton Research; Table A.2) are commercially available sparse matrix screens. The X screen (Table A.3) is a systematic screen developed by Zhaohui Xu. Crystallization screening is carried out in Cryshem 24-well sitting drop trays (Hampton Research). The Hampton screens are utilized by adding 500μL of the supplied precipitant to the well and 1-4μL of a 1:1 mixture of protein and precipitant from the well to the drop. Wells are immediately sealed and trays are stored in a 4°C or 20°C temperature- and humidity-controlled room and observed regularly for crystal growth. The X screen is utilized by first determining the pH stability of the protein. A 1:1 mixture of protein and one of a panel of pH stabilized 100mM buffers is observed at 4°C for 5-10min, then up to three buffers at particular pH values are chosen for which the protein remains soluble. The screen's precipitants are then mixed with each of the chosen buffers to a volume of 500μL in the well of the Cryshem tray and protein and well solution are mixed, sealed and stored as for the Hampton screen.

Once a crystal condition has been identified and optimized, a second round of screening can be performed in order to identify closely related crystal forms by the addition of other chemical species. For convenience the commercially available Hampton

Table A.2.1: Hampton Crystal Screen I

Condition #	Precipitant contents
1	30% (±)-2-methyl-2,4-pentanediol, 0.02M $CaCl_2 \cdot 2H_2O$, 0.1M sodium acetate·$3H_2O$ pH4.6
2	0.4M potassium sodium tartrate·$4H_2O$
3	0.4M $NH_4H_2PO_4$
4	2M $(NH_4)_2SO_4$, 0.1M Tris·HCl pH8.5
5	30% (±)-2-methyl-2,4-pentanediol, 0.2M trisodium citrate·$2H_2O$, 0.1M HEPES·Na pH7.5
6	30% PEG 4000, 0.2M $MgCl_2 \cdot 6H_2O$, 0.1M Tris·HCl pH8.5
7	1.4M sodium acetate·$3H_2O$, 0.1M sodium cacodylate·$3H_2O$ pH6.5
8	30% 2-propanol, 0.2M trisodium citrate·$2H_2O$, 0.1M sodium cacodylate·$3H_2O$ pH6.5
9	30% PEG 4000, 0.2M ammonium acetate, 0.1M trisodium citrate·$2H_2O$ pH5.6
10	30% PEG 4000, 0.2M ammonium acetate, 0.1M sodium acetate·$3H_2O$ pH4.6
11	1M $NH_4H_2PO_4$, 0.1M trisodium citrate·$2H_2O$ pH5.6
12	30% 2-propanol, 0.2M $MgCl_2 \cdot 6H_2O$, 0.1M HEPES·Na pH7.5
13	30% PEG 400, 0.2M trisodium citrate·$2H_2O$, 0.1M Tris·HCl pH8.5
14	28% PEG 400, 0.2M $CaCl_2 \cdot 2H_2O$, 0.1M HEPES·Na pH7.5
15	30% PEG 8000, 0.2M $(NH_4)_2SO_4$, 0.1M sodium cacodylate·$3H_2O$ pH6.5
16	1.5M $Li_2SO_4 \cdot H_2O$, 0.1M HEPES·Na pH7.5
17	30% PEG 4000, 0.2M $Li_2SO_4 \cdot H_2O$, 0.1M Tris·HCl pH8.5
18	20% PEG 8000, 0.2M magnesium acetate·$4H_2O$, 0.1M sodium cacodylate·$3H_2O$ pH6.5
19	30% 2-propanol, 0.2M ammonium acetate, 0.1M Tris·HCl pH8.5
20	25% PEG 4000, 0.2M $(NH_4)_2SO_4$, 0.1M sodium acetate·$3H_2O$ pH4.6
21	30% (±)-2-methyl-2,4-pentanediol, 0.2M magnesium acetate·$4H_2O$, 0.1M sodium cacodylate·$3H_2O$ pH6.5
22	30% PEG 4000, 0.2M sodium acetate·$3H_2O$, 0.1M Tris·HCl pH8.5
23	30% PEG 400, 0.2M $MgCl_2 \cdot 6H_2O$, 0.1M HEPES·Na pH7.5
24	20% 2-propanol, 0.2M $CaCl_2 \cdot 2H_2O$, 0.1M sodium acetate·$3H_2O$ pH4.6
25	1M sodium acetate·$3H_2O$, 0.1M imidazole pH6.5
26	30% (±)-2-methyl-2,4-pentanediol, 0.2M ammonium acetate, 0.1M trisodium citrate·$2H_2O$ pH5.6
27	20% 2-propanol, 0.2M trisodium citrate·$2H_2O$, 0.1M HEPES·Na pH7.5
28	30% PEG 8000, 0.2M sodium acetate·$3H_2O$, 0.1M sodium cacodylate·$3H_2O$ pH6.5
29	0.8M potassium sodium tartrate·$4H_2O$, 0.1M HEPES·Na pH7.5
30	30% PEG 8000, 0.2M $(NH_4)_2SO_4$
31	30% PEG 4000, 0.2M $(NH_4)_2SO_4$
32	2M $(NH_4)_2SO_4$
33	4M sodium formate
34	2M sodium formate, 0.1M sodium acetate·$3H_2O$ pH4.6
35	0.8M $NaH_2PO_4 \cdot H_2O$, 0.8M KH_2PO_4, 0.1M HEPES·Na pH7.5
36	8% PEG 8000, 0.1M Tris·HCl pH8.5
37	8% PEG 4000, 0.1M sodium acetate·$3H_2O$ pH4.6
38	1.4M trisodium citrate·$2H_2O$, 0.1M HEPES·Na pH7.5
39	2% PEG 400, 2M $(NH_4)_2SO_4$, 0.1M HEPES·Na pH7.5
40	20% 2-propanol, 20% PEG 4000, 0.1M trisodium citrate·$2H_2O$ pH5.6
41	10% 2-propanol, 20% PEG 4000, 0.1M HEPES·Na pH7.5
42	20% PEG 8000, 0.05M KH_2PO_4
43	30% PEG 1500
44	0.2M magnesium formate·$2H_2O$
45	18% PEG 8000, 0.2M Zinc acetate·$2H_2O$, 0.1M sodium cacodylate·$3H_2O$ pH6.5
46	18% PEG 8000, 0.2M Calcium acetate·$2H_2O$, 0.1M sodium cacodylate·$3H_2O$ pH6.5
47	2M $(NH_4)_2SO_4$, 0.1M sodium acetate·$3H_2O$ pH4.6
48	2M $NH_4H_2PO_4$, 0.1M Tris·HCl pH8.5
49	2% PEG 8000, 1M $Li_2SO_4 \cdot H_2O$
50	15% PEG 8000, 0.5M $Li_2SO_4 \cdot H_2O$

Concentrations given are those of the initial well solution

Table A.2.2: Hampton Crystal Screen II

Condition #	Precipitant contents
1	10% PEG 6000, 2M NaCl
2	0.01M hexadecyltrimethylammonium bromide, 0.5M NaCl, 0.01M $MgCl_2 \cdot 6H_2O$
3	25% ethylene glycol
4	35% 1,4-dioxane
5	5% 2-propanol, 2M $(NH_4)_2SO_4$
6	1M imidazole pH7.0
7	10% PEG 1000, 10% PEG 8000
8	10% ethanol, 1.5M NaCl
9	2M NaCl, 0.1M sodium acetate·$3H_2O$ pH4.6
10	30% (±)-2-methyl-2,4-pentanediol, 0.2M NaCl, 0.1M sodium acetate·$3H_2O$ pH4.6
11	1M 1,6-hexanediol, 0.01M $CoCl_2 \cdot 6H_2O$, 0.1M sodium acetate·$3H_2O$ pH4.6
12	30% PEG 400, 0.1M $CdCl_2 \cdot H_2O$, 0.1M sodium acetate·$3H_2O$ pH4.6
13	30% PEG MME 2000, 0.2M $(NH_4)_2SO_4$, 0.1M sodium acetate·$3H_2O$ pH4.6
14	2M $(NH_4)_2SO_4$, 0.2M potassium sodium tartrate·$4H_2O$, 0.1M trisodium citrate·$2H_2O$ pH5.6
15	1M $Li_2SO_4 \cdot H_2O$, 0.5M $(NH_4)_2SO_4$, 0.1M trisodium citrate·$2H_2O$ pH5.6
16	2% ethylene imine polymer, 0.5M NaCl, 0.1M trisodium citrate·$2H_2O$ pH5.6
17	35% *t*-butanol, 0.1M trisodium citrate·$2H_2O$ pH5.6
18	10% Jeffamine M-600, 0.01M $FeCl_3 \cdot 6H_2O$, 0.1M trisodium citrate·$2H_2O$ pH5.6
19	2.5M 1,6-hexanediol, 0.1M trisodium citrate·$2H_2O$ pH5.6
20	1.6M $MgSO_4 \cdot 7H_2O$, 0.1M MES·H_2O pH6.5
21	2M NaCl, 0.1M $NaH_2PO_4 \cdot H_2O$, 0.1M KH_2PO_4, 0.1M MES·H_2O pH6.5
22	12% PEG 20000, 0.1M MES·H_2O pH6.5
23	10% 1,4-dioxane, 1.6M $(NH_4)_2SO_4$, 0.1M MES·H_2O pH6.5
24	30% Jeffamine M-600, 0.05M CsCl, 0.1M MES·H_2O pH6.5
25	1.8M $(NH_4)_2SO_4$, 0.01M $CoCl_2 \cdot 6H_2O$, 0.1M MES·H_2O pH6.5
26	30% PEG MME 5000, 0.2M $(NH_4)_2SO_4$, 0.1M MES·H_2O pH6.5
27	25% PEG MME 550, 0.01M $ZnSO_4 \cdot 7H_2O$, 0.1M MES·H_2O pH6.5
28	1.6M trisodium citrate·$2H_2O$ pH6.5
29	30% (±)-2-methyl-2,4-pentanediol, 0.5M $(NH_4)_2SO_4$, 0.1M HEPES pH 7.5
30	10% PEG 6000, 0.1M HEPES pH 7.5
31	20% Jeffamine M-600, 0.1M HEPES pH 7.5
32	1.6M $(NH_4)_2SO_4$, 0.1M NaCl, 0.1M HEPES pH 7.5
33	2M ammonium formate, 0.1M HEPES pH 7.5
34	1M Sodium acetate·$3H_2O$, 0.05M $CdSO_4 \cdot H_2O$, 0.1M HEPES pH 7.5
35	70% (±)-2-methyl-2,4-pentanediol, 0.1M HEPES pH 7.5
36	4.3M NaCl, 0.1M HEPES pH 7.5
37	10% PEG 8000, 8% ethylene glycol, 0.1M HEPES pH 7.5
38	20% PEG 10000, 0.1M HEPES pH 7.5
39	3.4M 1,6-hexanediol, 0.2M $MgCl_2 \cdot 6H_2O$, 0.1M Tris pH8.5
40	25% *t*-butanol, 0.1M Tris pH8.5
41	1M $Li_2SO_4 \cdot H_2O$, 0.01M $NiCl_2 \cdot 6H_2O$, 0.1M Tris pH8.5
42	12% glycerol, 1.5M $(NH_4)_2SO_4$, 0.1M Tris pH8.5
43	50% (±)-2-methyl-2,4-pentanediol, 0.2M $NH_4H_2PO_4$, 0.1M Tris pH8.5
44	20% ethanol, 0.1M Tris pH8.5
45	20% PEG MME 2000, 0.01M $NiCl_2 \cdot 6H_2O$, 0.1M Tris pH8.5
46	20% PEG MME 550, 0.1M NaCl, 0.1M bicine pH9.0
47	2M $MgCl_2 \cdot 6H_2O$, 0.1M bicine pH9.0
48	2% 1,4-dioxane, 10% PEG 20000, 0.1M bicine pH9.0

Concentrations given are those of the initial well solution

Table A.3.1: X Screen initial pH screen

Condition #	Buffer species
1	Sodium acetate pH4.5
2	Sodium cacodylate pH5.5
3	PIPES pH6.5
4	HEPES pH7.5
5	Tris pH8.5
6	Glycine pH9.5

Table A.3.2: X Screen additional buffer screen

Condition #	Precipitant contents
1	0.8M NaH_2PO_4/KH_2PO_4 pH5.2
2	1.6M NaH_2PO_4/KH_2PO_4 pH5.2
3	2.4M NaH_2PO_4/KH_2PO_4 pH5.2
4	0.8M NaH_2PO_4/KH_2PO_4 pH6.8
5	1.6M NaH_2PO_4/KH_2PO_4 pH6.8
6	2.4M NaH_2PO_4/KH_2PO_4 pH6.8
7	0.8M NaH_2PO_4/KH_2PO_4 pH8.2
8	1.6M NaH_2PO_4/KH_2PO_4 pH8.2
9	2.4M NaH_2PO_4/KH_2PO_4 pH8.2
10	1M $NH_4H_2PO_4$ pH6.5
11	1.5M $NH_4H_2PO_4$ pH6.5
12	2M $NH_4H_2PO_4$ pH6.5
13	0.8M sodium citrate pH6.0
14	1.2M sodium citrate pH6.0
15	1.6M sodium citrate pH6.0
16	1.5M sodium formate pH8.0
17	2.5M sodium formate pH8.0
18	3.5M sodium formate pH8.0
19	0.5M sodium tartrate pH7.0
20	1M sodium tartrate pH7.0
21	1.5M sodium tartrate pH7.0
22	1M ammonium acetate pH7.5
23	2M ammonium acetate pH7.5
24	3M ammonium acetate pH7.5

Concentrations given are those of the initial well solution

Table A.3.3: X Screen precipitants to be mixed with variable buffer species

Condition #	Set 1 precipitant contents	Set 2 precipitant contents	Set 3 precipitant contents
1	1.2M $(NH_4)_2SO_4$	8% PEG 2000	20% MPD
2	1.2M $(NH_4)_2SO_4$, 2% MPD	8% PEG 2000, 5% MPD	20% MPD, 0.2M LiCl
3	1.2M $(NH_4)_2SO_4$, 5% ethanol	8% PEG 2000, 10% ethanol	20% MPD, 5% PEG 8000
4	1.2M $(NH_4)_2SO_4$, 0.25M Li_2SO_4	8% PEG 2000, 0.2M calcium acetate	35% MPD
5	2M $(NH_4)_2SO_4$	16% PEG 2000	35% MPD, 0.2M LiCl
6	2M $(NH_4)_2SO_4$, 2% MPD	16% PEG 2000, 5% MPD	35% MPD, 5% PEG 8000
7	2M $(NH_4)_2SO_4$, 5% ethanol	16% PEG 2000, 10% ethanol	50% MPD
8	2M $(NH_4)_2SO_4$, 0.25M Li_2SO_4	16% PEG 2000, 0.2M calcium acetate	50% MPD, 0.2M LiCl
9	2.8M $(NH_4)_2SO_4$	24% PEG 2000	50% MPD, 5% PEG 8000
10	2.8M $(NH_4)_2SO_4$, 2% MPD	24% PEG 2000, 5% MPD	20% PEG 300, 0.2M LiCl
11	2.8M $(NH_4)_2SO_4$, 5% ethanol	24% PEG 2000, 10% ethanol	30% PEG 300, 0.2M LiCl
12	2.8M $(NH_4)_2SO_4$, 0.25M Li_2SO_4	24% PEG 2000, 0.2M calcium acetate	40% PEG 300, 0.2M LiCl
13	0.5M $CaCl_2$	8% PEG 8000	20% PEG 600, 0.2M LiCl
14	1M $CaCl_2$	8% PEG 8000, 0.2M LiCl	30% PEG 600, 0.2M LiCl
15	2M $CaCl_2$	8% PEG 8000, 0.2M $MgCl_2$	40% PEG 600, 0.2M LiCl
16	0.5M Li_2SO_4	8% PEG 8000, 0.2M $(NH_4)_2SO_4$	20% ethanol
17	1M Li_2SO_4	16% PEG 8000	30% ethanol
18	2M Li_2SO_4	16% PEG 8000, 0.2M LiCl	40% ethanol
19	0.5M $MgSO_4$	16% PEG 8000, 0.2M $MgCl_2$	10% 2-propanol
20	1M $MgSO_4$	16% PEG 8000, 0.2M $(NH_4)_2SO_4$	20% 2-propanol
21	2M $MgSO_4$	24% PEG 8000	30% 2-propanol
22	1M NaCl	24% PEG 8000, 0.2M LiCl	25% ethylene glycol
23	2M NaCl	24% PEG 8000, 0.2M $MgCl_2$	35% ethylene glycol
24	4M NaCl	24% PEG 8000, 0.2M $(NH_4)_2SO_4$	40% ethylene glycol

All precipitants include 0.1M of a chosen buffer species at a specific pH value
Concentrations given are those of the initial well solution

Table A.4: Hampton Additive Screens

Condition #	Screen 1	Screen 2	Screen 3
1	0.01M $BaCl_2 \cdot 2H_2O$	0.1M NaI	0.1M $(NH_4)_2SO_4$
2	0.01M $CdCl_2 \cdot 2H_2O$	0.01M L-cysteine	0.1M CsCl
3	0.01M $CaCl_2 \cdot 2H_2O$	0.01M EDTA·Na salt	0.1M KCl
4	0.01M $CoCl_2 \cdot 6H_2O$	0.01M β-NAD	0.1M LiCl
5	0.01M $CuCl_2 \cdot 2H_2O$	0.01M ATP·2Na salt	0.2M NaCl
6	0.01M $MgCl_2 \cdot 6H_2O$	3% D(+)-glucose·H_2O	0.05M NaF
7	0.01M $MnCl_2 \cdot 4H_2O$	3% D(+)-sucrose	0.2M NaSCN
8	0.01M $SrCl_2 \cdot 6H_2O$	3% xylitol	3% dextran sulfate·Na salt
9	0.01M $YtCl_3 \cdot 6H_2O$	0.01M spermidine	5% Jeffamine M-600 pH7.0
10	0.01M $ZnCl_2$	0.01M spermine·4HCl	4% 2,5-hexanediol
11	3% ethylene glycol	3% 6-aminocaproic acid	4% (±)-1,3-butanediol
12	3% glycerol anhydrous	3% 1,5-diaminopentane·2HCl	4% PPG P 400
13	3% 1,6-hexanediol	3% 1,6-diaminohexane	4% 1,4-butanediol
14	3% MPD	3% 1,8-diaminooctane	4% *t*-butanol (v)
15	5% PEG 400	0.1M glycine	4% 1,3-propanediol (v)
16	0.01M $(CH_3)_3N \cdot HCl$	0.03M glycyl-glycyl-glycine	4% acetonitrile (v)
17	0.1M guanidine·HCl	0.01M $[Co(NH_3)_6]Cl_3$	4% 4-butyrolactone (v)
18	0.01M urea	0.01M taurine	4% *n*-propanol (v)
19	1.5% 1,2,3-heptanetriol	0.01M betaine·H_2O	0.5% ethyl acetate (v)
20	2% benzamidine·HCl	0.5% polyvinylpyrrolidine K15	4% acetone (v)
21	3% dioxane (v)	0.3M NDSB 195	0.025% CH_2Cl_2 (v)
22	3% ethanol (v)	0.2M NDSB 201	0.7% *n*-butanol (v)
23	3% isopropanol (v)	0.01M phenol	4% TFE (v)
24	3% methanol (v)	3% DMSO (v)	0.01M DTT (v)

Concentrations given are those of the initial drop
Conditions followed by (v) are volatile

Additive screens I, II, and III (Hampton Research; Table A.4) are employed. For non-volatile additives, 500μL precipitant is added to the well and the drop is composed of 4μL 5:4:1 protein:precipitant:additive. For volatile additives, the precipitant is modified to include the additive and added to the well and the drop is composed of 1:1 protein:precipitant. Wells are immediately sealed and trays are stored in a 4°C or 20°C temperature- and humidity-controlled room and observed regularly for crystal growth.

Preparation of SeMet substituted minimal MOPS media

The composition of SeMet substituted minimal MOPS media is complicated because Met must be avoided in all media components. As a result, several stock solutions are composed in advance to simplify the process. All stocks are autoclaved or contain autoclaved water and were filtered with a sterile 0.22μm filter. In addition, only sterile tools are used to minimize Met contamination from outside sources.

Six 1L cultures are typically grown at once. 1L of media is composed of 660mL ddH_2O, 200mL 5× amino acid and nucleotide stock (4mM Ala, 14.3mM Arg, 2mM Asn, 2mM Asp, 0.5mM Cys, 3mM Glu, 3mM Gln, 1mM His, 2mM Phe, 2mM Pro, 50mM Ser, 2mM Thr, 0.5mM Trp, 4mM Iso, 8mM Leu, 4mM Lys, 2mM Tyr, 6mM Val, 1mM adenine, 1mM guanine, 1mM cytosine, 1mM thymine), 94mL 10× MOPS stock (426mM MOPS, 43mM tricine, 3mM K_2SO_4, 5μM $CaCl_2$, 6mM $MgCl_2$, 532mM NaCl), 30mL 20% glucose stock, 10mL 132mM K_2HPO_4 stock, 5mL 1.9M NH_4Cl stock, 1mL antibiotic, 500μL 2000× vitamin stock (20mM thiamine·HCl, 20mM pantothenic acid·0.5Ca, 23mM *p*-hydroxybenzoic acid, 20mM *p*-aminobenzoic acid, 20mM 2,3-dihydroxybenzoic acid), 20μL 5000× micronutrients stock (706μM $(NH_4)_6Mo_7O_{24}·4H_2O$,

20mM H_3Bo_3, 6mM $CoCl_2 \cdot 6H_2O$, 344μM $CuSO_4 \cdot 5H_2O$, 4mM $MnCl_2 \cdot 4H_2O$, 501μM $ZnSO_4 \cdot 7H_2O$), 122mM SeMet stock, and 1mL 10mM $FeSO_4$ stock. It is noted that the 5× amino acid and nucleotide stock can remain cloudy with undissolved components even after several days of stirring. As a result, the actual concentrations of some components may be lower than listed here. The concentration and type of antibiotic used is dependent on the expression vector used. The 122mM SeMet stock and the 10mM $FeSO_4$ stock are made fresh immediately before use.

REFERENCES

Ausubel, F. M., Brent, R., Kingston, R. E., Moore, D. D., Seidman, J. G., Smith, J. A., Struhl, K., Albright, L. M., Coen, D. M., and Varki, A., Eds. (1998). Current Protocols in Molecular Biology. Vol. 1. Current Protocols. Edited by Chanda, V. B. 4 vols: John Wiley & Sons, Inc.